GL-TR-90-0279(I)

AD-A231 894

Laboratory Particle Velocity Experiments
on (JVE) Analog Rock

S. A. Miller
A. L. Florence

SRI International
333 Ravenswood Avenue
Menlo Park, CA 94025-3493

October 1990

Final Report
24 August 1988-30 November 1990

GEOPHYSICS LABORATORY
AIR FORCE SYSTEMS COMMAND
UNITED STATES AIR FORCE
HANSCOM AIR FORCE BASE, MASSACHUSETTS 01731-5000

91 2 13 · 007

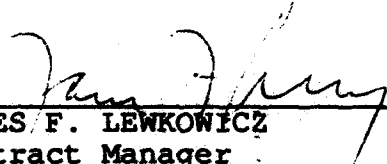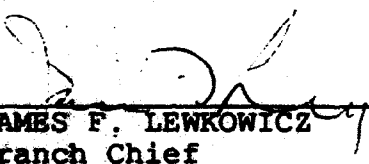The views and conclusions contained in this document are those of the authors and should not be interpreted as representing the official policies, either expressed or implied, of the Defense Advanced Research Projects Agency or the U.S. Government.

This technical report has been reviewed and is approved for publication.

JAMES F. LEWKOWICZ
Contract Manager
Solid Earth Geophysics Branch
Earth Sciences Division

JAMES F. LEWKOWICZ
Branch Chief
Solid Earth Geophysics Branch
Earth Sciences Division

FOR THE COMMANDER

DONALD H. ECKHARDT, Director
Earth Sciences Division

REPORT DOCUMENTATION PAGE

Form Approved
OMB No. 0704-0188

Public reporting burden for this collection of information is estimated to average 1 hour per response, including the time for reviewing instructions, searching existing data sources, gathering and maintaining the data needed, and completing and reviewing the collection of information. Send comments regarding this burden estimate or any other aspect of this collection of information, including suggestions for reducing this burden, to Washington Headquarters Services, Directorate for Information Operations and Reports, 1215 Jefferson Davis Highway, Suite 1204, Arlington, VA 22202-4302, and to the Office of Management and Budget, Paperwork Reduction Project (0704-0188), Washington, DC 20503.

1. AGENCY USE ONLY (Leave blank)	2. REPORT DATE October 1990	3. REPORT TYPE AND DATES COVERED Final - 88/8/24 - 90/11/30

4. TITLE AND SUBTITLE
LABORATORY PARTICLE VELOCITY EXPERIMENTS ON (JVE) ANALOG ROCK

5. FUNDING NUMBERS
Contract:
F19628-88-K-0051
PE 62714E
PR 8A10 TADAWUAO

6. AUTHOR(S)
Miller, S. A. and Florence, A. L.

7. PERFORMING ORGANIZATION NAME(S) AND ADDRESS(ES)
SRI International
333 Ravenswood Avenue
Menlo Park, CA 94025-3493

8. PERFORMING ORGANIZATION REPORT NUMBER
SRI Project 6645

9. SPONSORING/MONITORING AGENCY NAME(S) AND ADDRESS(ES)
Geophysics Laboratory
Hanscom AFB, MA 01731-5000

Def Advanced Rsch Proj Ag.
Nuclear Monitoring Rsch Off.
1400 Wilson Boulevard
Arlington, VA 22209-2808

Contract Manager: James F. Lewkowicz/LWH

10. SPONSORING/MONITORING AGENCY REPORT NUMBER
GL-TR-90-0279(I)

11. SUPPLEMENTARY NOTES

12a. DISTRIBUTION/AVAILABILITY STATEMENT
Approved for public release;
distribution unlimited

12b. DISTRIBUTION CODE

13. ABSTRACT (Maximum 200 words)

This project was performed in support of the Defense Advanced Research Projects Agency (DARPA) program to calibrate a Soviet nuclear test site by generating spherical waves in granite obtained from a borehole drilled adjacent to the site of the joint verification experiment (JVE). The objectives were to determine effects of pore condition and effective stress on spherical wave propagation and attenuation and to investigate coupling and attenuation properties in different low porosity "hard" rocks to find a suitable analog to the JVE rock and determine if attenuation is independent of the hard rock constituents. Particle velocity histories in cores of Sierra White granite and rocks obtained from a site on Mt. Katahdin, Maine, were measured in laboratory spherical wave experiments. Effects of initial porosity on attenuation were determined by comparing results from low porosity Katahdin limestone and high porosity Indiana limestone.

The effects of pore condition on attenuation were determined by experiments on Sierra White granite with three initial conditions: (1) dry, (2) saturated with zero effective stress, and (3) saturated with 11.7 MPa initial effective stress. Coupling and attenuation properties in different low porosity hard rocks were determined by experiments on Katahdin coarse- and fine-grained granite and

14. SUBJECT TERMS		15. NUMBER OF PAGES 104
Underground explosions Spherical waves Granite	Limestone Energy coupling Potentials	16. PRICE CODE

17. SECURITY CLASSIFICATION OF REPORT UNCLASSIFIED	18. SECURITY CLASSIFICATION OF THIS PAGE UNCLASSIFIED	19. SECURITY CLASSIFICATION OF ABSTRACT UNCLASSIFIED	20. LIMITATION OF ABSTRACT SAR

CLASSIFIED BY:

DECLASSIFY ON:

13.   ABSTRACT (Continued)

Katahdin limestone. The experimental results showed that (1) the pore condition (i.e., dry versus saturated) and initial effective stress conditions had little, if any, effect on velocity and displacement attenuation in low porosity Sierra White granite; and (2) the attenuation of peak displacements in Sierra White granite, Katahdin coarse- and fine-grained granite, and Katahdin limestone was the same within the scatter of the experimental data. Comparisons of high porosity Indiana limestone and low porosity Katahdin limestone showed a substantial effect of initial porosity on attenuation.

Accession For	
NTIS GRA&I	☑
DTIC TAB	☐
Unannounced	☐
Justification	
By	
Distribution/	
Availability Codes	
Dist	Avail and/or Special
A-1	

DTIC
COPY
INSPECTED

SUMMARY

This project was performed to support the Defense Advanced Research Projects Agency (DARPA) program for calibrating the Soviet nuclear test site at Semipalatinsk by generating spherical waves in granite obtained from a borehole adjacent to the site of the Joint Verification Experiment (JVE). Particle velocity histories in cores of Sierra White granite and rocks obtained from a site on Mt. Katahdin, Maine, were measured in laboratory spherical wave experiments. The objectives were to (1) determine effects of pore condition and effective stress on spherical wave propagation and attenuation, and (2) investigate coupling and attenuation properties in different low porosity "hard" rocks to find a suitable analog to the JVE rock and determine if attenuation is independent of the hard rock constituents. Effects of initial porosity, n, on attenuation were determined by comparing results from Katahdin limestone (n = 1%) and Indiana limestone (n = 13%).

The spherical wave source was a 3/8-g charge of PETN powder packed to a density of 1.0 g/cm^3. Particle velocity histories were measured at different ranges by using concentric copper loops placed in machined grooves along the midplane of the specimen. An external axial magnetic field was applied to the specimen, and the particle velocity was measured by monitoring the induced voltage generated by the gages as they moved through the magnetic field. The particle velocity is proportional to the induced voltage, the conductor length, and the magnetic field strength according to Faraday's law.

To determine the effects of pore condition on attenuation, experiments were performed in Sierra White granite (n ≈ 1%) with three initial conditions: (1) dry, (2) saturated with zero effective stress, and (3) saturated with 11.7 MPa initial effective stress. To determine coupling and attenuation properties in different low porosity hard rocks, experiments were performed in Katahdin coarse- and fine-grained granite and Katahdin limestone.

The experimental results showed that (1) the pore condition (i.e., dry versus saturated) and initial effective stress conditions had little, if any, effect on velocity and displacement attenuation in low porosity Sierra White granite; and (2) the attenuation of peak displacements in Sierra White granite, Katahdin coarse- and fine-grained granite, and Katahdin limestone was the same within the scatter of the experimental data. Comparisons of high porosity (13%) Indiana limestone and low porosity (1%) Katahdin limestone showed a substantial effect of initial porosity on attenuation.

iii

PREFACE

TABLE OF CONTENTS

LIST OF ILLUSTRATIONS

LIST OF ILLUSTRATIONS (CONTINUED)

LIST OF ILLUSTRATIONS (CONTINUED)

LIST OF ILLUSTRATIONS (CONTINUED)

LIST OF ILLUSTRATIONS (CONCLUDED)

SECTION 1

INTRODUCTION

The objective of this research project was to support the Defense Advanced Research Projects Agency (DARPA) program for calibrating the Soviet nuclear test site at Semipalatinsk by generating spherical waves in granite obtained from a borehole drilled adjacent to the site of the joint verification experiment (JVE). Because the Semipalatinsk region is geologically diverse in terms of physical properties and degrees of saturation, additional objectives were established during the course of the DARPA program: (1) to investigate the effect of initial pore condition on wave propagation in low porosity (<1%) hard rock and (2) to investigate a variety of low porosity hard rocks to determine how variability in the rock constituents affects wave propagation and attenuation.

We performed three spherical wave experiments in Sierra White granite under different initial pore conditions to determine how pore fluid and initial effective stress affect wave propagation and attenuation. The initial pore conditions were (1) dry, (2) saturated with zero initial effective stress (i.e., equal overburden and pore pressure), and (3) saturated with 11.7 MPa initial effective stress. The granite specimens had initial porosities less than 1%.

Mt. Katahdin, Maine, has been proposed to be geologically analogous to the Soviet test site. We performed spherical wave experiments in three different hard rocks obtained from the Mt. Katahdin site to compare the results with those from specimens from the JVE site and to investigate the more general question of how rock constituents in low porosity hard rock affect coupling and attenuation. The Mt. Katahdin specimens tested included (1) coarse-grain granite, (2) fine-grain granite, and (3) metamorphosed limestone. Each of these rocks had initial porosities less than 1%.

In this report, we present (1) the results of spherical wave experiments in Sierra White granite, in which we investigated the effects of pore fluid and initial effective stress on wave propagation; (2) the results of spherical wave experiments in different hard rocks obtained from Mt. Katahdin, Maine; and (3) comparisons between high and low porosity limestone that demonstrate how initial porosity affects coupling and attenuation. The results of the spherical wave experiments in the rock obtained from the site of the JVE experiment are presented in a separate report.

1

In Section 2, we describe the experimental technique and configuration for the spherical wave experiments. In Section 3, we present the experimental results obtained in Sierra White granite and the Mt. Katahdin specimens. A few results from a separate effort in a high porosity (13%) Indiana limestone are also presented for comparison with the results from the low porosity (1%) Katahdin limestone. Section 4 describes our conclusions from this work and recommendations for additional research. Strain histories and strain path data from these experiments are shown in Appendix A, and reduced displacement potential (RDP) and reduced velocity potential (RVP) histories are shown in Appendix B. Figures are grouped together at the end of the report and each appendix.

SECTION 2

EXPERIMENTAL CONFIGURATION

The configuration for the spherical wave experiments is shown in Figure 1. (All figures are at the end of the text.) In these experiments, a 3/8-g charge of PETN powder is detonated at the center of a 16.5-cm-diameter cylindrical specimen, and particle velocity histories are measured at different radii from the center of the charge. Each sample is prepared by grinding its face flat and machining a spherical cavity for the charge and grooves for the particle velocity (PV) gages.

The gages used to measure particle velocity are copper loops that are mounted into the machined grooves in the specimen. A constant axial magnetic field is applied by a solenoid surrounding the specimen, and the particle velocity is measured by monitoring the induced voltage generated by the copper loop as it moves at the local particle velocity through the magnetic field. According to Faraday's law, the induced voltage is proportional to the length of the conductor, the magnetic field strength, and the particle velocity. The magnetic field strength is determined in each test by measuring the current supplied to the solenoid. The charge is detonated by a strand of 2-grain mild detonating fuse (MDF) that is channelled through a stainless steel tube extending out of the pressure vessel and initiated by an exploding bridge wire.

Although the stainless steel tube is not stemmed, code calculations of our experimental geometry have shown that the reduction in cavity pressure due to venting in the tube is small during the recording period and the effect on the propagated pulse in the medium is negligible.

For experiments where the specimen was dry, we isolated the external pressurizing fluid (overburden) from the sample by applying a rubber seal to the outside of the specimen. In experiments where the specimen was saturated and the pore pressure was equal to the overburden pressure (zero effective stress), we first saturated the specimen in a separate vessel and then installed the explosive charge. The specimen was then put into the test chamber containing the solenoid, and the overburden pressure was applied. In the experiment with nonzero effective stress, the pore pressure was isolated from the overburden pressure by first surrounding the saturated specimen with a fine wire mesh that acted as a reservoir and flow path for the pore fluid. The sample and mesh were then

3

surrounded by a thin aluminum sleeve around the circumference and end caps on the top and bottom with feedthroughs for the hydraulic line and wire egress. This assembly was inserted in a rubber jacket and epoxied to the end caps. Pressure gages were installed to measure the overburden pressure and pore pressure separately.

The specimens were saturated by (1) applying and maintaining a vacuum for 12 to 24 hours to remove air from the pore space, and (2) immersing the specimen in deionized/degassed water and applying an overburden pressure to the sample with a flatjack for an additional 12 to 24 hours.

SECTION 3

EXPERIMENTAL RESULTS

In this section, we present results from (1) experiments in Sierra White granite under different initial pore conditions and (2) experiments in specimens obtained from Mt. Katahdin, Maine, and (3) a comparison of results from low porosity and high porosity limestone.

EFFECTS OF PORE FLUID AND INITIAL EFFECTIVE STRESS

We performed three experiments in Sierra White granite with porosity <1% to compare the response for different pore conditions. These conditions were (1) dry (Test 564), (2) saturated with equal overburden and pore pressure (i.e., zero effective stress) (Test 564), and (3) saturated with an initial effective stress (P_c) of 11.7 MPa (Test 565).

Sets of the particle velocity records from gages at the same location in each experiment are shown superimposed in Figures 2 through 9. Unfortunately, we did not recover data from the gages at the 50-mm and 65-mm ranges in Test 563 because of a malfunction in the recording equipment. As shown in Figures 6 and 7, the peak velocities at the 30-mm and 40-mm ranges in Test 565 were not captured because of an apparent loss in high frequency response of the recording equipment for these channels; therefore, these data are not included in the peak particle velocity attenuation plot (Figure 10). Posttest cavity diameters were measured to be about 1.3 cm.

Particle displacement histories were obtained by temporal integration of the velocity records. Sets of particle displacement histories at each gage location for the three different pore conditions are shown superimposed in Figures 11 through 18, and attenuation of peak displacement with range is shown in Figure 19. The velocity and displacement attenuation exponents shown in Figures 10 and 19 are 1.23 and 1.15, respectively.

Overall, the agreement between velocity and displacement histories for the different pore conditions is quite good, and any effects of pore fluid or initial effective stress cannot easily be resolved within the scatter of the experimental data. This result applies only to very low porosity rocks (<1%), and probably does not extend to rocks with higher initial porosities.

5

On the basis of the results in Sierra White granite, the experiments on the JVE and Mt. Katahdin specimens were performed under saturated, zero effective stress conditions, which is the least complicated sample preparation scheme.

EXPERIMENTAL RESULTS FROM MT. KATAHDIN SPECIMENS

Our objective in these experiments was to determine how variabilities in the constituents of low porosity hard rock affect coupling and attenuation. The Mt. Katahdin, Maine, site has been proposed to be geologically analogous to the Soviet test site. We performed spherical wave experiments in three different hard rocks obtained from the Mt. Katahdin site: (1) fine-grained Katahdin granite, (2) coarse-grained Katahdin granite, and (3) low porosity Katahdin limestone.

Although other rock types were obtained from the Katahdin site, recovery of cores of the size we need for our experiments was limited to these three specimen types. The fine-grain and coarse-grain granites represent two members of the Katahdin batholith. These rocks are essentially structureless and are about two-thirds feldspar and one-third quartz, with 5-10% biotite. The limestone is reefal and reef detritus; it is sheared and penetrated with joints healed with silaceous or calcareous cement. Each of these rocks had initial porosities lower than 1%.

We recovered data from four of the six experiments performed in the Katahdin specimens. Unfortunately, the charge apparently burned instead of detonated in two of the experiments (one Katahdin coarse-grain granite and one Katahdin limestone), causing these specimens to fracture from the long-duration loading of the cavity.

The results from the Katahdin granite specimens (Tests 571, 577, and 579) are shown with the results from an experiment in Sierra White granite (Test 563) for comparison with another low porosity hard rock. In a separate comparison, the results from the Katahdin limestone experiment (Test 572) are shown with those from a Katahdin fine-grain granite (Test 571).

The time of arrival is shown as a function of the gage distance from the center of the source for the granite experiments in Figure 20(a). A least-squares fit to the data results in a wave velocity of about 5.6 km/s. The single Katahdin limestone experiment showed a wave velocity of about 6.6 km/s [Figure 20(b)].

The measured particle velocity histories at each measurement location for Sierra White granite and fine- and coarse-grained Katahdin granite are shown superimposed in

6

Figures 21 through 27. Signals recorded at the 40-mm location are not included because a malfunction in the recording equipment erroneously attenuated the signal.

Overall, the results show very similar energy coupling in each of the different types of granite, characterized by an initial sharp rise to the peak velocity, followed by positive (outward) motion lasting about 6-7 μs, and a negative (rebound) phase increasing in duration with propagation distance. Because of the very fast rise time in this material, the peak particle velocity shows experimental scatter on the order of 20%. After the peak, the material response is essentially the same in each type of granite.

The results from each measurement location in the Katahdin limestone specimen (Test 572) are shown superimposed with those from a typical granite experiment (Katahdin fine-grain, Test 571) in Figures 28 through 33. The results show a longer rise time and a lower peak particle velocity in the limestone, but the pulse shapes after the peak are similar. We believe that the lower peak particle velocity in limestone is a real effect, but because the repeat experiment in limestone was unsuccessful, we can not confirm this result. These differences, however, do not have a significant effect on either the peak displacements or displacement histories.

Attenuation of peak velocity for the Sierra White granite and Katahdin specimens is shown in Figure 34. Except for the limestone specimen, the peak velocity attenuation shows a scatter of about 20%. The very fast rise time in granite makes it difficult to separate any material effects (on peak particle velocity) from experimental artifacts such as failure to capture the peak because of the sampling rate and frequency response of the recording equipment. For example, in two experiments, Tests 577 and 579, we increased the sampling rate of the digital oscilloscope from 50 ns/point to 20 ns/point, and we observed an increase in peak particle velocity of about 20%. However, capturing peak velocity has little effect on the displacements.

The displacement histories at each gage location for the experiments on Katahdin specimens are shown in Figures 35 through 41. These data provide the displacement gradients needed to obtain approximate strain and strain path information from these experiments. Peak displacement attenuations for Sierra White granite, Katahdin fine- and coarse-grained granite, and Katahdin limestone are shown superimposed in Figure 42. As seen in Figure 42, the peak displacements for the different rock types are grouped in a narrow band, and any differences between the rock types can not easily be distinguished from the scatter in the experimental data.

EFFECTS OF INITIAL POROSITY

In a previous experimental effort,[1] we generated particle velocity histories using a 3/8-g spherical explosive source in saturated Indiana limestone. The total porosity of Indiana limestone was about 12.6%. A comparison of the particle velocity records for this limestone and the Katahdin limestone at one representative gage location (50 mm) is shown in Figure 43. The corresponding displacements are shown in Figure 44, and attenuation of peak displacement with range for each gage location is shown in Figure 45. These results demonstrate the effect of initial porosity on coupling and attenuation and show a much longer particle velocity pulse duration (and corresponding displacement) in the high porosity Indiana limestone than in the lower porosity (1%) Katahdin limestone.

---

[1]S. A. Miller and A. L. Florence, "Spherical Waves in Limestone," SRI Technical Report DNA-TR-89-263, August 1990.

8

SECTION 4

CONCLUSIONS AND RECOMMENDATIONS

The results of the spherical wave experiments showed

- Little effect of the initial pore fluid condition on attenuation in low porosity (<1%) granite.

- Similar energy coupling and attenuation in different types of low porosity hard rock, although lower peak velocities were observed in limestone than in granite.

- A significant difference in wave shape and attenuation between low porosity (<1%) and high porosity (13%) limestone.

We recommend (1) additional experiments for different initial pore conditions in higher porosity specimens to determine how effective stress affects wave propagation and attenuation, and (2) additional experiments on JVE specimens for comparison with the results presented here.

External Magnetic
Field

Overburden
Pressure

MDF
Tube

8 cm

3/8 gram
PETN
Charge

PV
Gages

(a) Side View

16.5 cm

Specimen
Boundary

RADIUS

0.5 cm (charge)
1.0 cm (PV1)
1.5 cm (PV2)
2.0 cm (PV3)
2.5 cm (PV4)
3.0 cm (PV5)
4.0 cm (PV6)
5.0 cm (PV7)
6.5 cm (PV8)

(b) Top View

RA-M-6645-1D
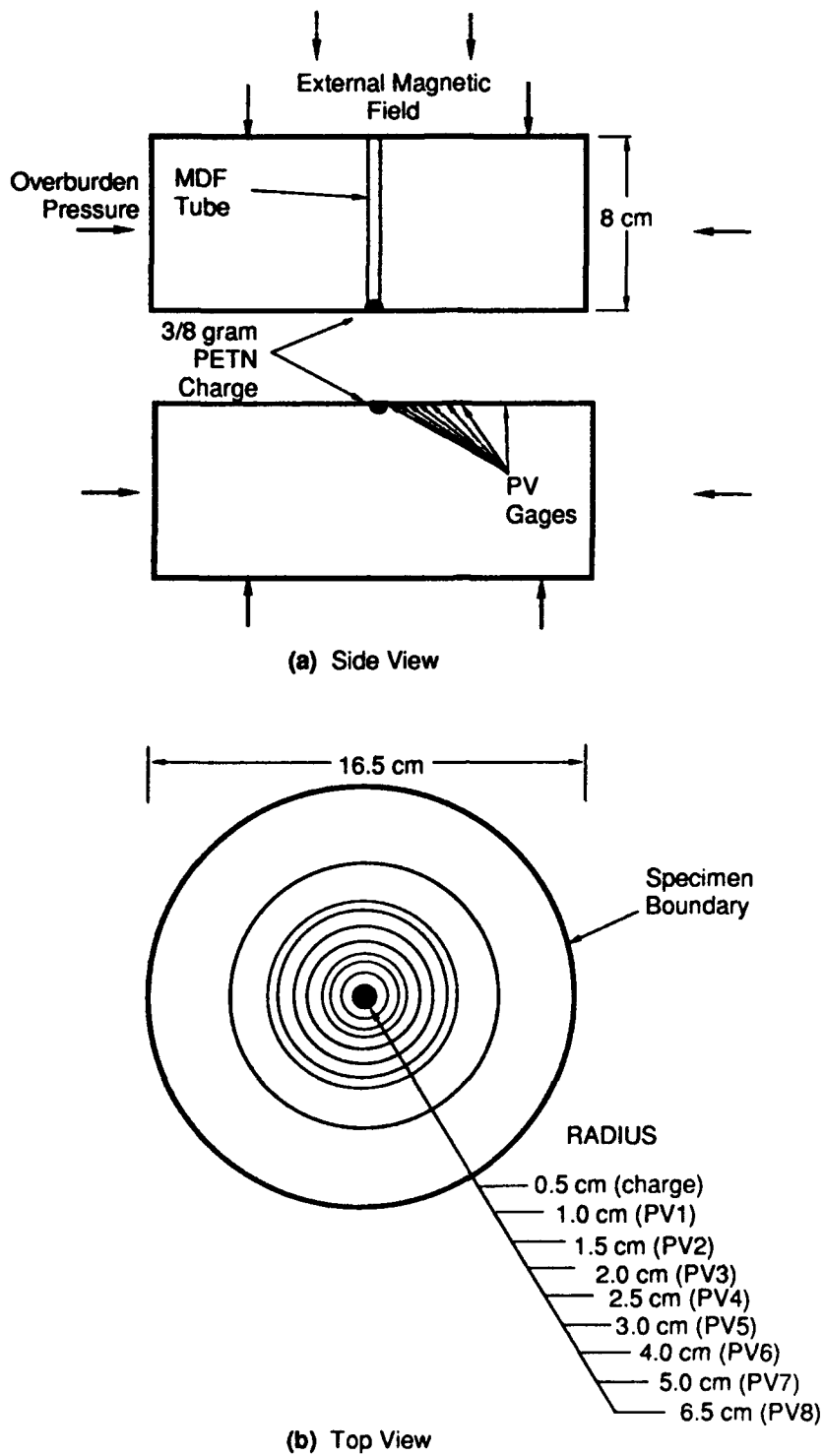
Figure 1. Configuration of spherical wave particle velocity experiments
in Sierra White granite and Katahdin specimens.

10
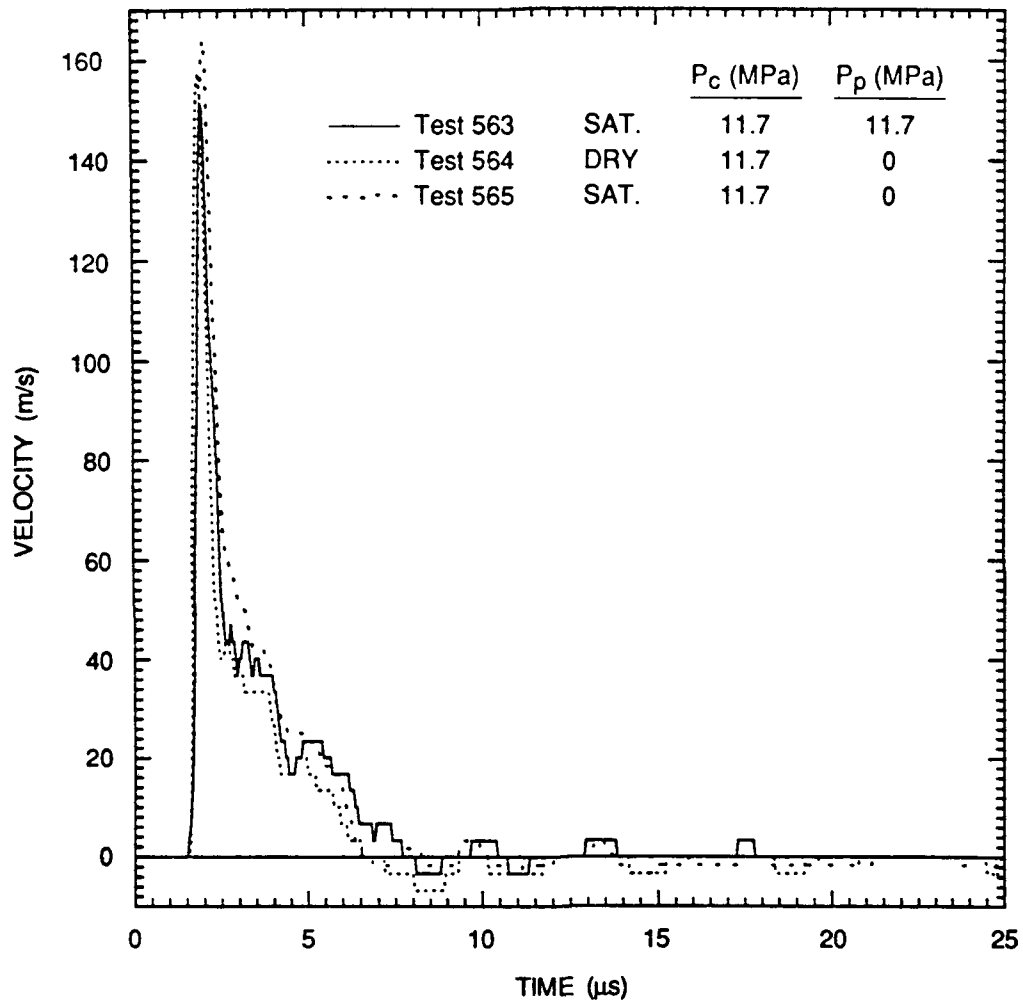
Figure 2. Particle velocity histories for three different pore conditions at 10-mm range in Sierra White granite.
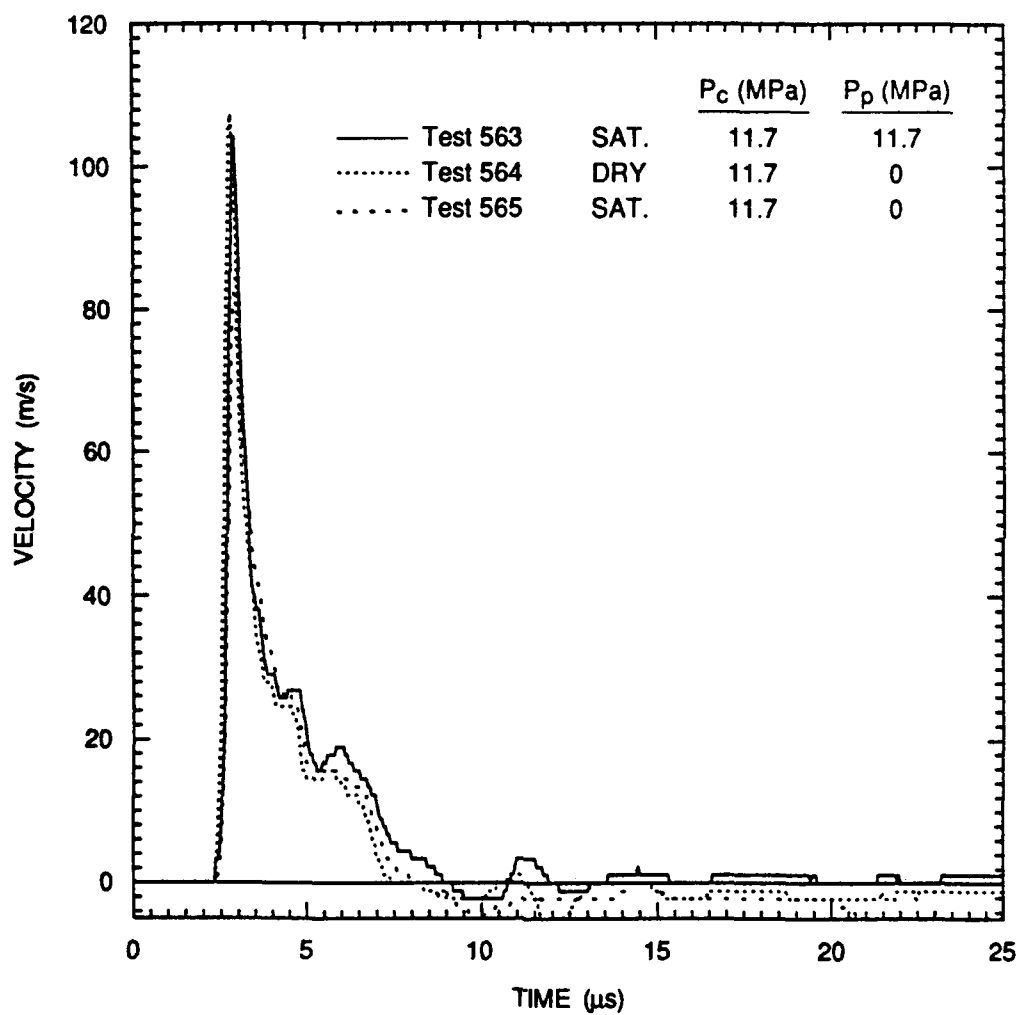
Figure 3. Particle velocity histories for three different pore conditions at 15-mm range in Sierra White granite.

RA-6645-9

12

Figure 4. Particle velocity histories for three different pore conditions at 20-mm range in Sierra White granite.

RA-6645-10

13

RA-6645-11

Figure 5. Particle velocity histories for three different pore conditions at 25-mm range in Sierra White granite.

14

Figure 6. Particle velocity histories for three different pore conditions at 30-mm range in Sierra White granite.

RA-6645-12

15

Figure 7.   Particle velocity histories for three different pore conditions at 40-mm range in Sierra White granite.
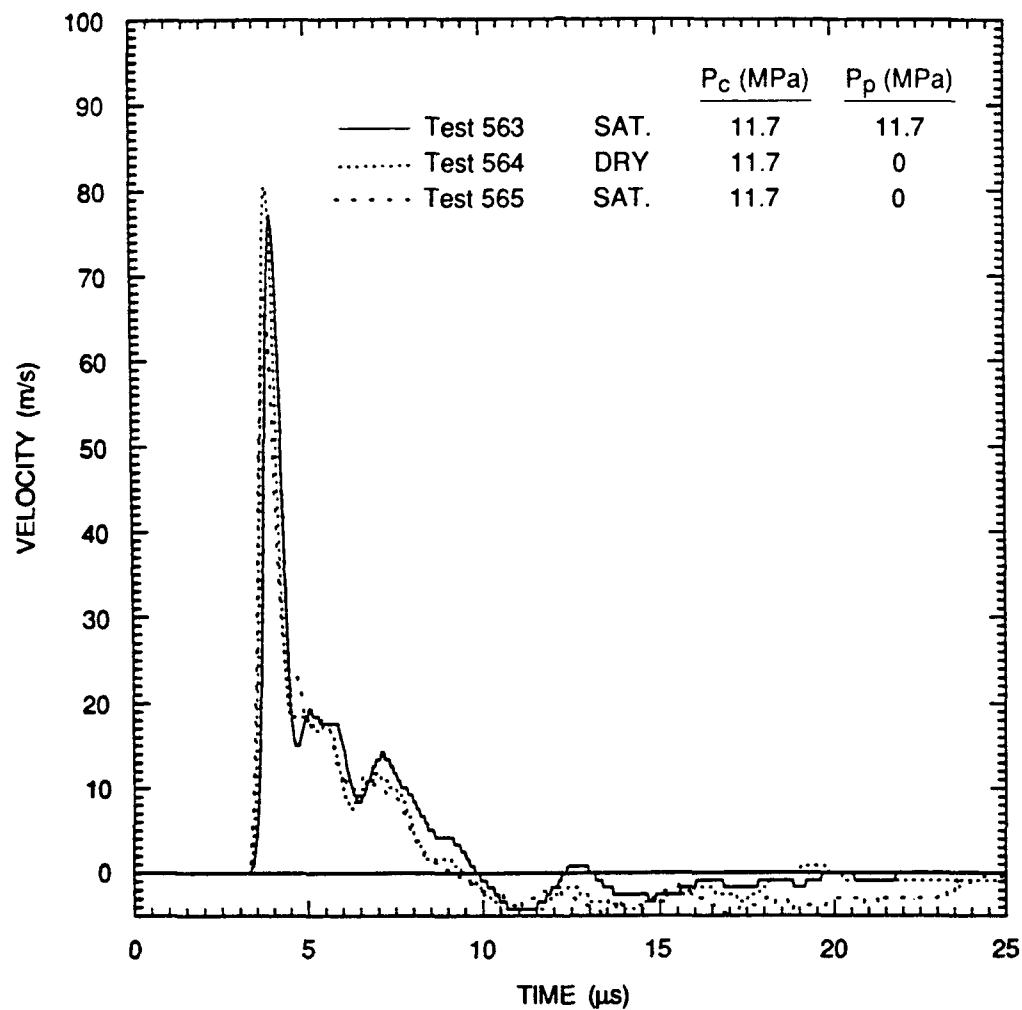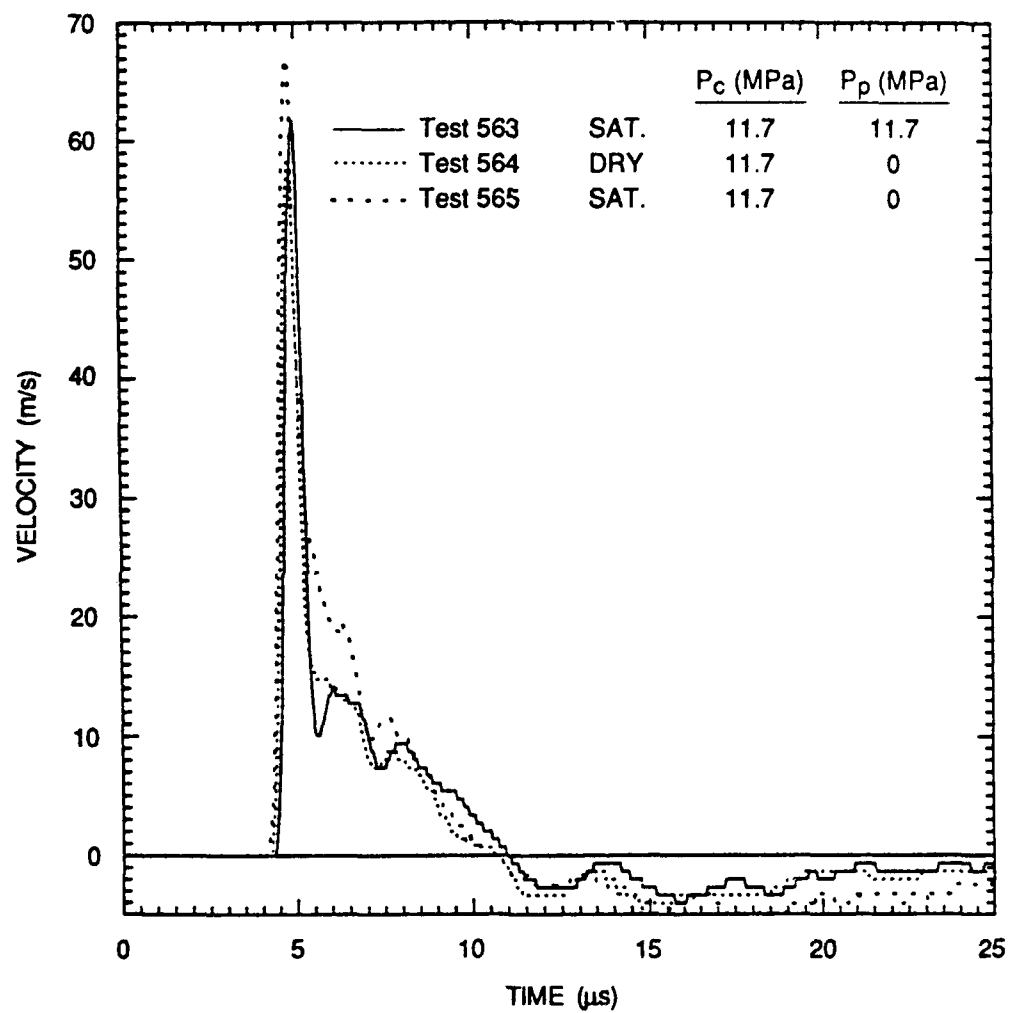
RA-6645-13

16

Figure 8.   Particle velocity histories for different pore conditions at 50-mm range in Sierra White granite.

17

RA-6645-15

Figure 9. Particle velocity histories for different pore conditions at 65-mm range in Sierra White granite.

18

Figure 10.   Attenuation of peak velocity for three different pore conditions in Sierra White granite.
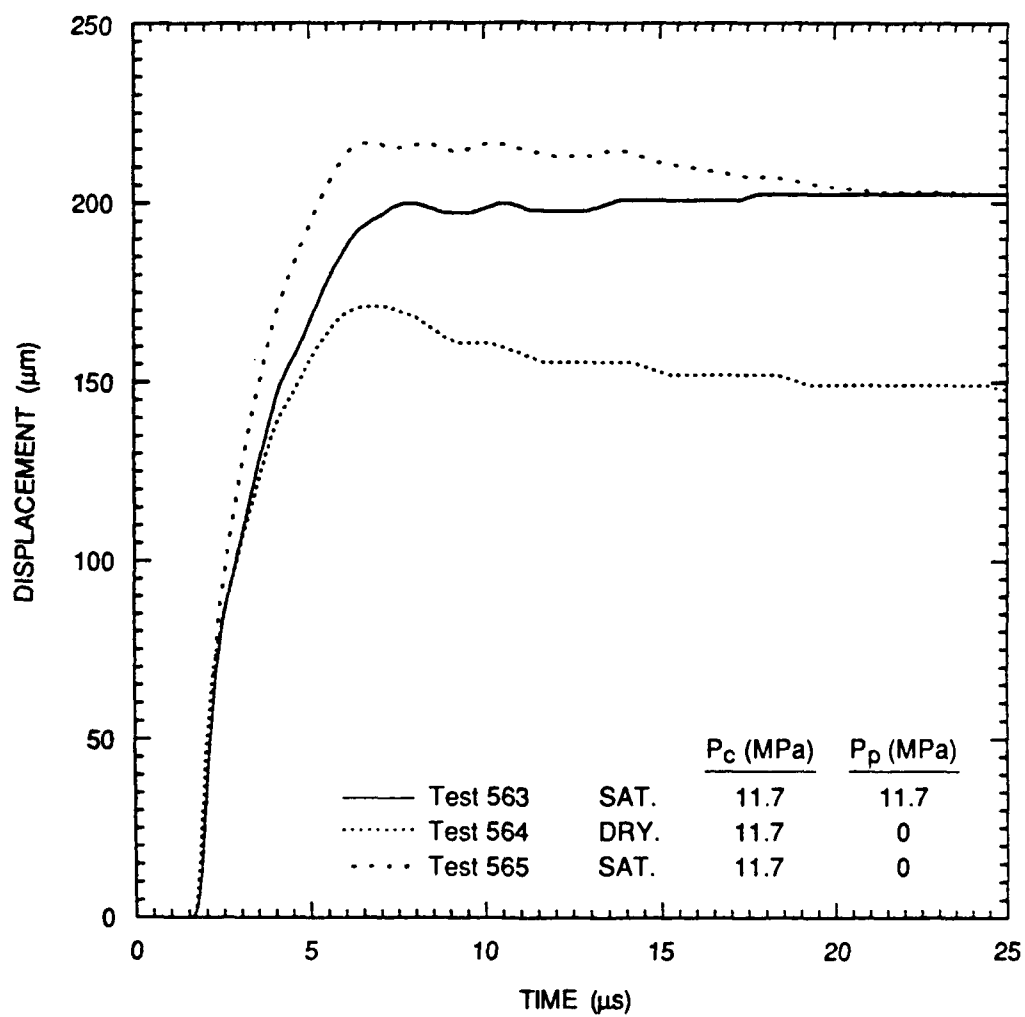
Figure 11. Displacement histories for three different pore conditions at 10-mm range in Sierra White granite.

20
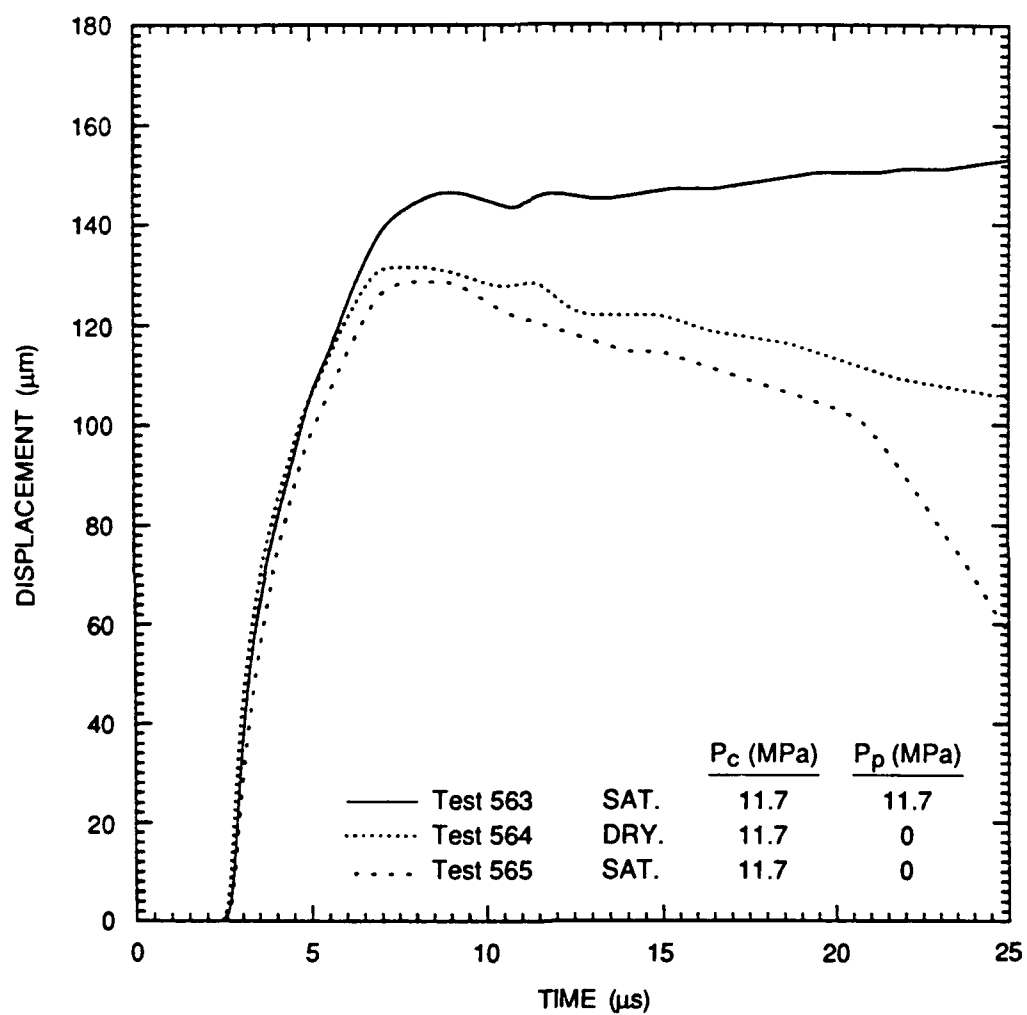
RA-6645-18

Figure 12. Displacement histories for three different pore conditions at 15-mm range in Sierra White granite.

21
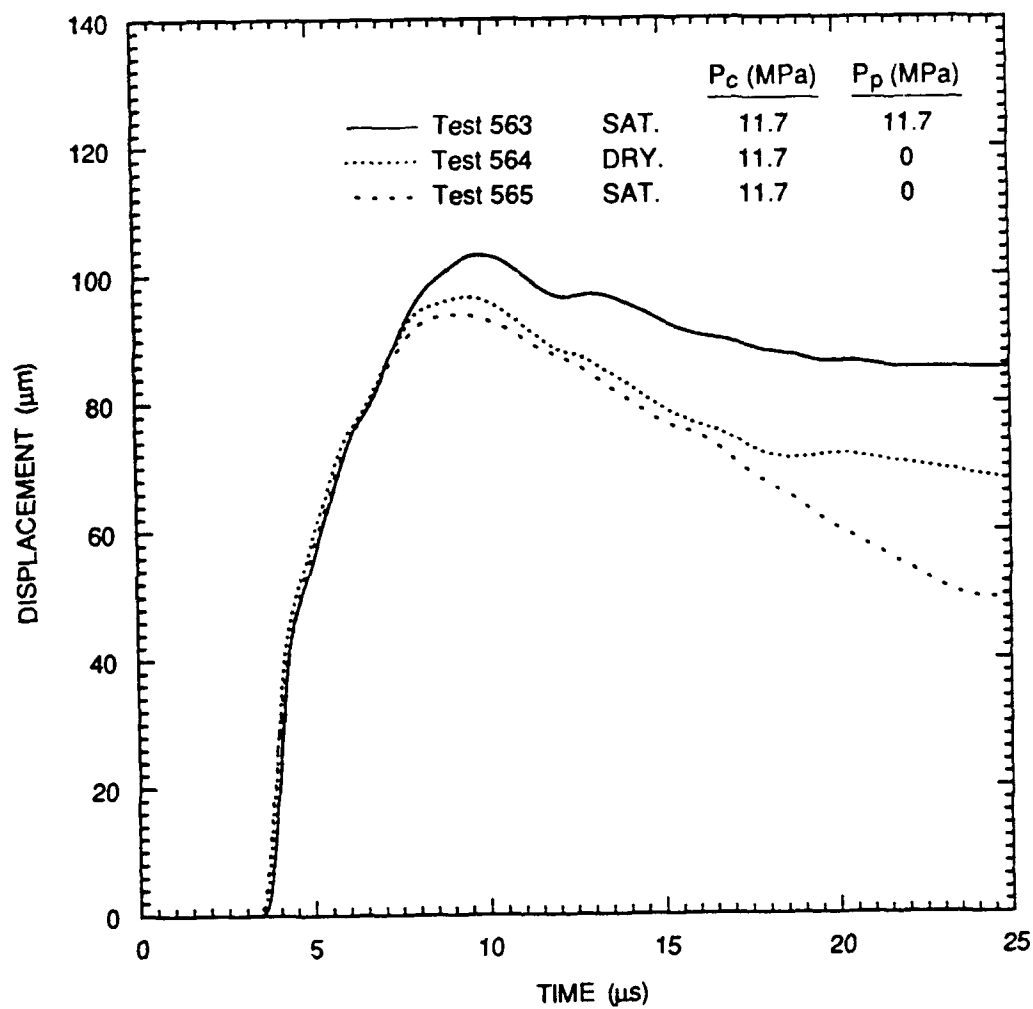
Figure 13. Displacement histories for three different pore conditions at 20-mm range in Sierra White granite.
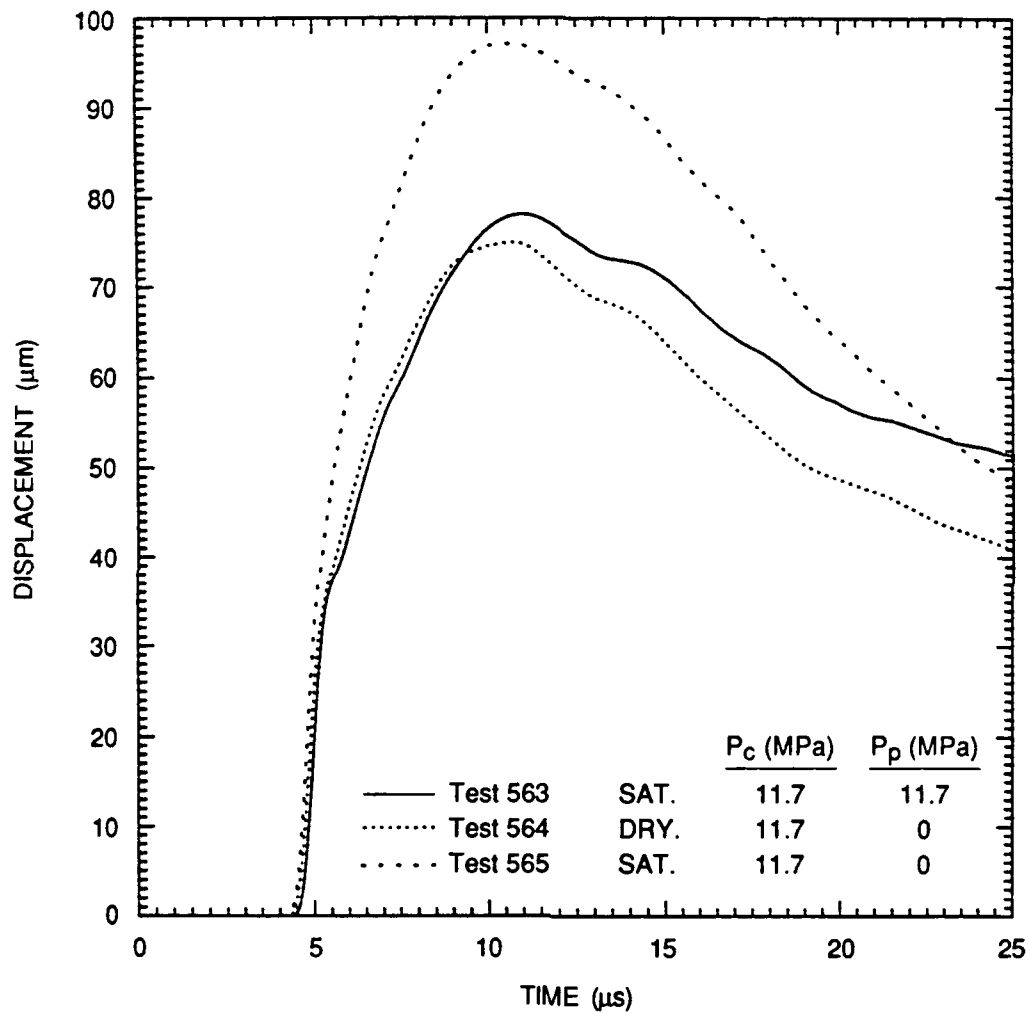
Figure 14. Displacement histories for three different pore conditions at 25-mm range in Sierra White granite.

RA-6645-20

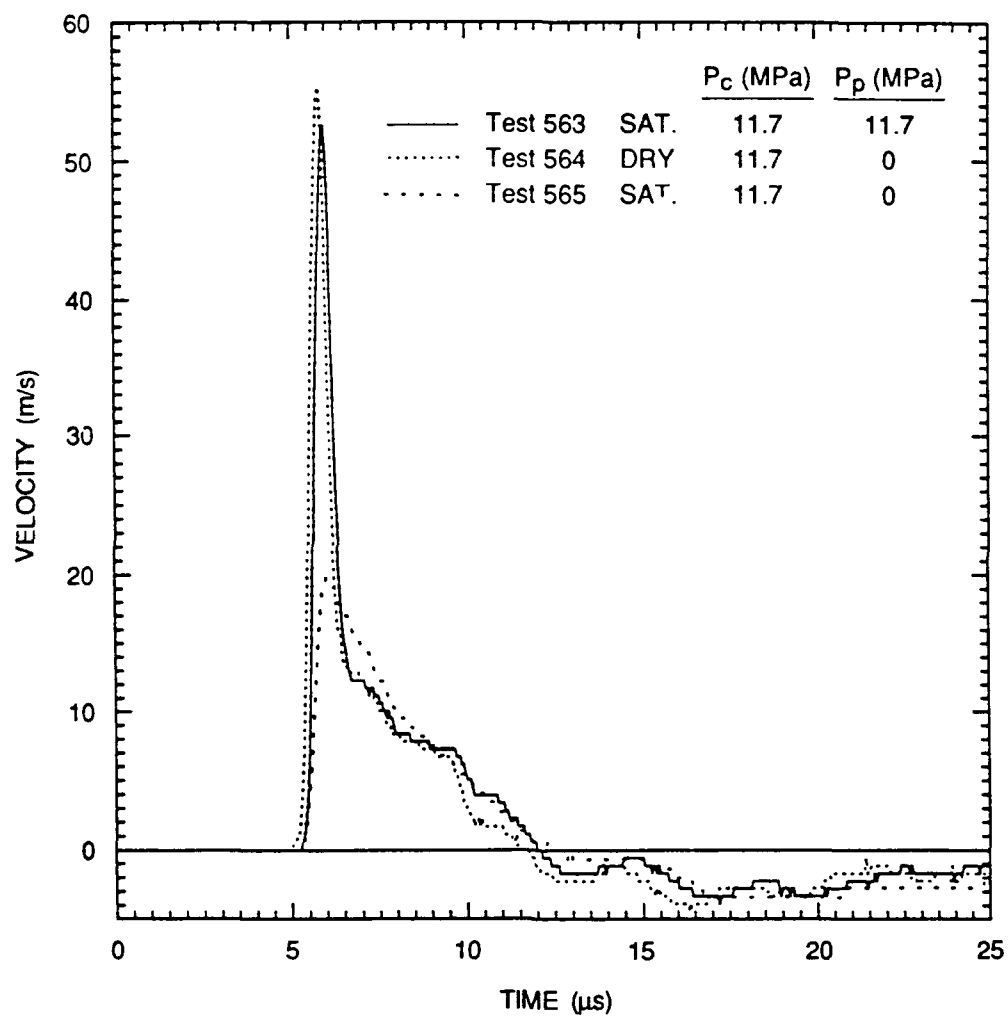23
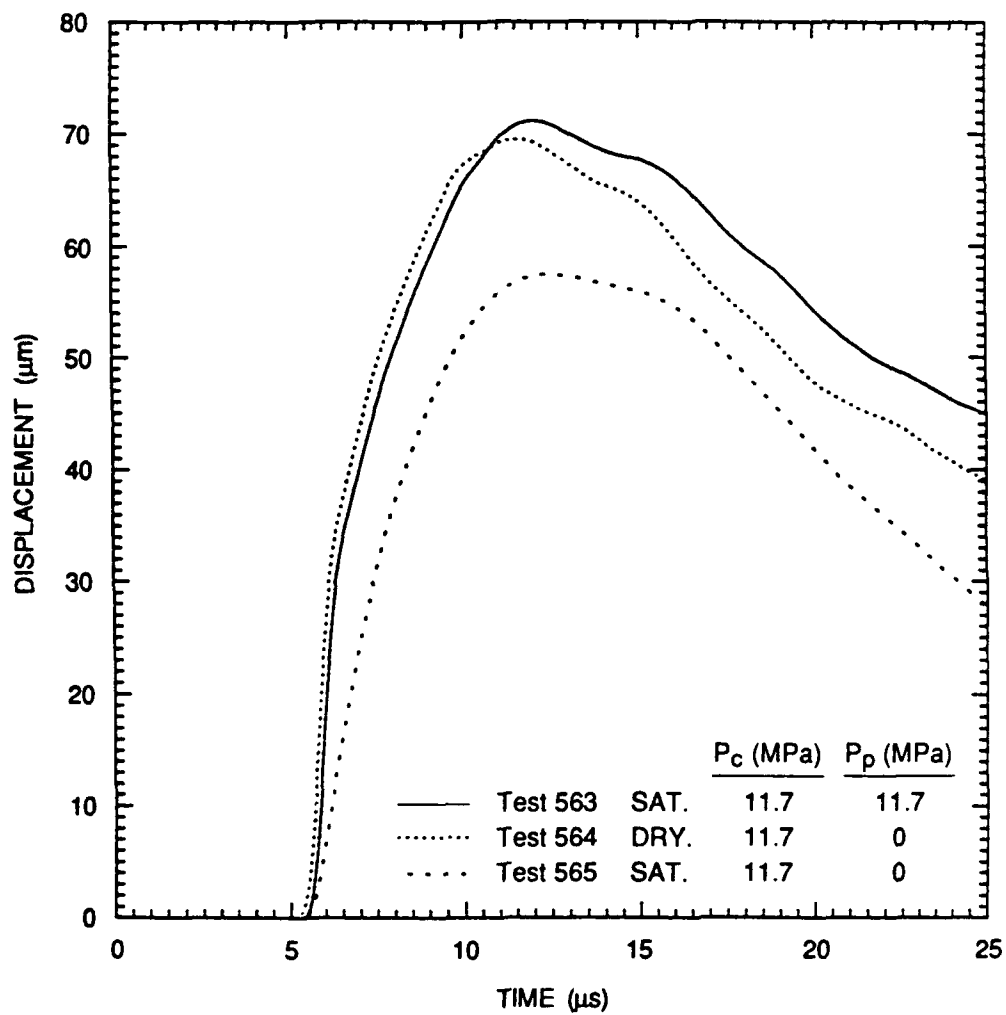
RA-6645-21

Figure 15. Displacement histories for three different pore conditions at 30-mm range in Sierra White granite.

24
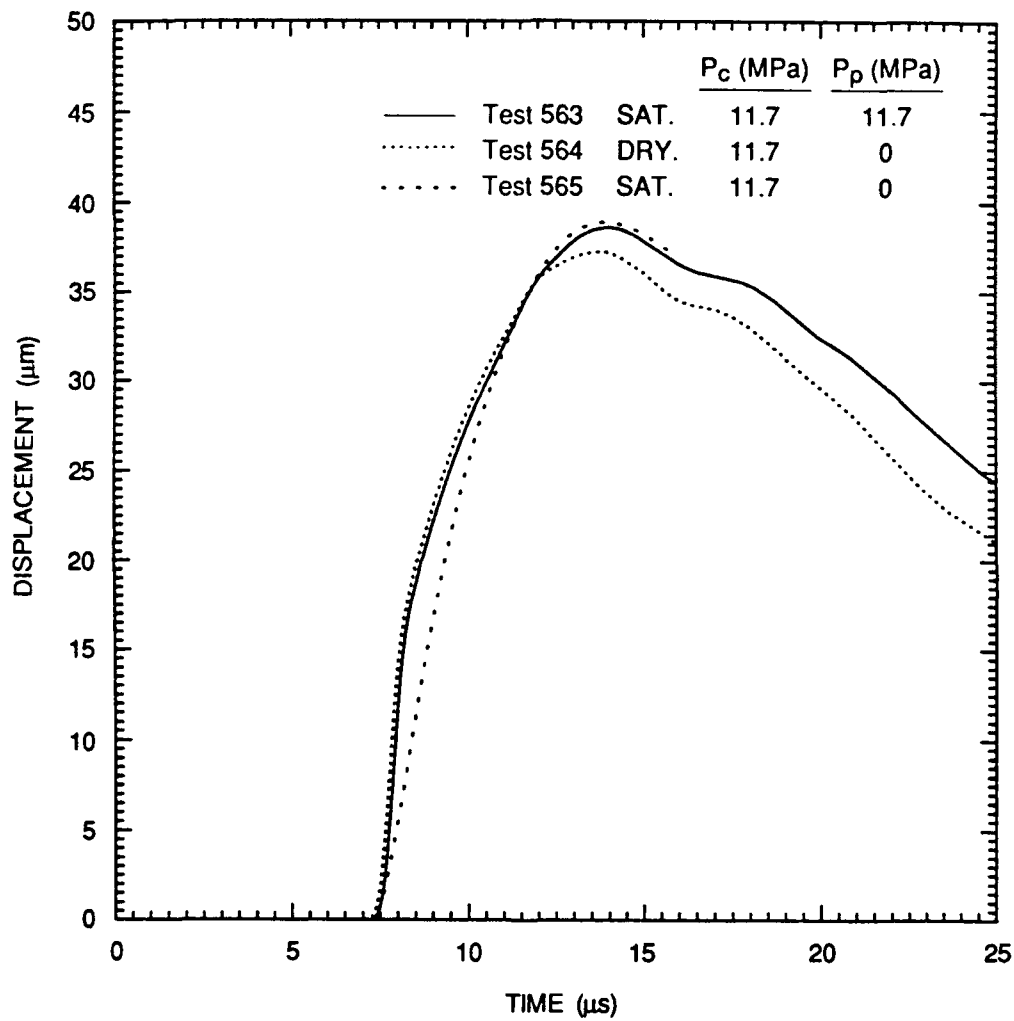
RA-6645-22

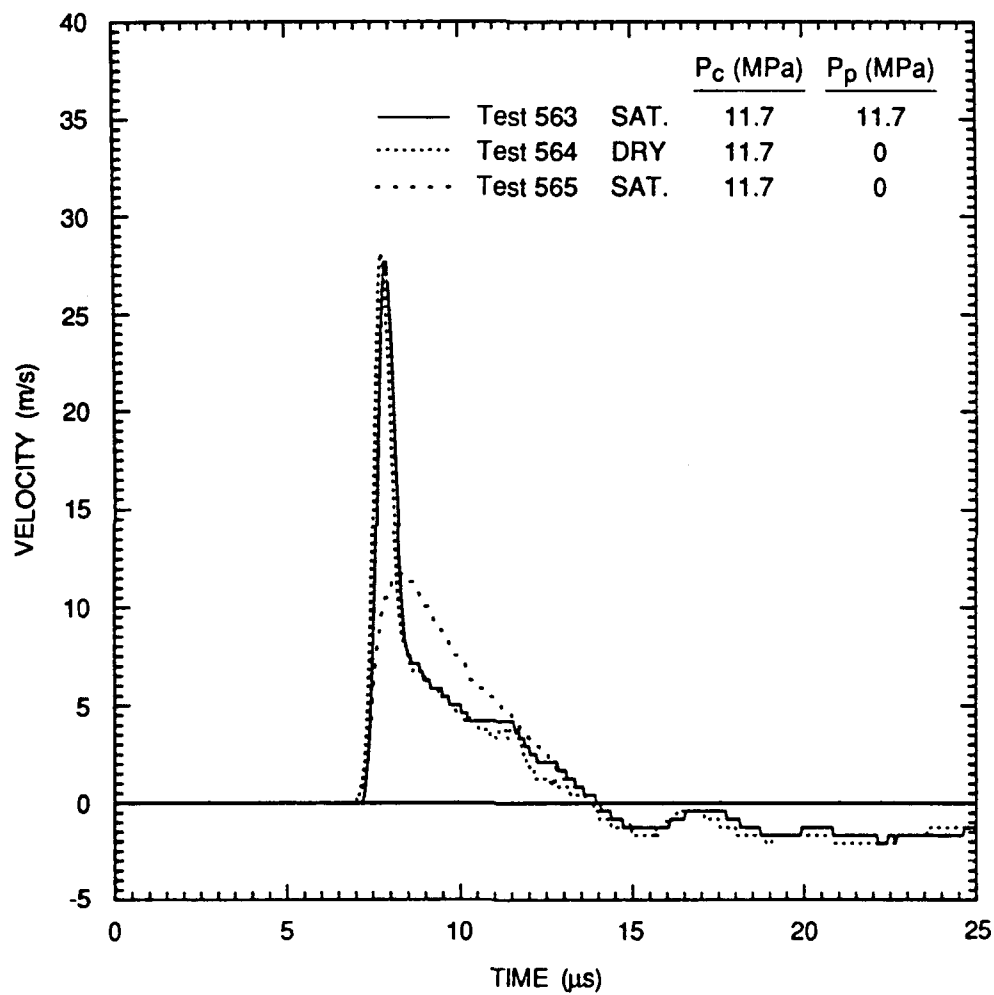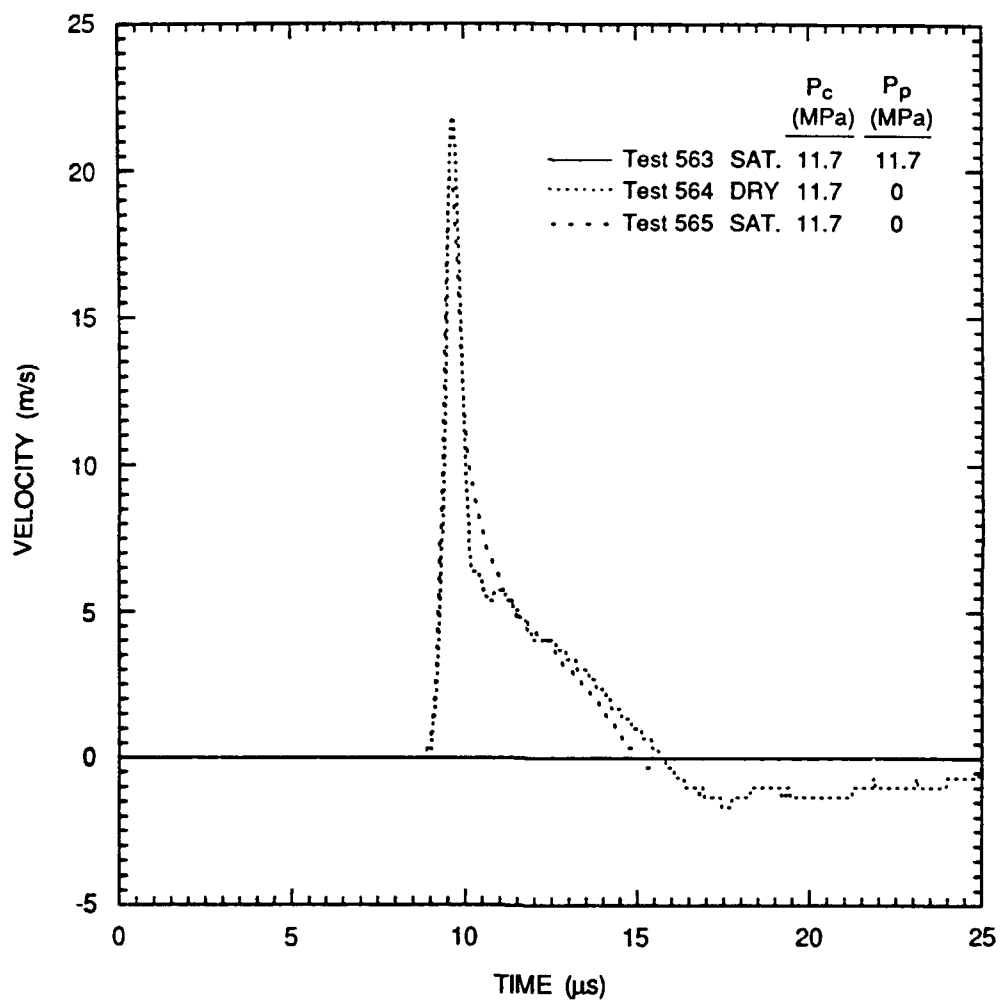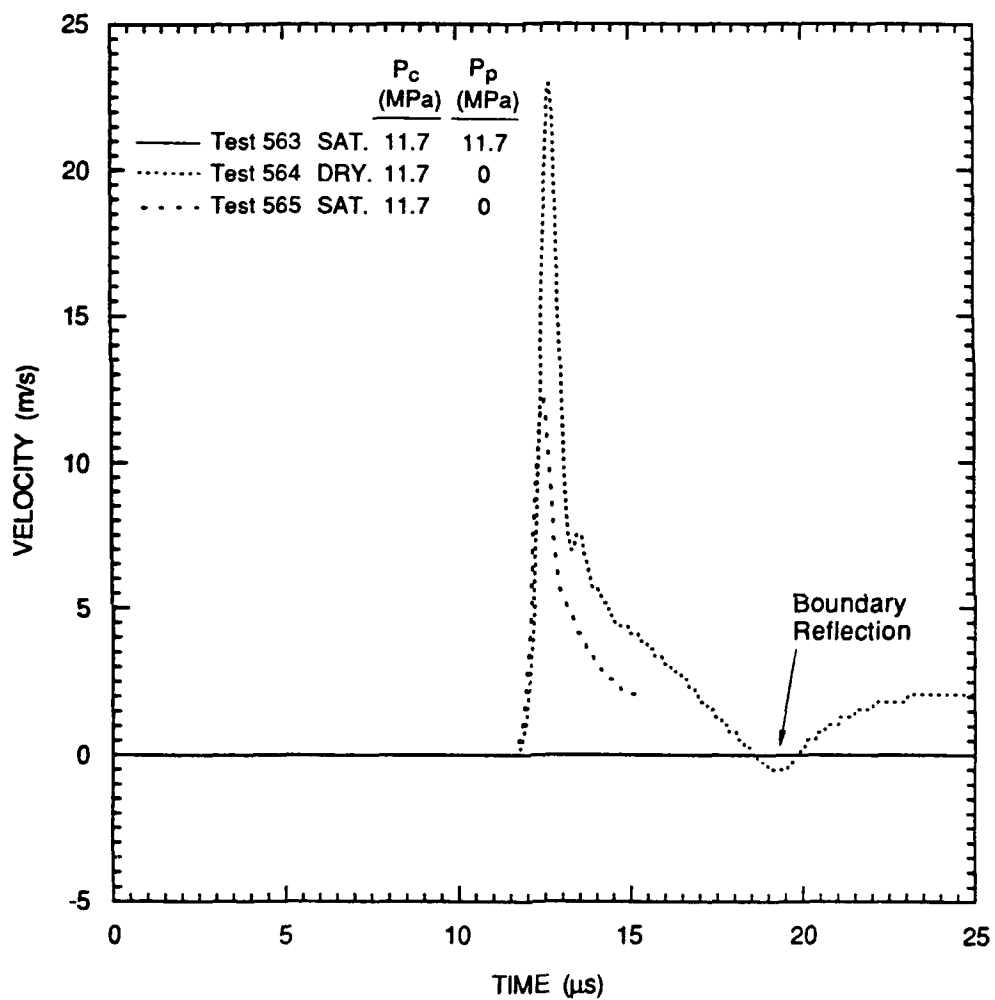Figure 16. Displacement histories for three different pore conditions at 40-mm range in Sierra White granite.

25
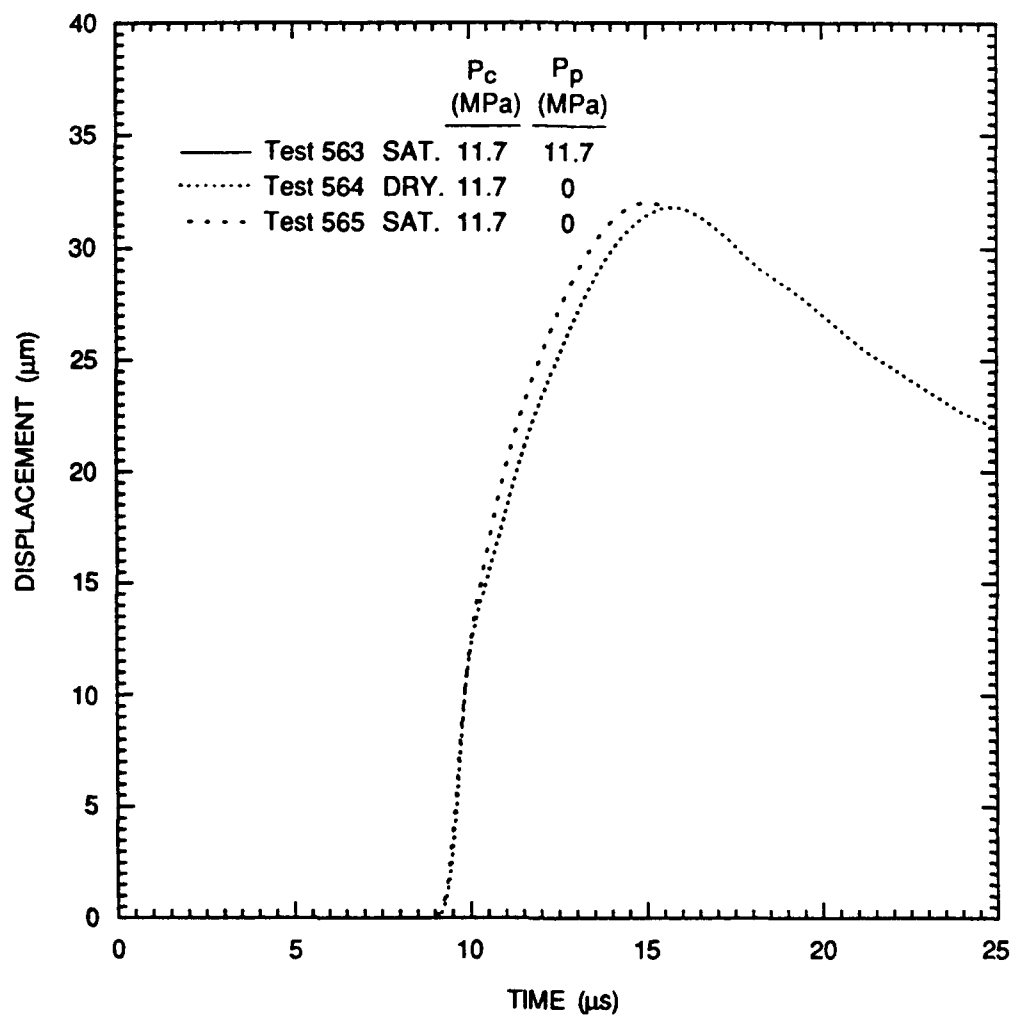
Figure 17. Displacement histories for different pore conditions at 50-mm range in Sierra White granite.

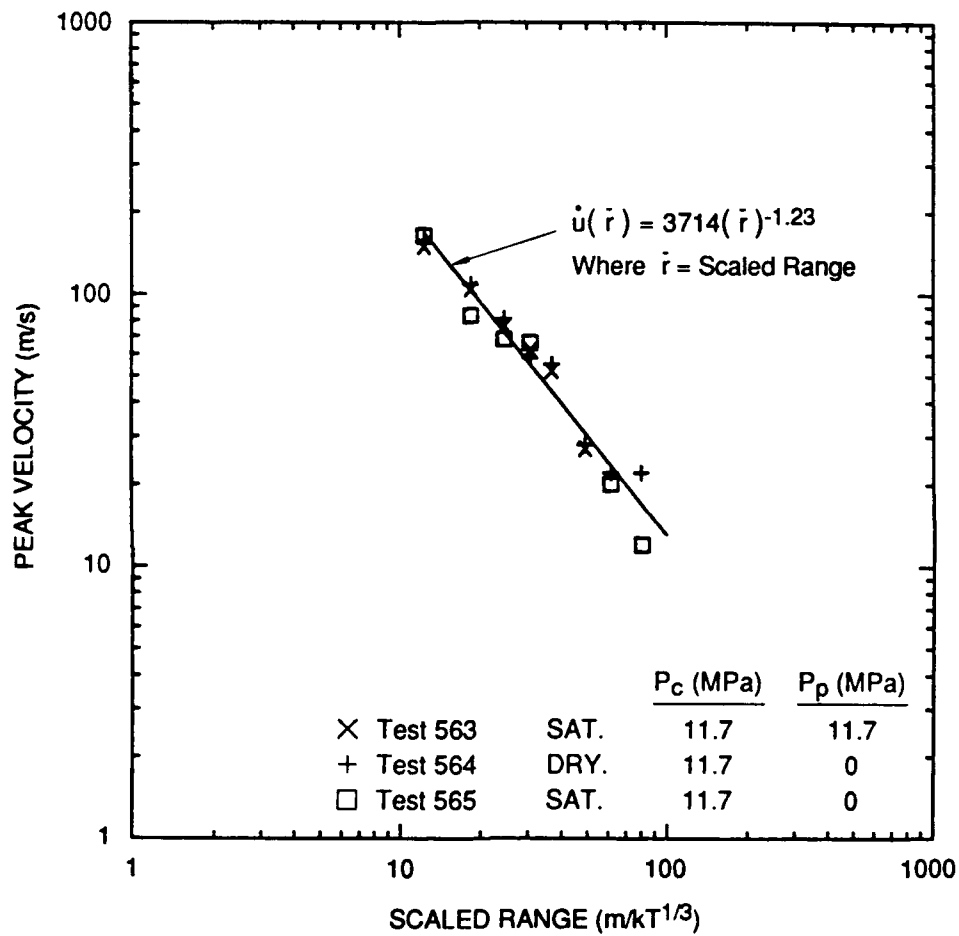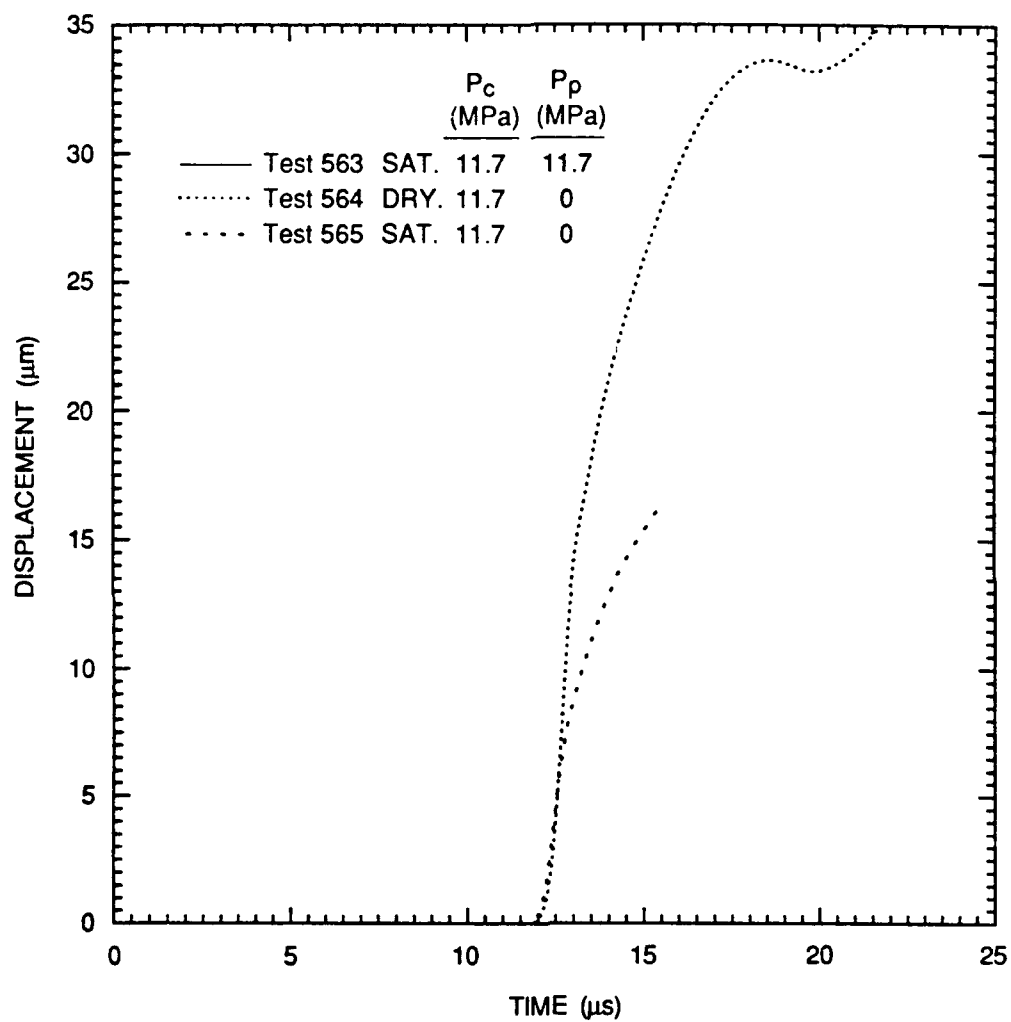Figure 18.   Displacement histories for different pore conditions at 65-mm range
in Sierra White granite.

RA-6645-24

27
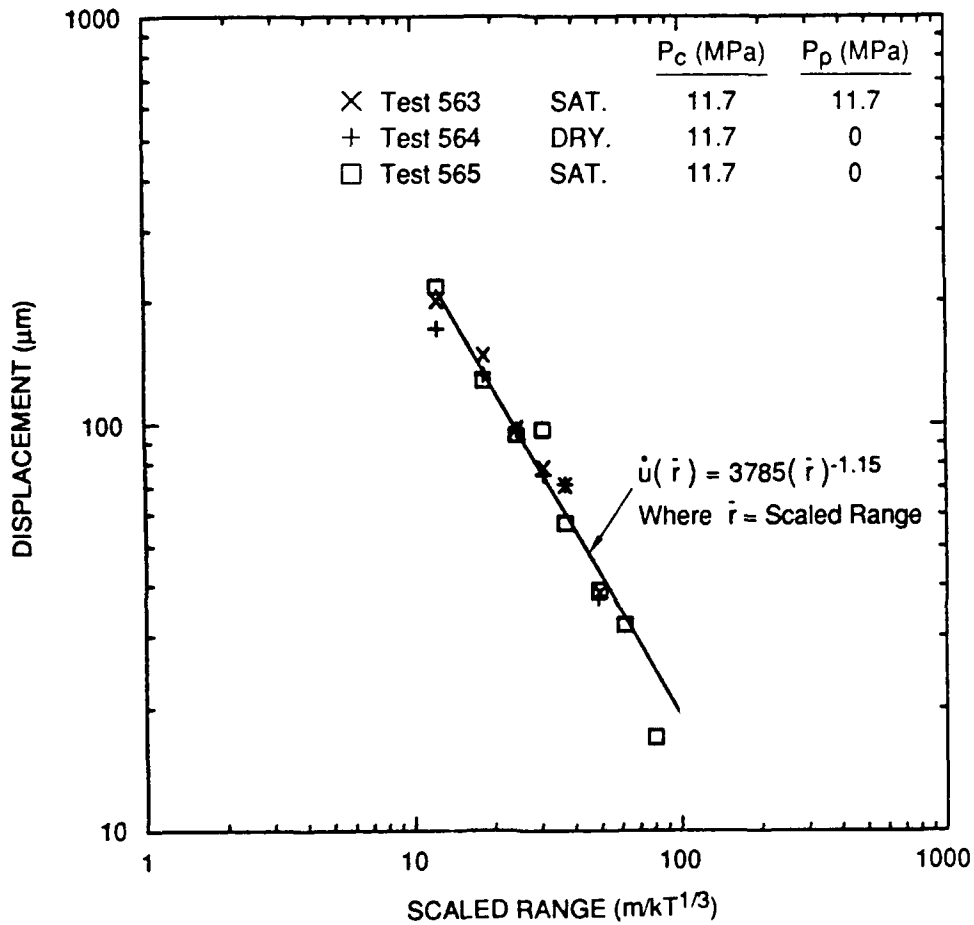
Figure 19. Attenuation of peak displacement for three different pore conditions in *Sierra White granite.*
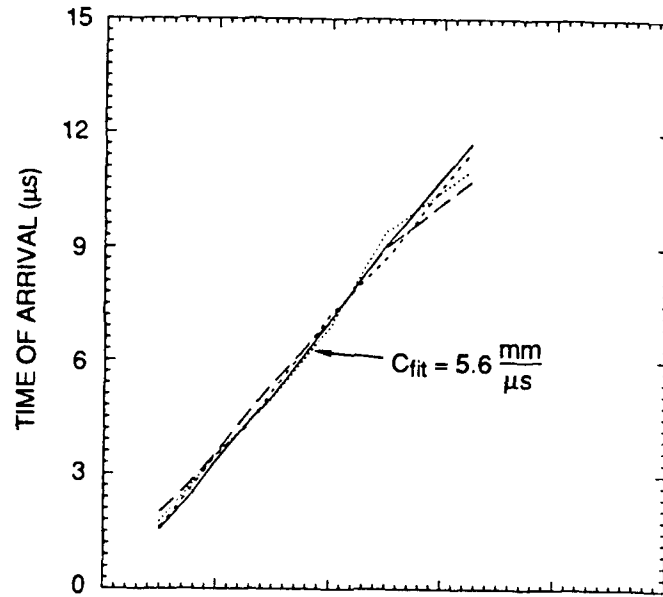
(a) Sierra White and Katahdin granite experiments.
(Tests 563, 571, 577, and 579)
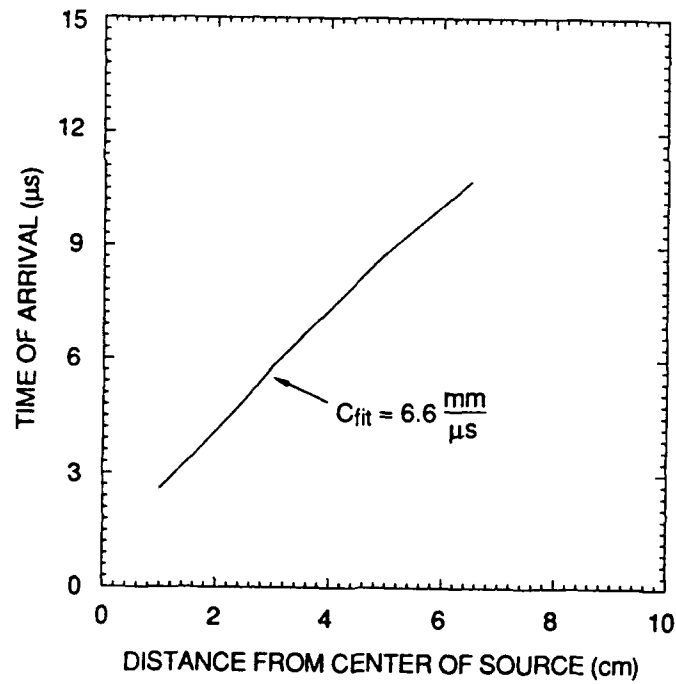
(b) Katahdin limestone experiment

RA-6645-76

Figure 20. Time of arrival as a function of distance from center
of source for granite and limestone specimens.

29
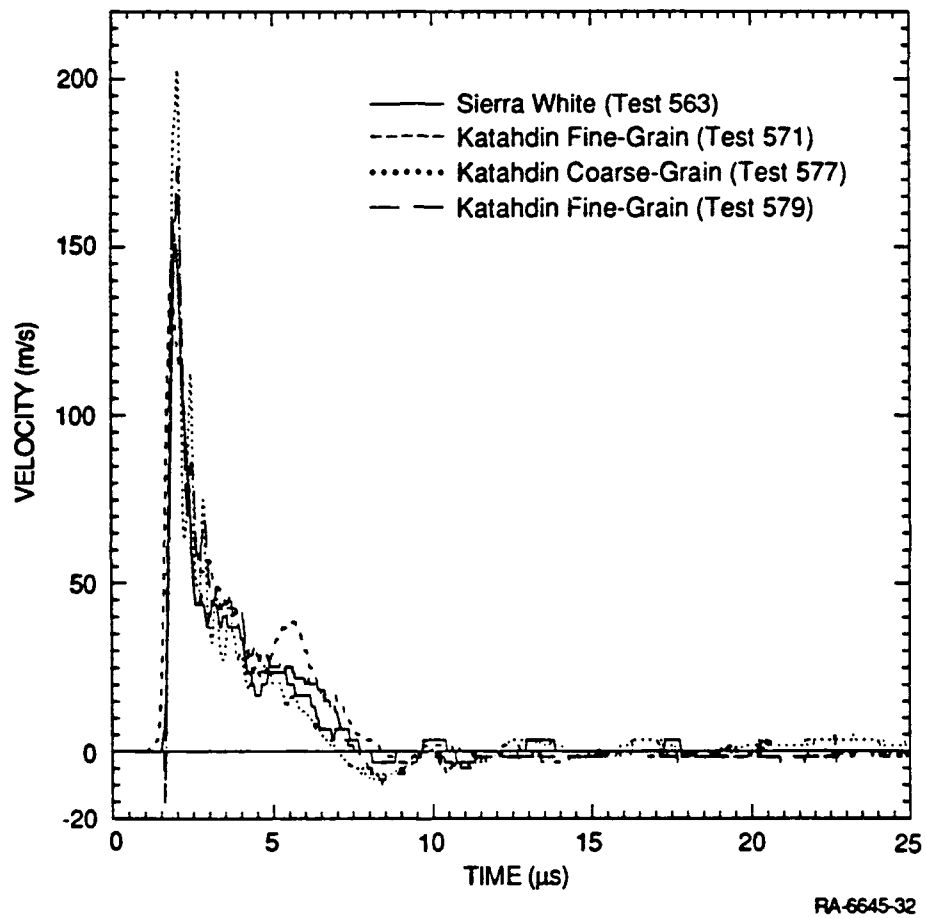
Figure 21.   Particle velocity histories measured at 10-mm range in different types
of granite.

30
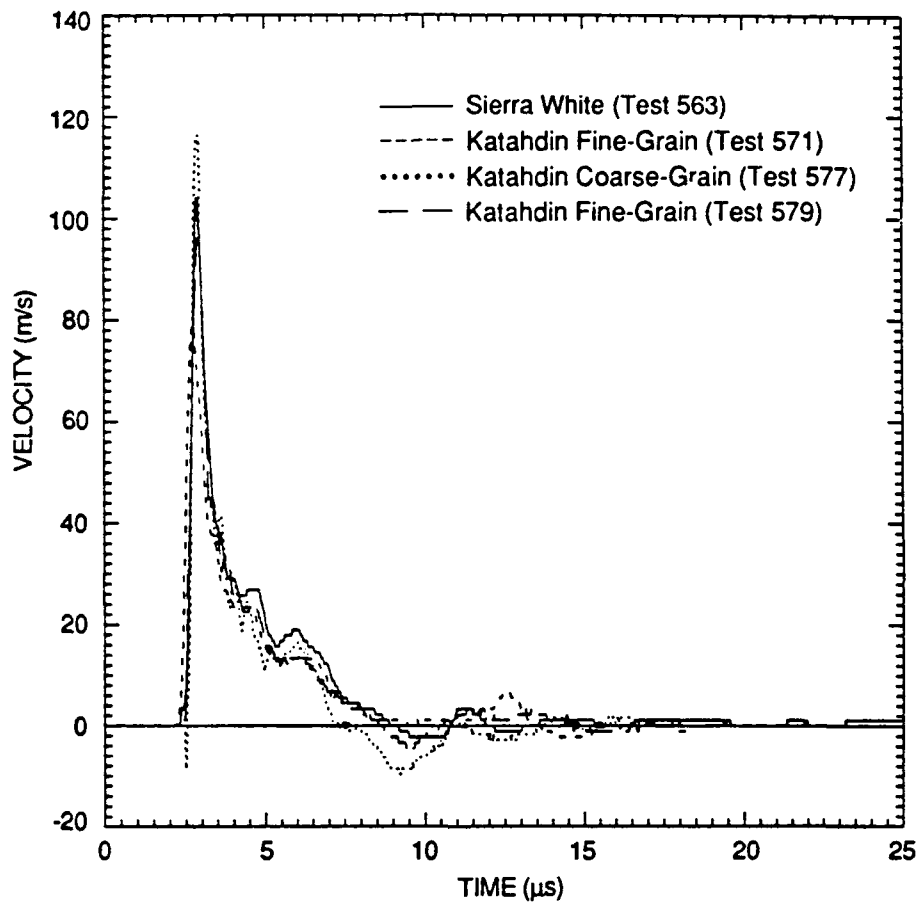
Figure 22. Particle velocity histories measured at 15-mm range in different types of granite.

31
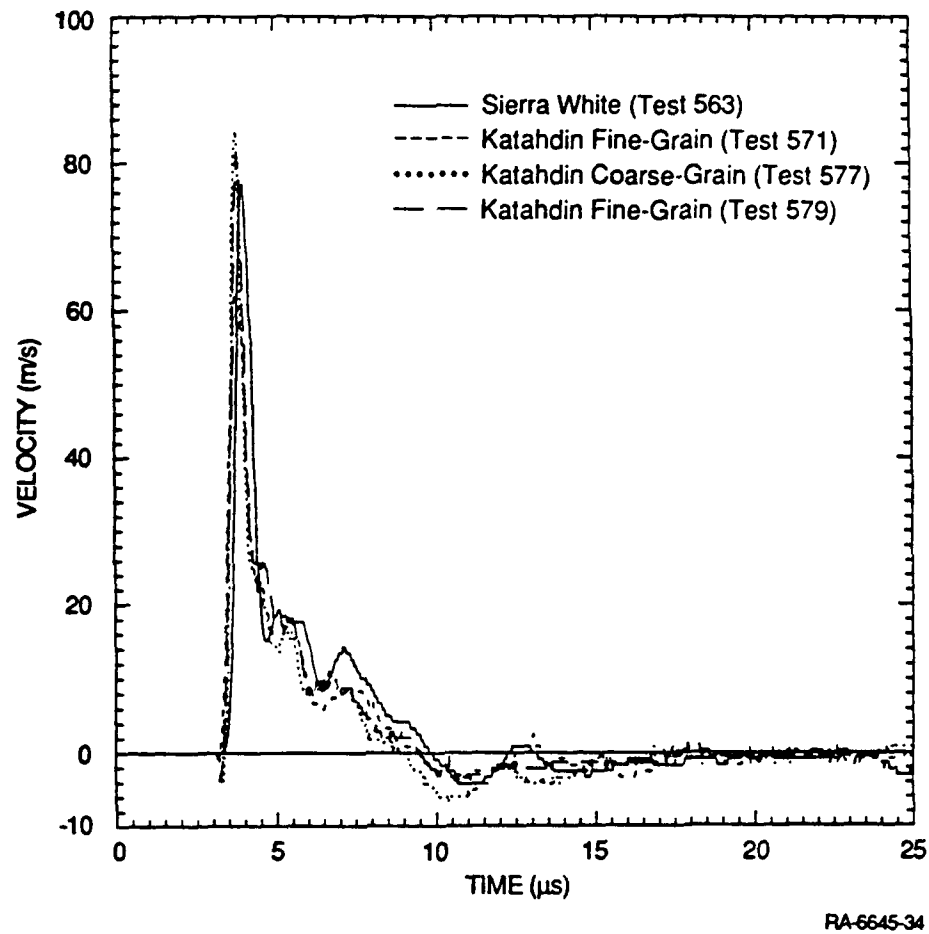
RA-6645-34

Figure 23.   Particle velocity histories measured at 20-mm range in different types of granite.

32
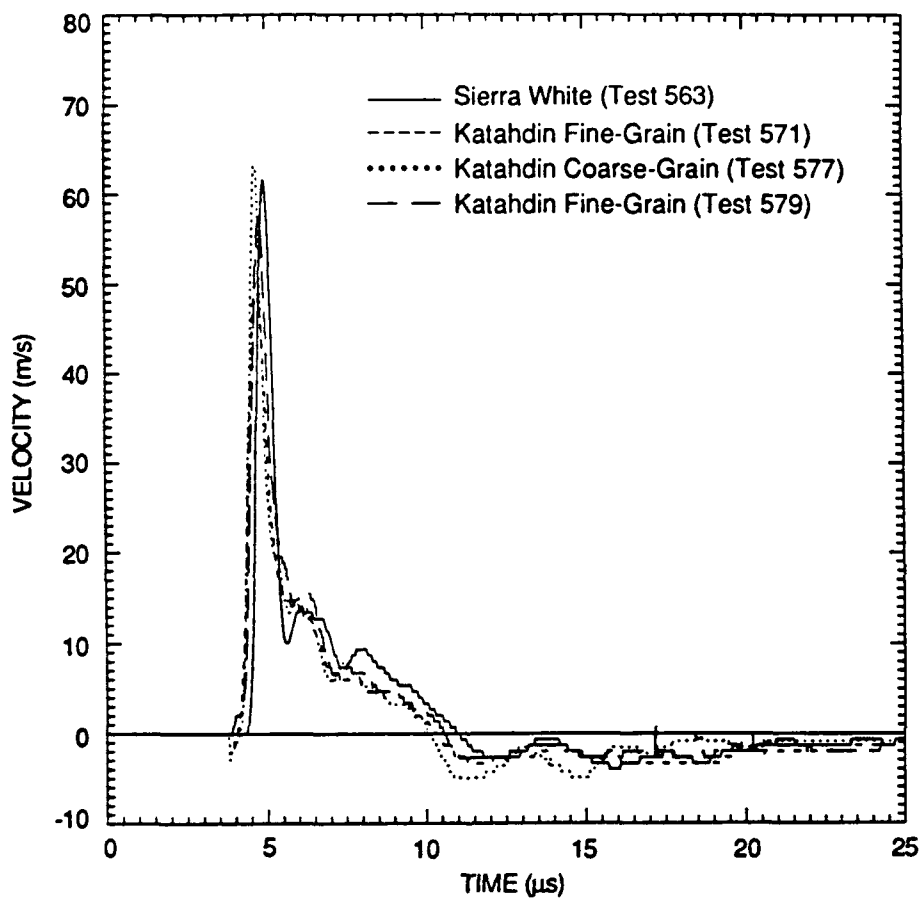
RA-6645-35

Figure 24.   Particle velocity histories measured at 25-mm range in different types of granite.
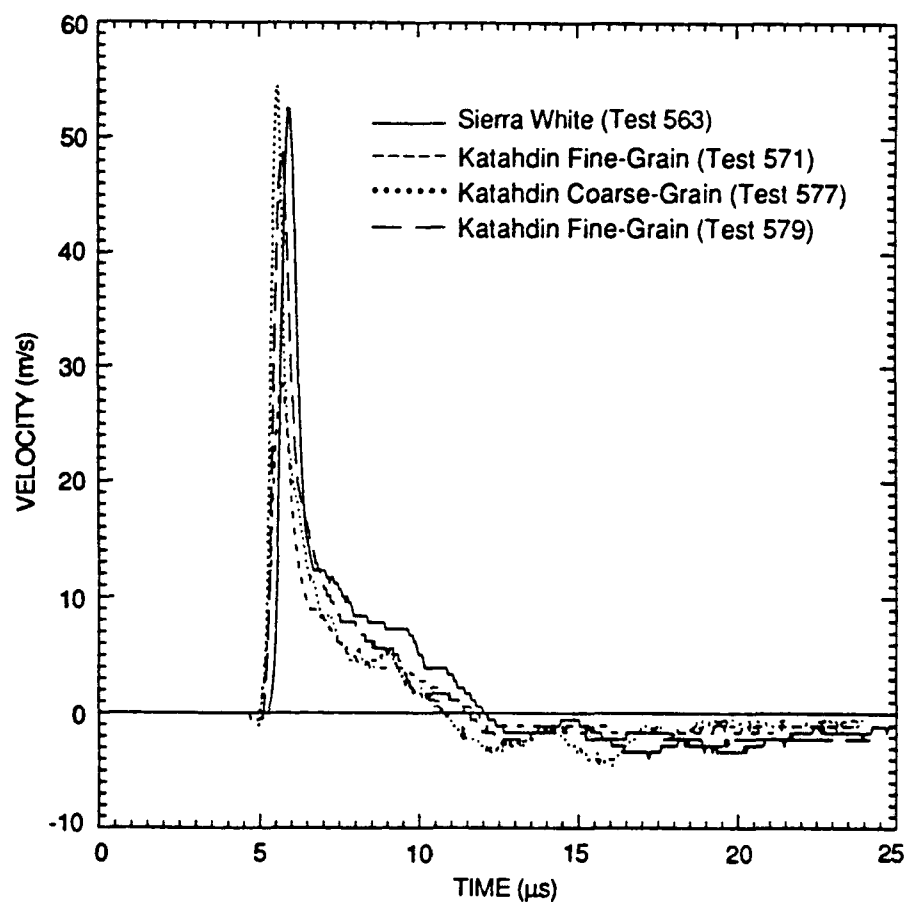
Figure 25. Particle velocity histories measured at 30-mm range in different types of granite.

34

RA-6645-37
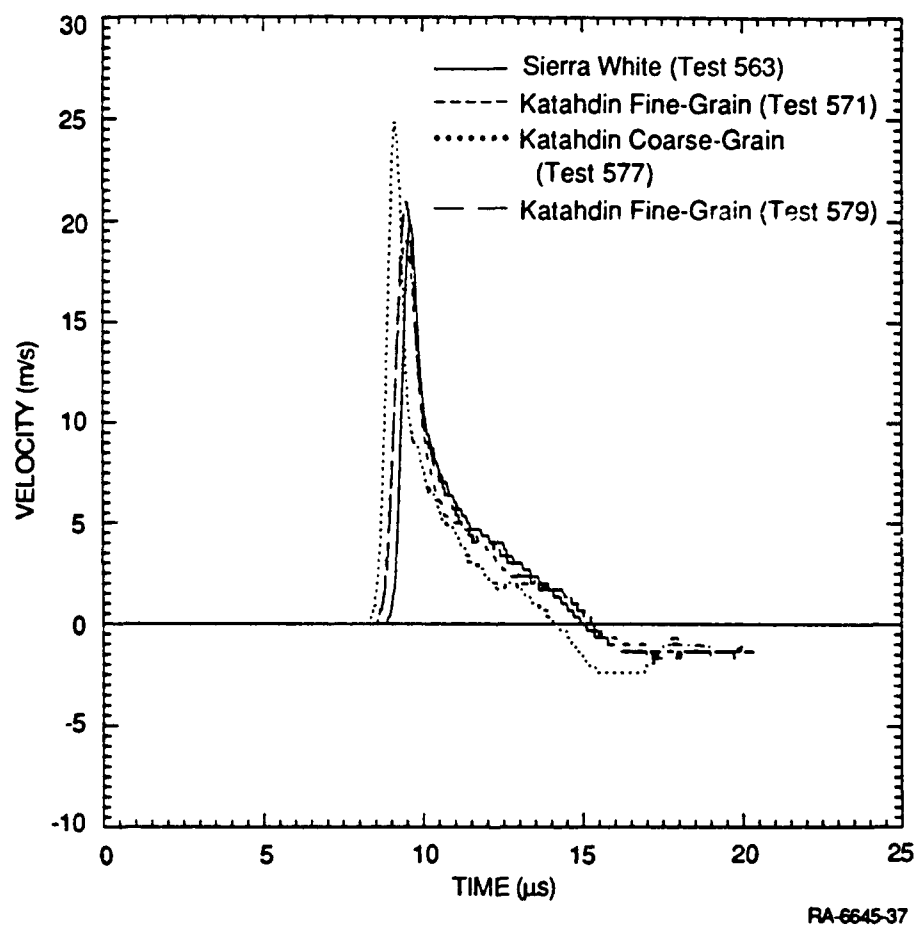
Figure 26. Particle velocity histories measured at 50-mm range in different types of granite.

35
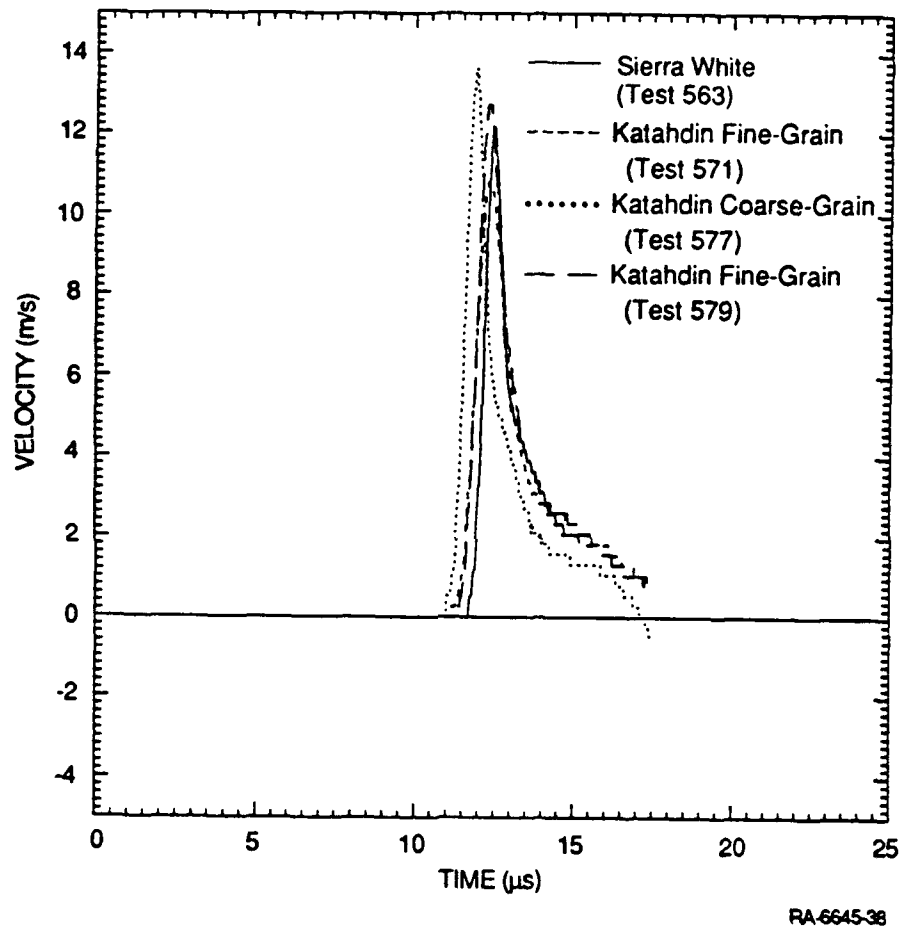
Figure 27. Particle velocity histories measured at 65-mm range in different types of granite.
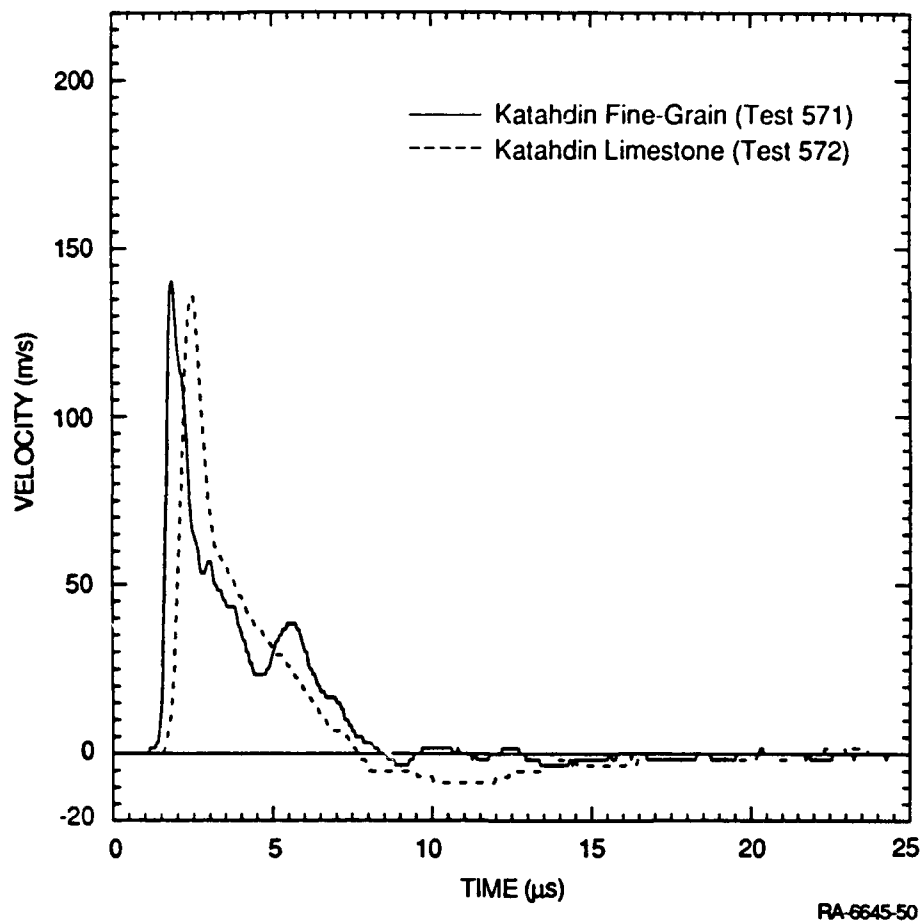
Figure 28.   Comparison of velocity histories at 10-mm range for Katahdin fine-grain granite and Katahdin limestone.

37
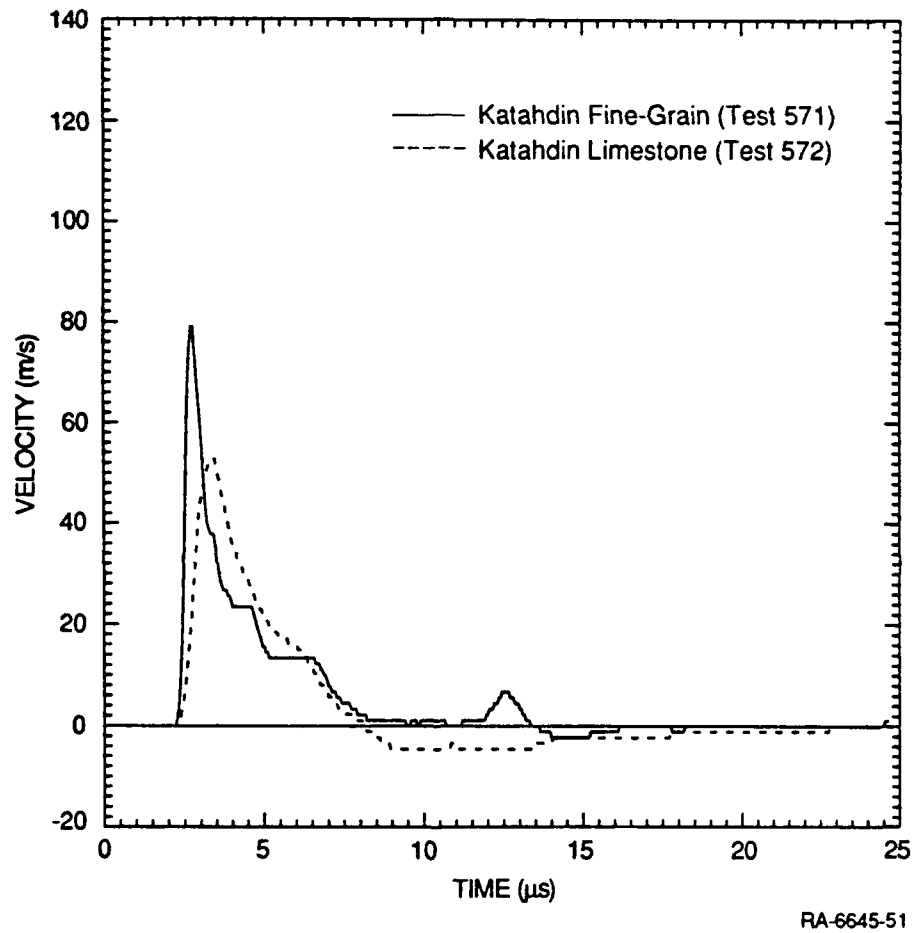
RA-6645-51

Figure 29.   Comparison of velocity histories at 15-mm range for Katahdin fine-grain granite and Katahdin limestone.

38
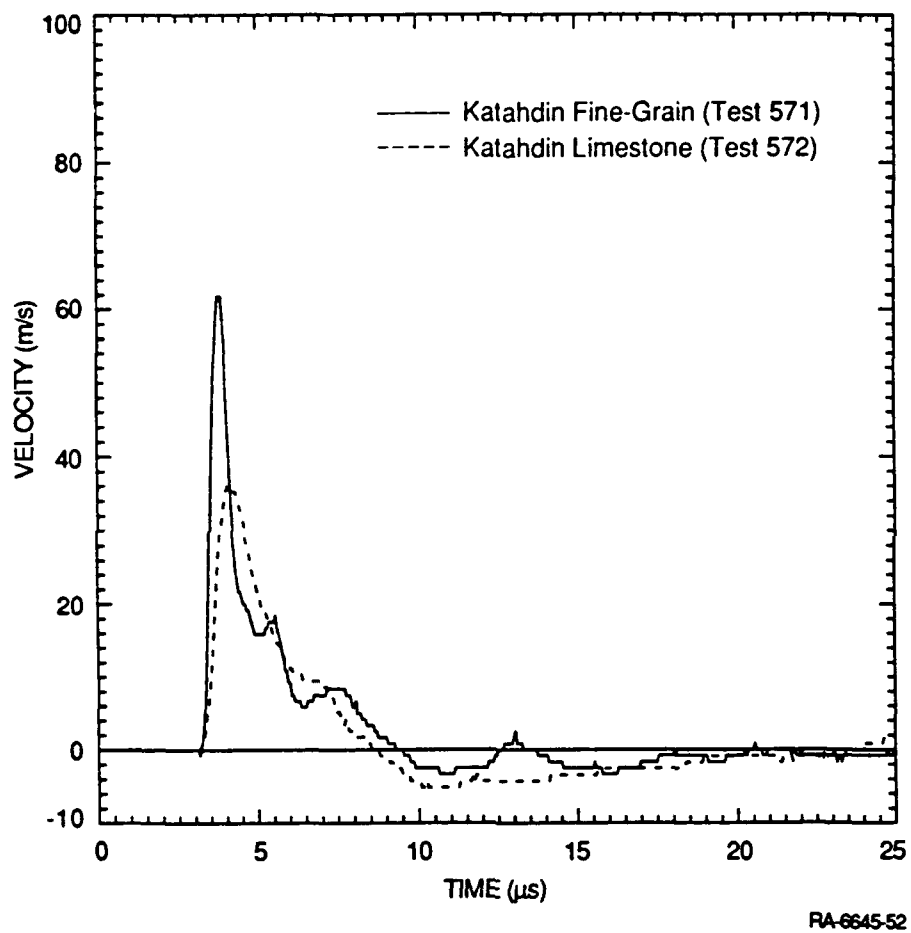
Figure 30. Comparison of velocity histories at 20-mm range for Katahdin fine-grain granite and Katahdin limestone.
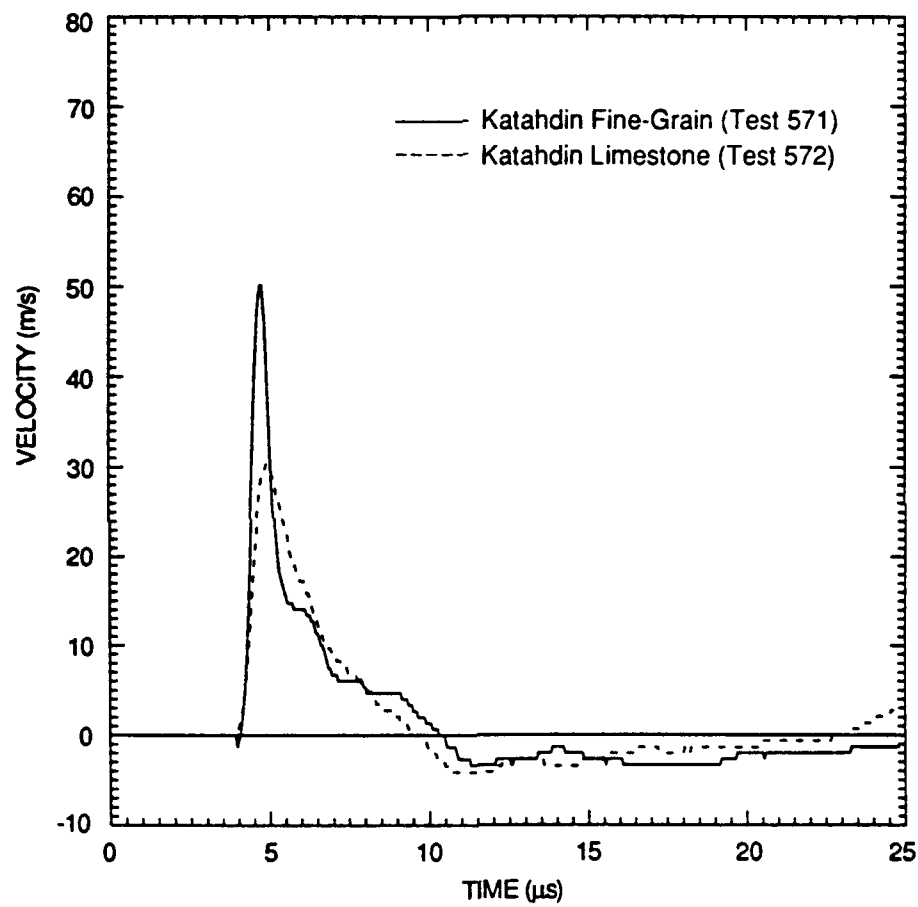
RA-6645-53

Figure 31. Comparison of velocity histories at 25-mm range for Katahdin fine-grain granite and Katahdin limestone.

40
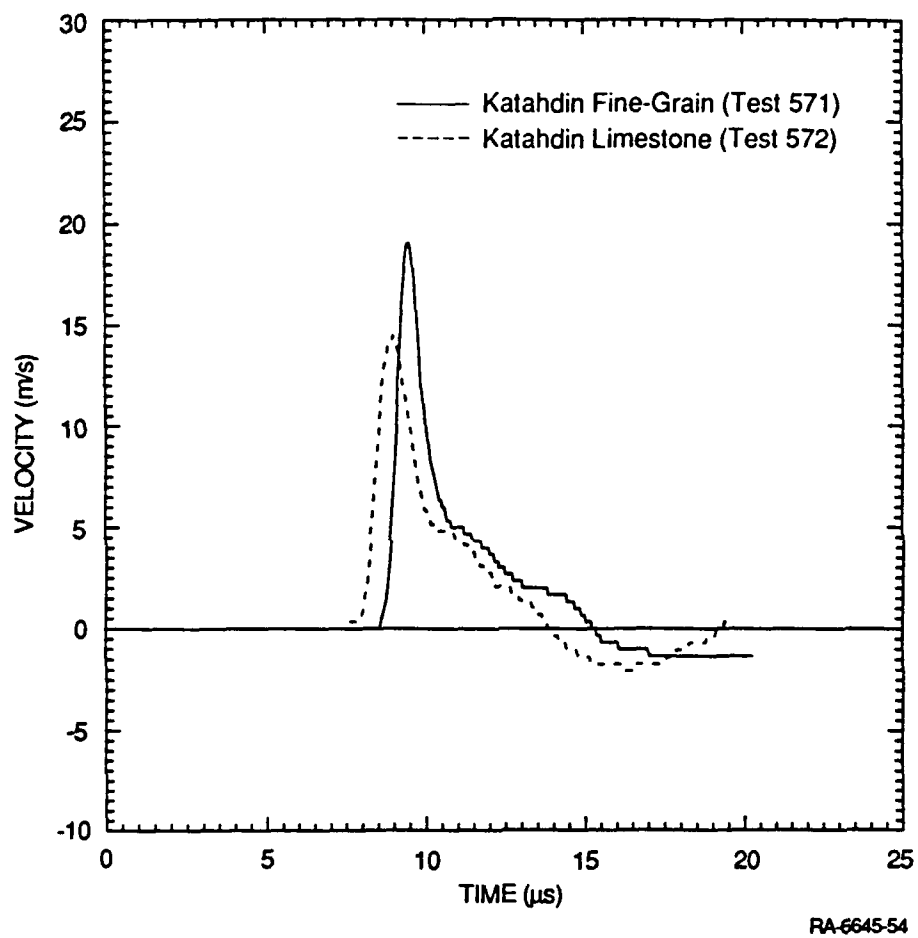
Figure 32. Comparison of velocity histories at 50-mm range for Katahdin fine-grain granite and Katahdin limestone.
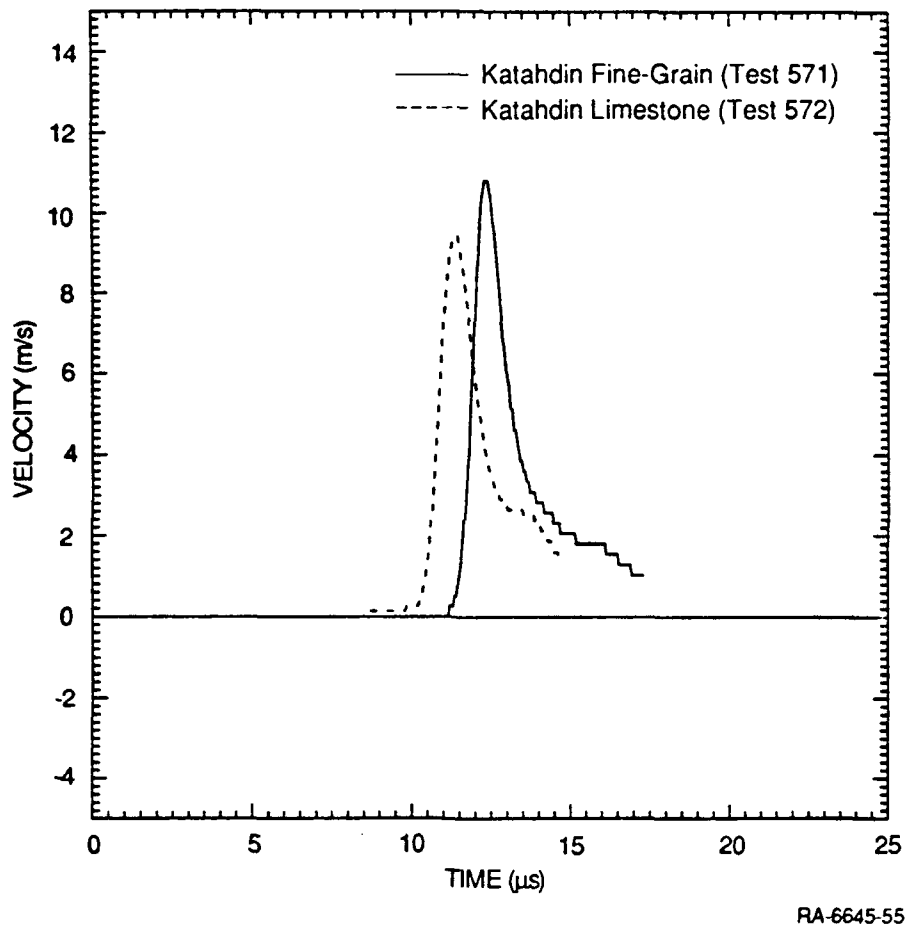
RA-6645-55

Figure 33.   Comparison of velocity histories at 65-mm range for Katahdin fine-grain
granite and Katahdin limestone.

42
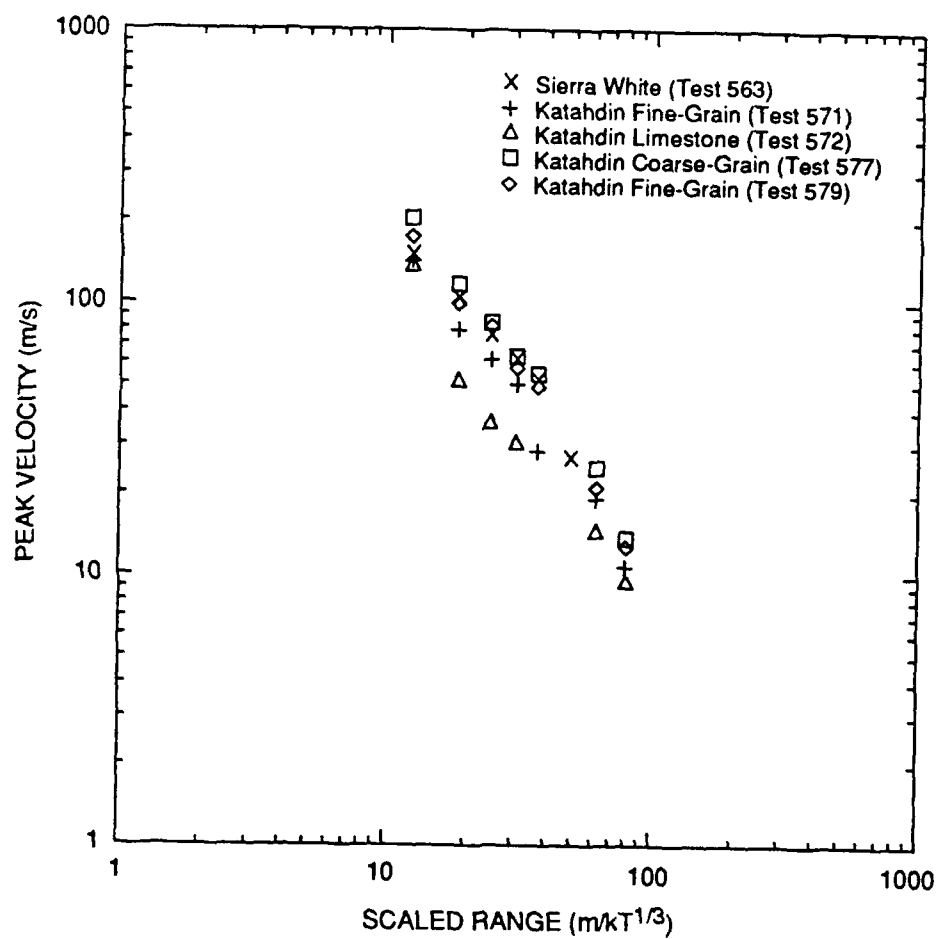
Figure 34. Attenuation of peak particle velocity in Sierra White granite and
Katahdin granites and limestone.
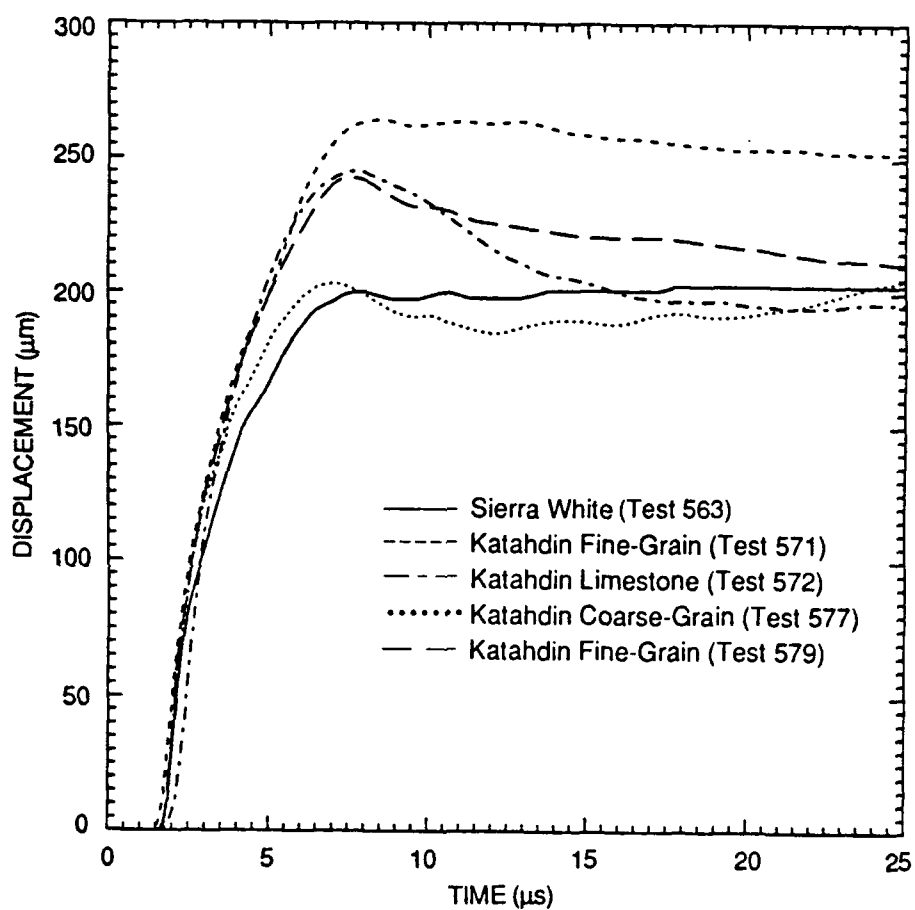
RA-6645-43

Figure 35. Displacement histories measured at 10-mm range in different types of granite and Katahdin limestone.

44
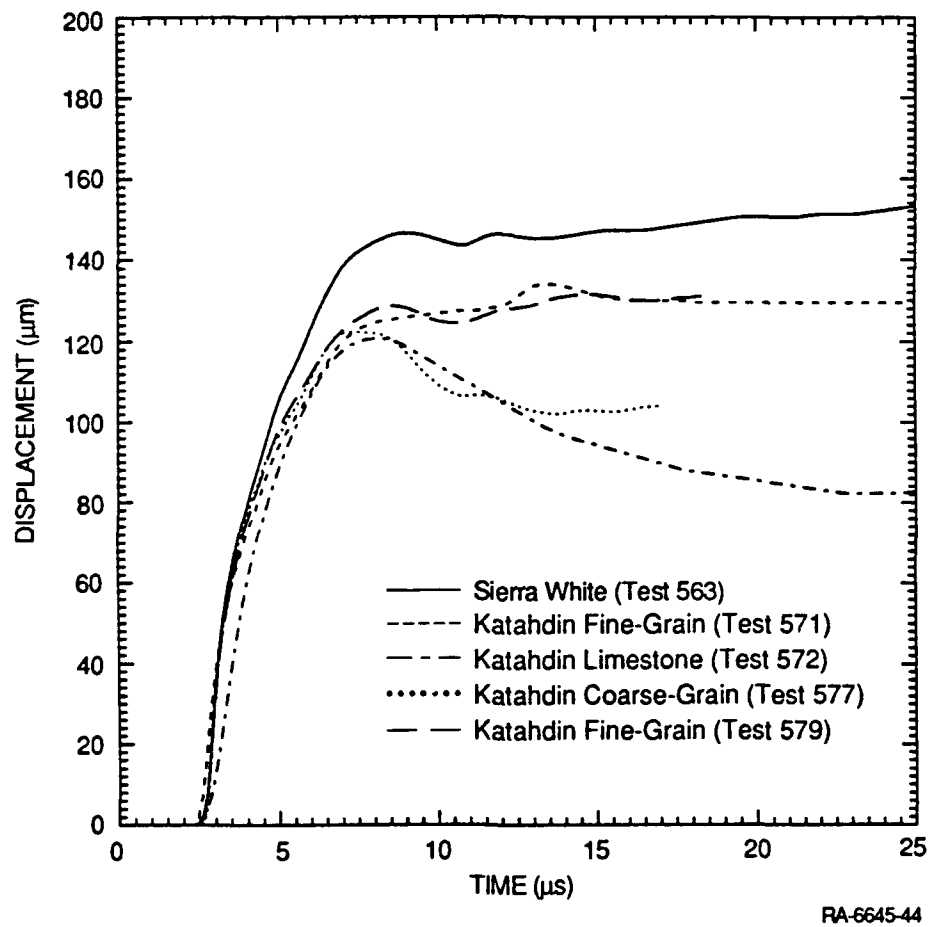
Figure 36. Displacement histories measured at 15-mm range in different types of granite and Katahdin limestone.
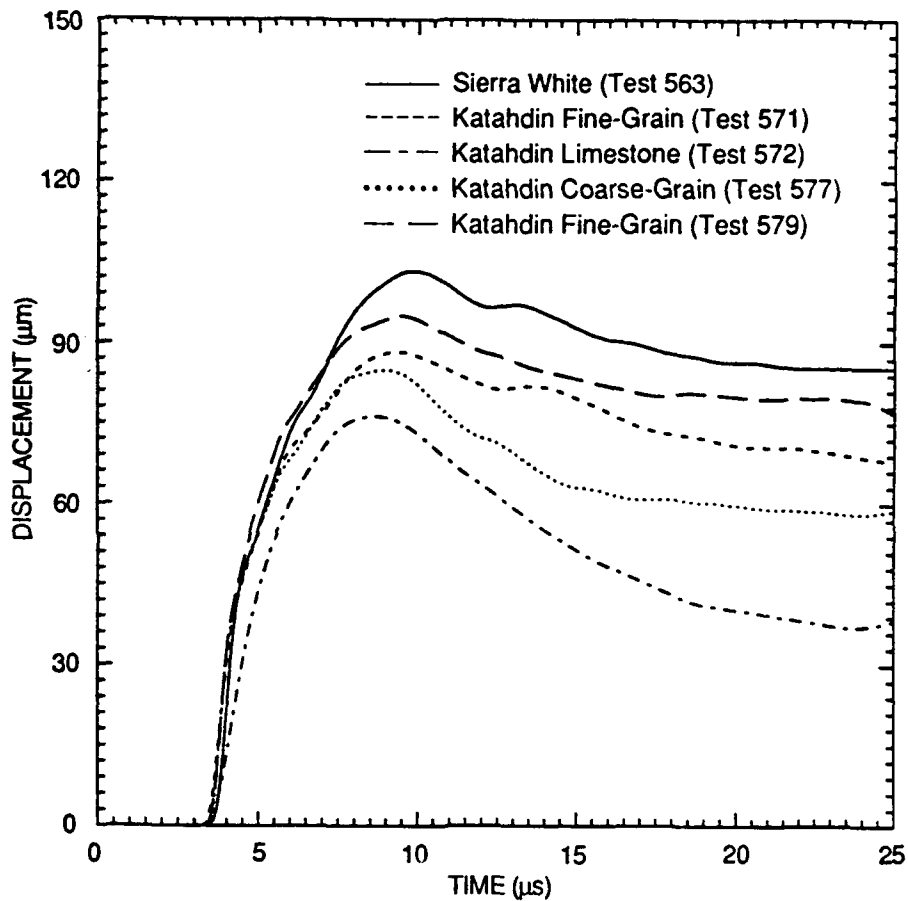
Figure 37. Displacement histories measured at 20-mm range in different types of granite and Katahdin limestone.
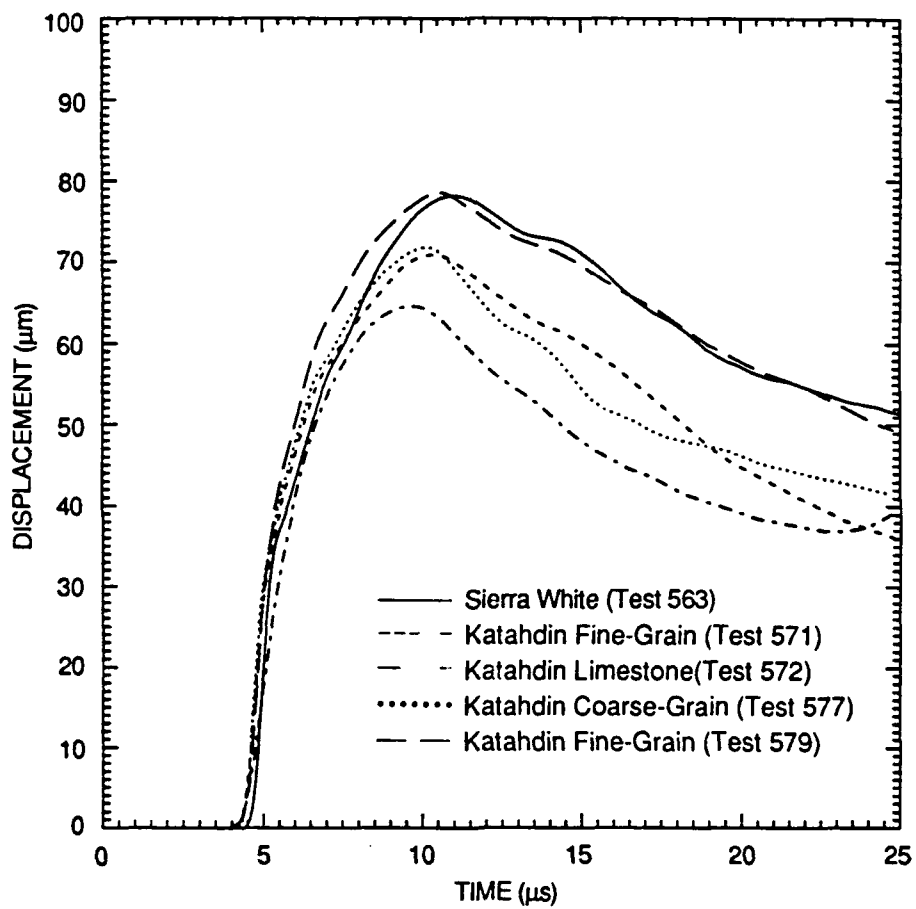
46

Figure 38. Displacement histories measured at 25-mm range in different types of granite and Katahdin limestone.
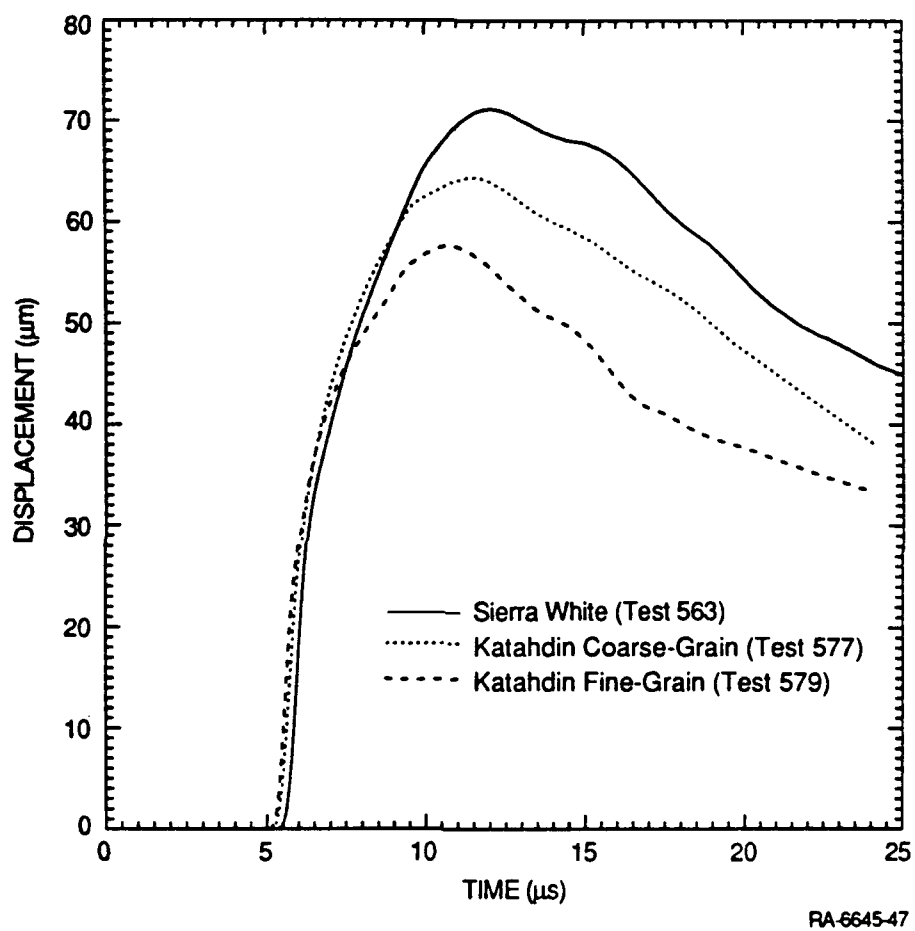
Figure 39. Displacement histories at 30-mm range in different types of granite.
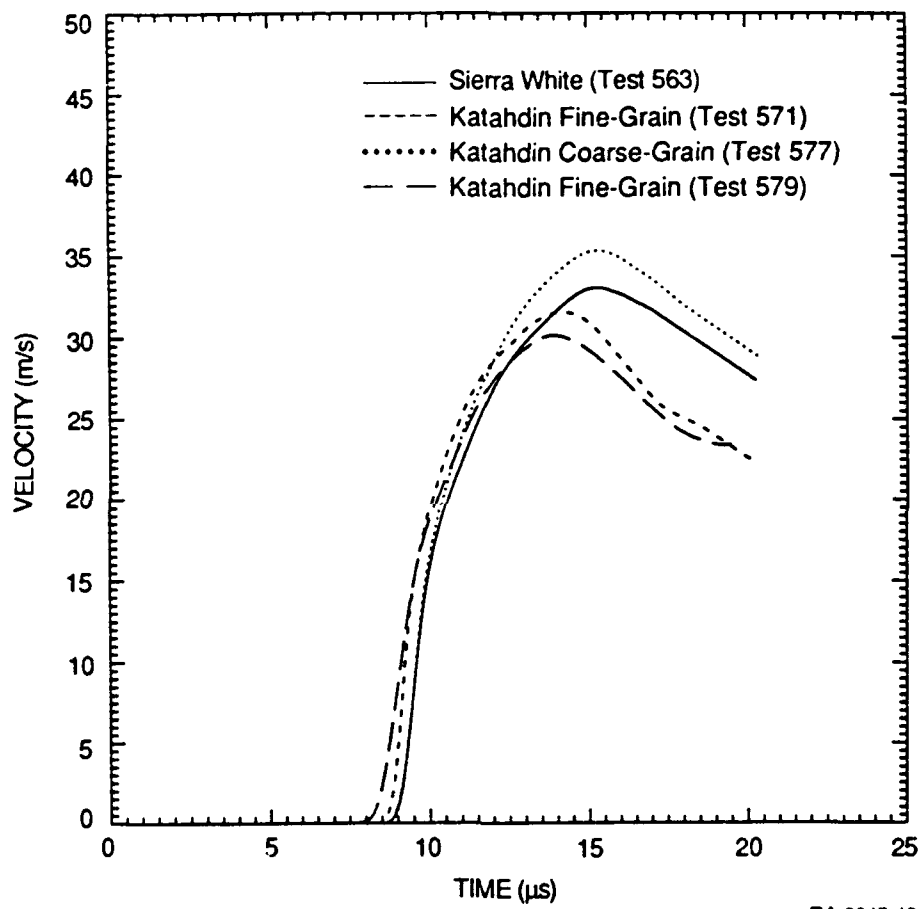
48

Figure 40. Displacement histories at 50-mm range in different types of granite.
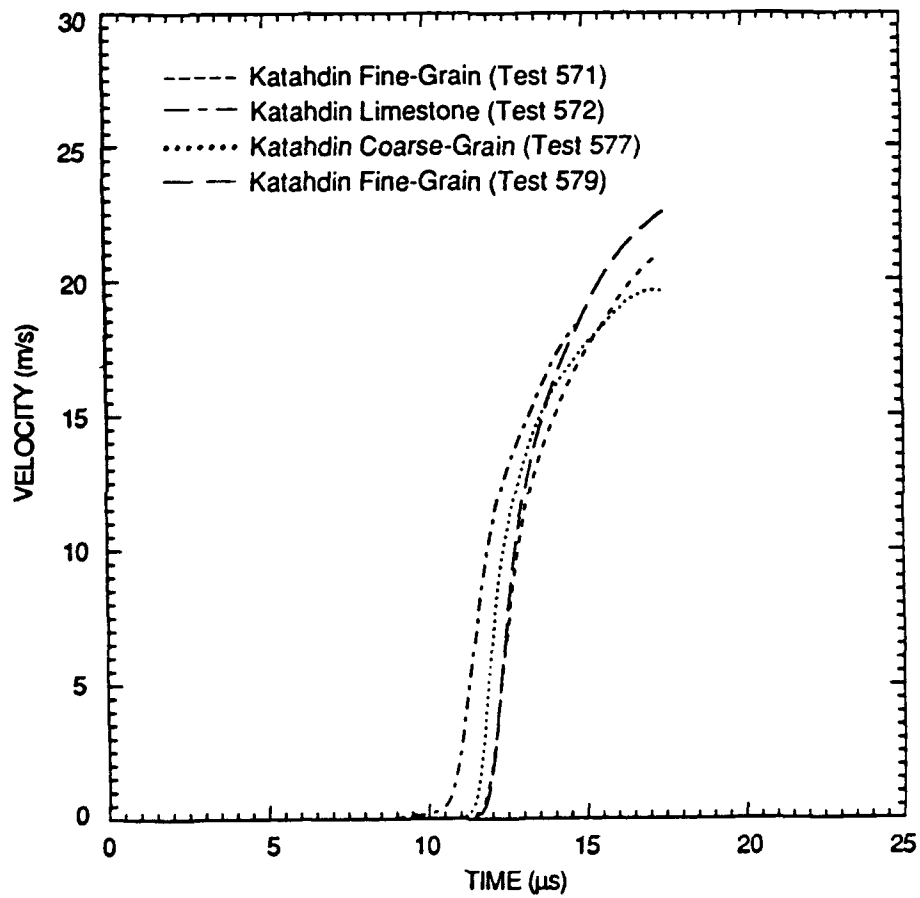
Figure 41. Displacement histories at 65-mm range in Katahdin granites and limestone.
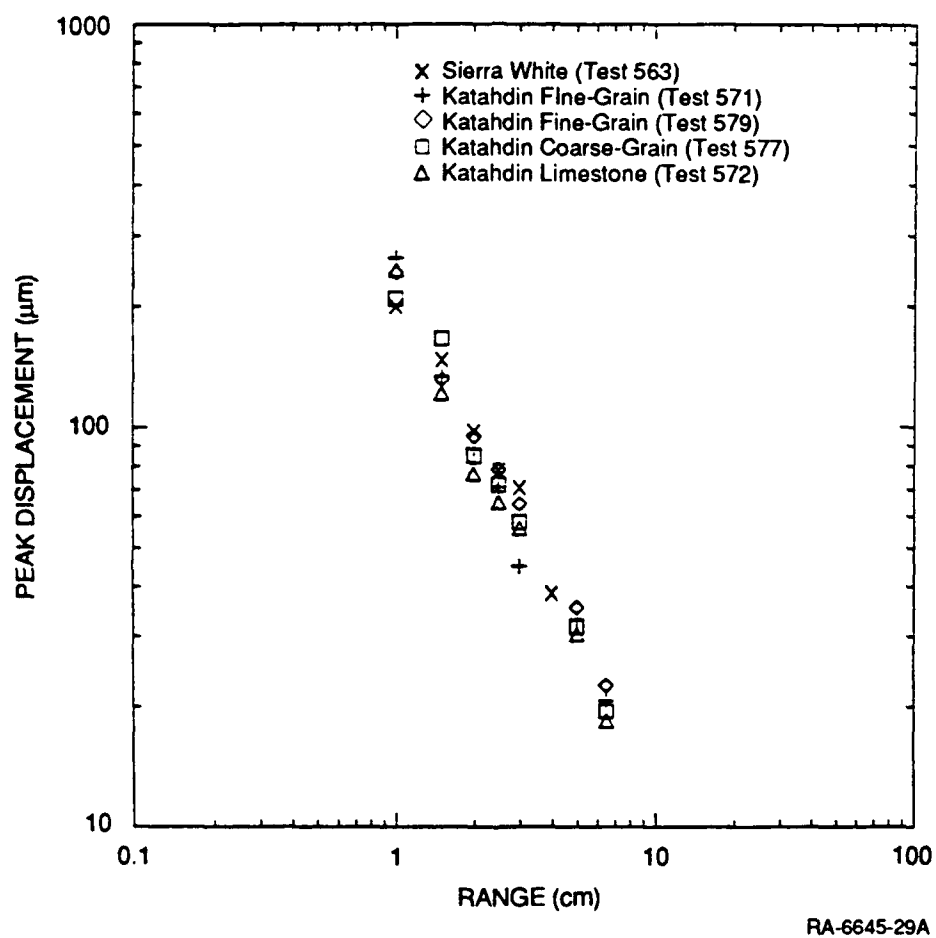
Figure 42. Attenuation of peak displacement with range in Sierra White granite and Katahdin granites and limestone.

RA-6645-29A

51
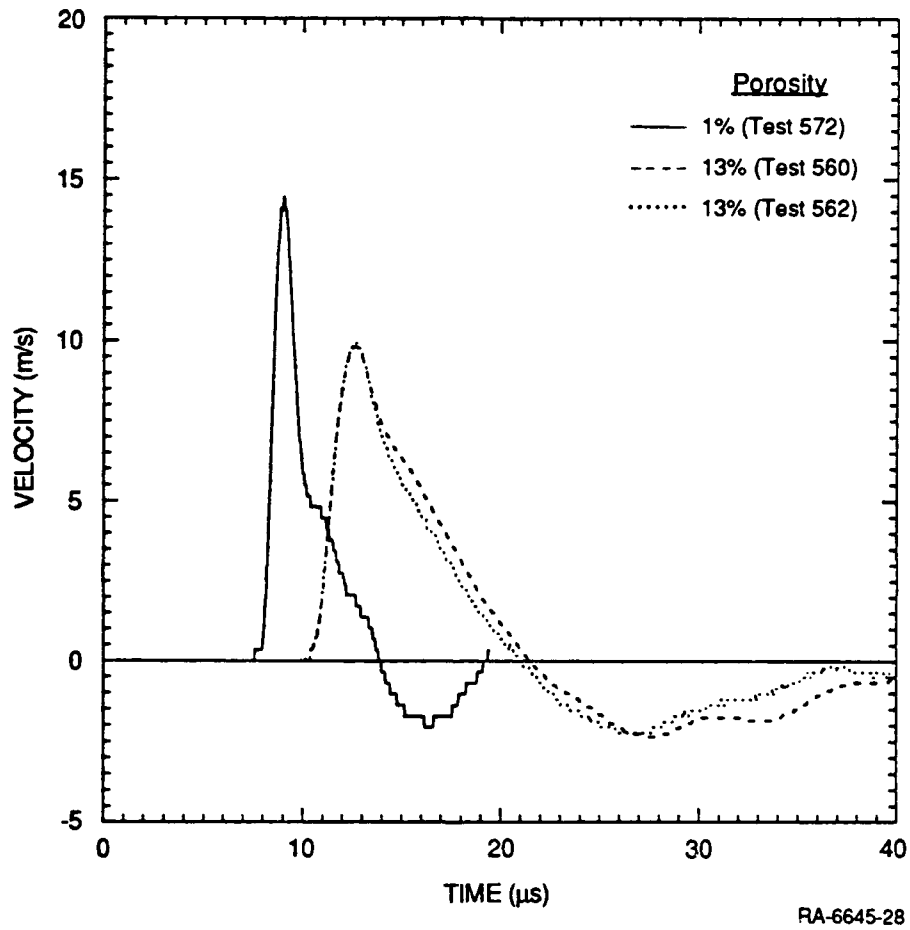
Figure 43. Comparison of velocity histories at 50-mm range for low-porosity
(1%) Katahdin limestone and high-porosity (13%) Indiana limestone.

RA-6645-28

52
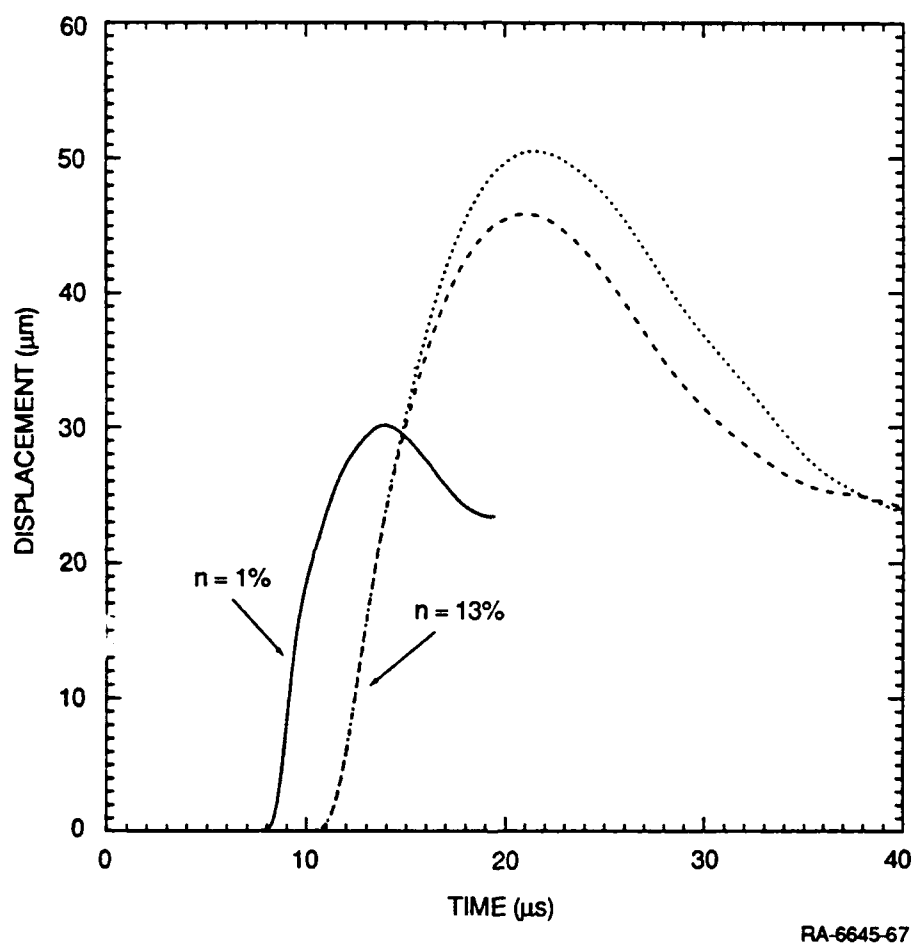
RA-6645-67

Figure 44. Comparison of displacement histories at 50-mm range for low-porosity (1%) Katahdin limestone and high-porosity (13%) Indiana limestone.

53
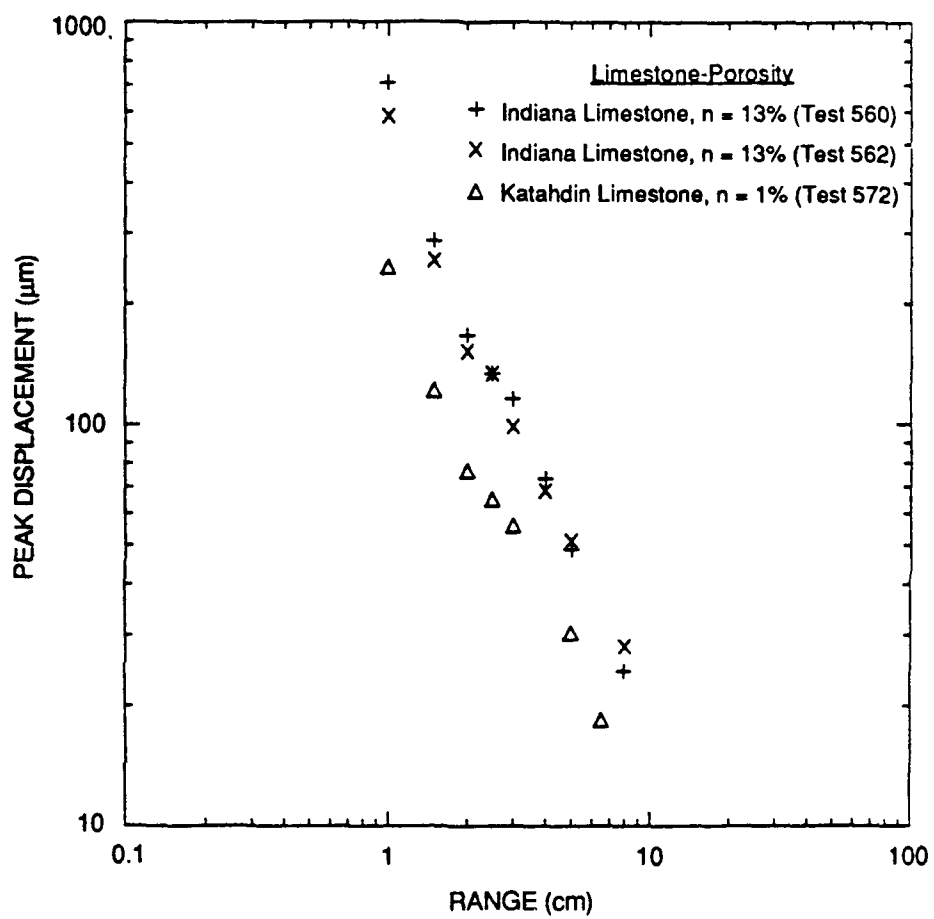
Figure 45. Comparison of peak displacement attenuation with range for low-
porosity Katahdin limestone and high-porosity Indiana limestone.

RA-6645-26A

54

APPENDIX A

STRAIN HISTORIES AND STRAIN PATHS

The radial displacement histories allow us to determine the spatial distribution of radial displacement, u_r, at fixed times, each spatial point corresponding to the range of a gage. From the spatial distribution of displacements, we obtain approximations for the radial strain, $\varepsilon_r = \partial u_r/\partial_r$, at a fixed time. The tangential strain component is simply $\varepsilon_\theta = u_r/r$; where r is the radius.

Because the accuracy of the spatial gradient of displacements is limited by the separation between gage positions, we present the strain results for locations where the gage separation is the minimum (i.e., 5 mm). The radial and tangential strain histories in different low porosity hard rocks at the 15- to 20-mm, 20- to 25-mm, and 25- to 30-mm ranges are shown superimposed in Figures A-1 through A-3, and the strain paths for each test are shown in Figures A-4 through A-8. Repeatability between tests is demonstrated for the three positions in Figures A-9 through A-11.
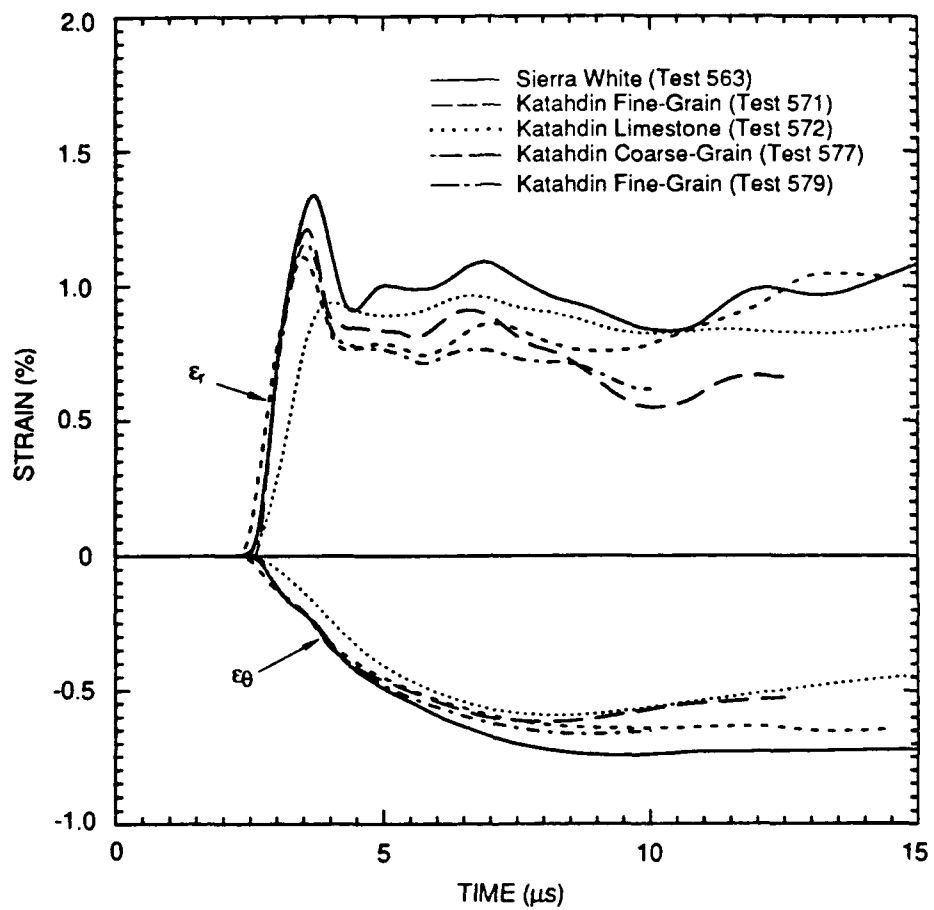
Figure A-1. Strain histories for 15- to 20-mm range in Sierra White granite and Katahdin granites and limestone.

A-2
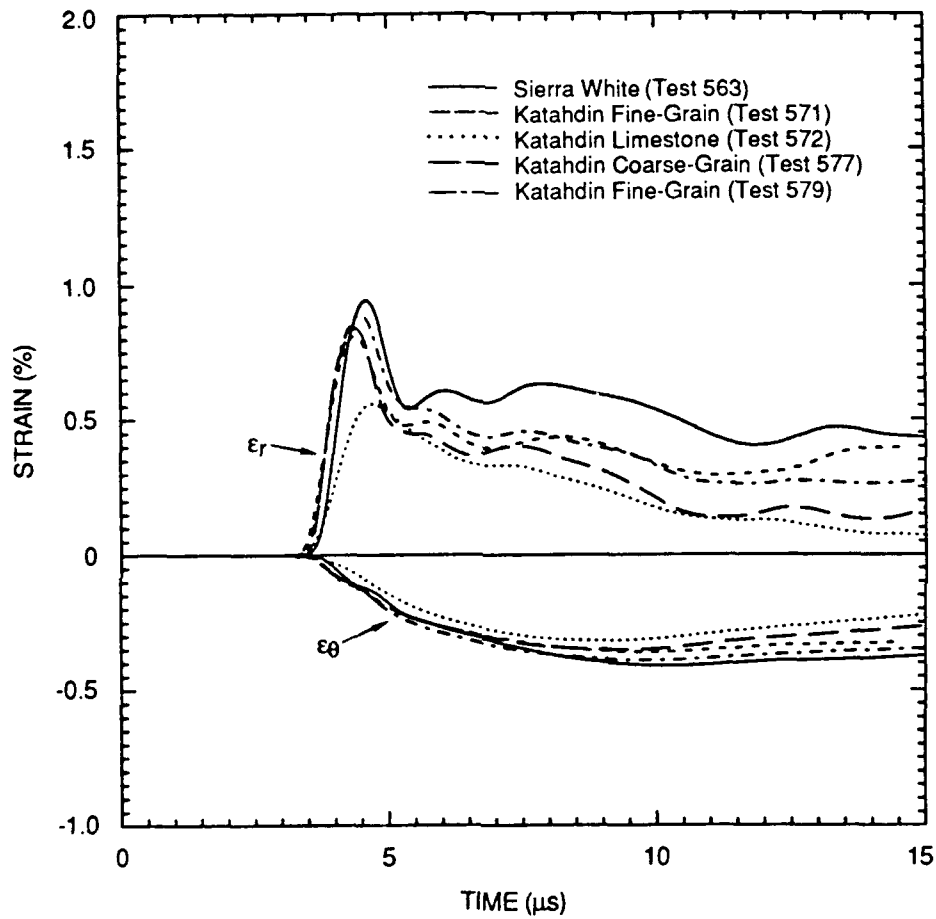
RA 6645-57

Figure A-2. Strain histories for 20 to 25-mm range in Sierra White granite
and Katahdin granites and limestone.

A-3
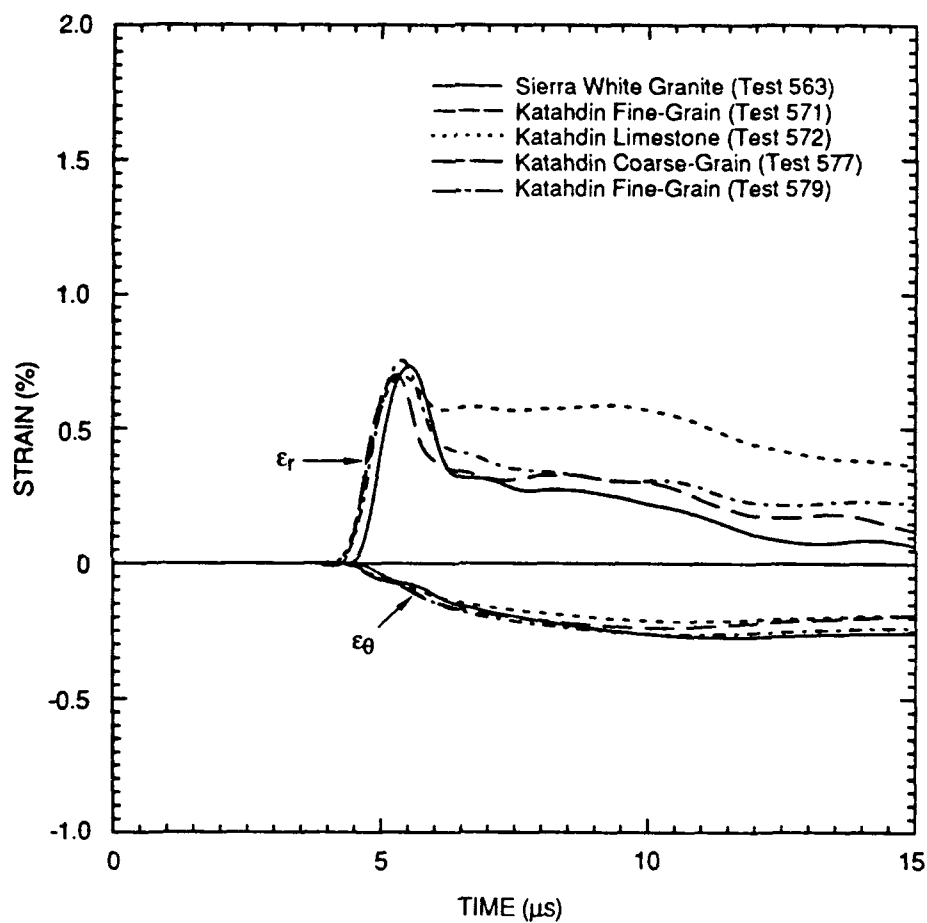
Figure A-3. Strain histories for 25 to 30-mm range in Sierra White granite and Katahdin granites and limestone.
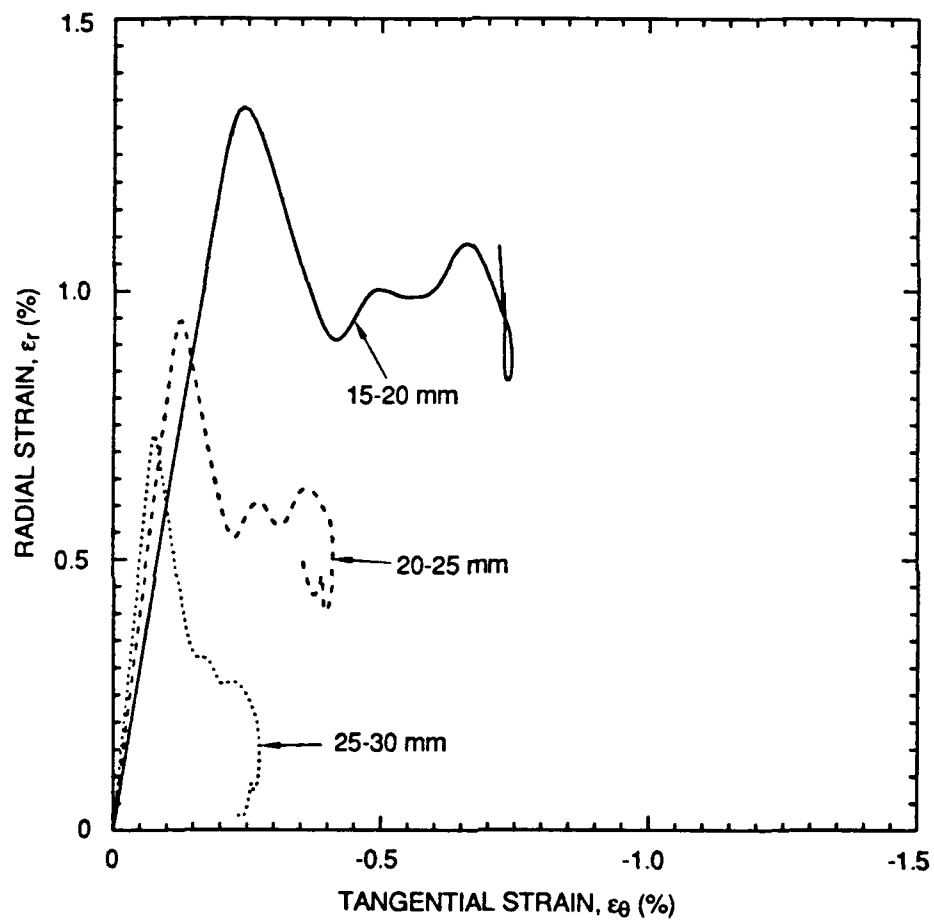
RA-6645-58

Figure A-4. Strain paths at different ranges in Sierra White granite (Test 563).
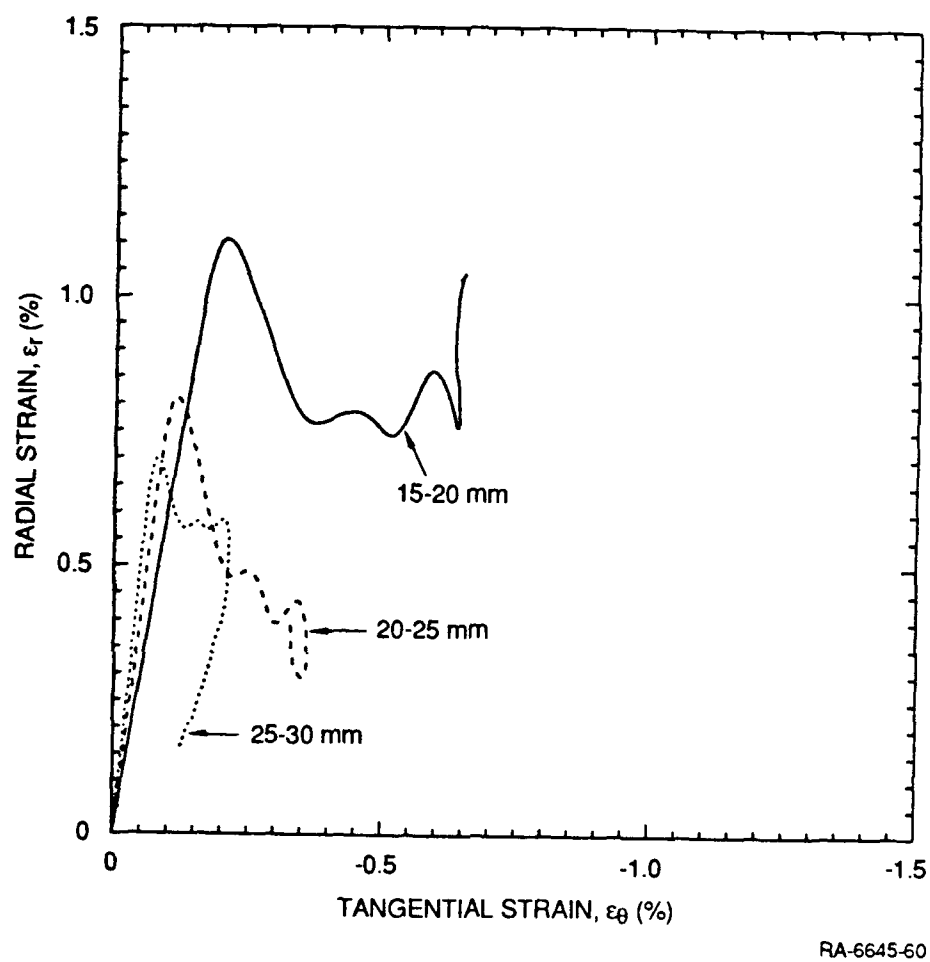
RA-6645-59

Figure A-5. Strain paths at different ranges in Katahdin fine-grain granite (Test 571).

RA-6645-60

A-6
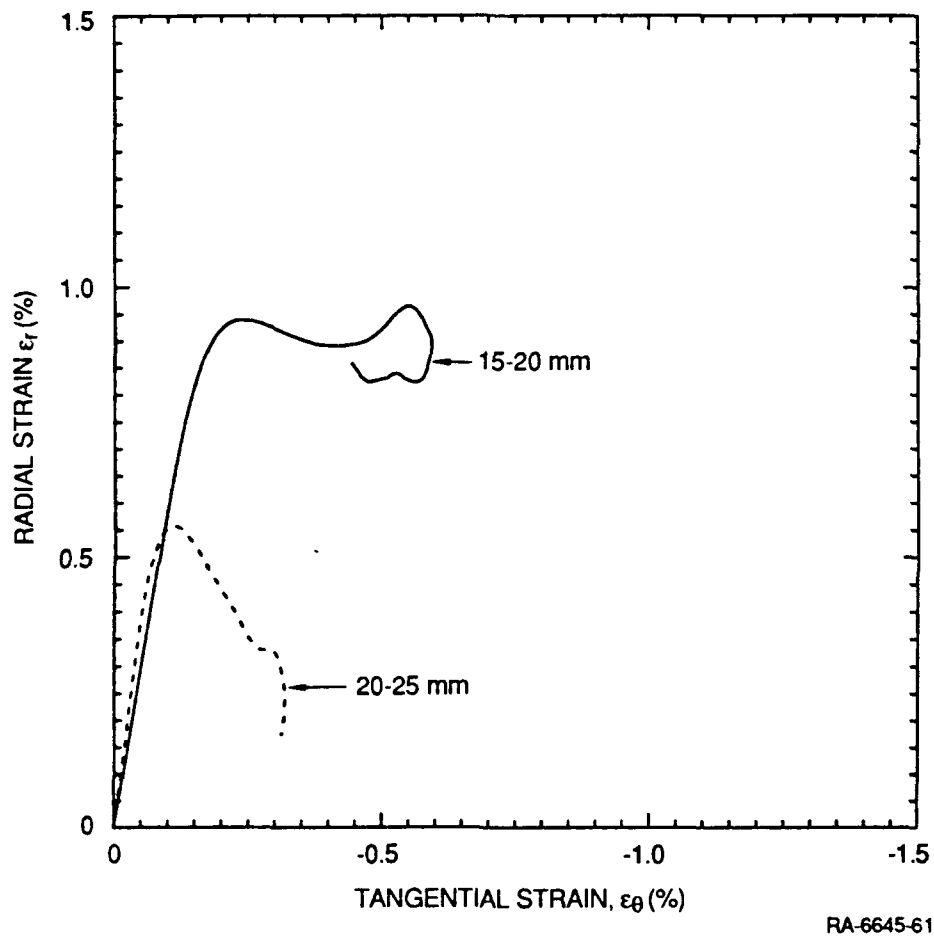
Figure A-6.   Strain paths at different ranges in Katahdin limestone (Test 572).
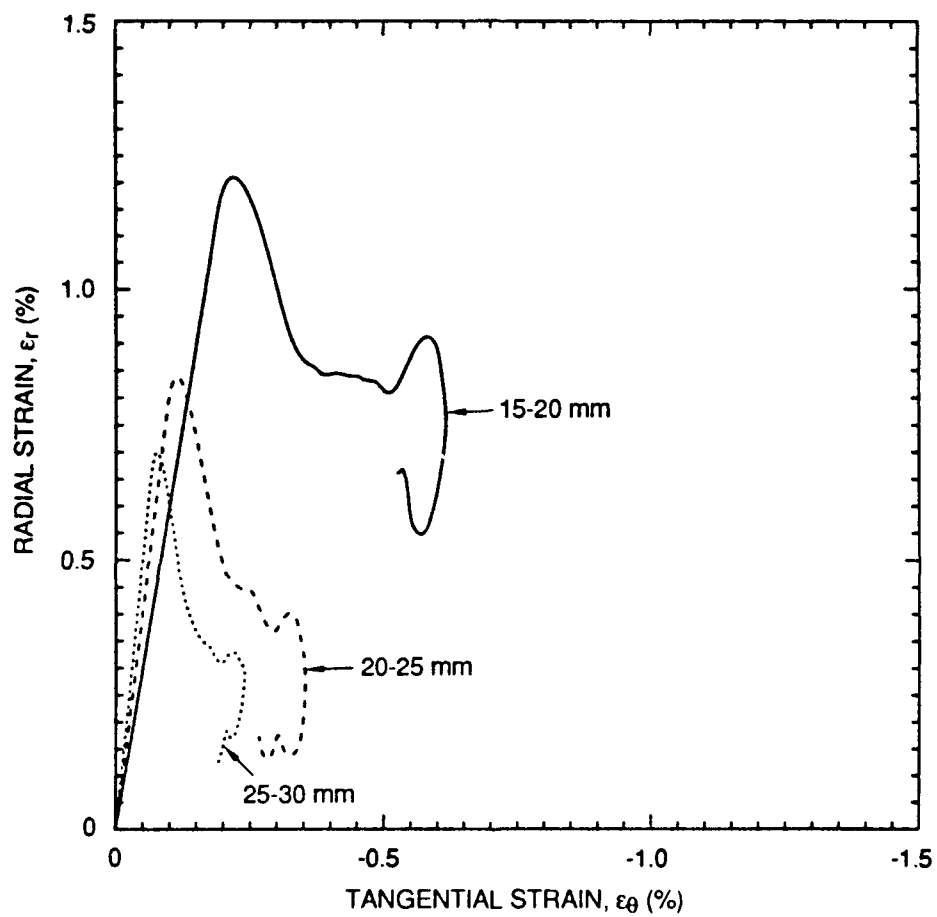
Figure A-7. Strain paths at different ranges in Katahdin coarse-grain granite
(Test 577).

RA-6645-62

A-8
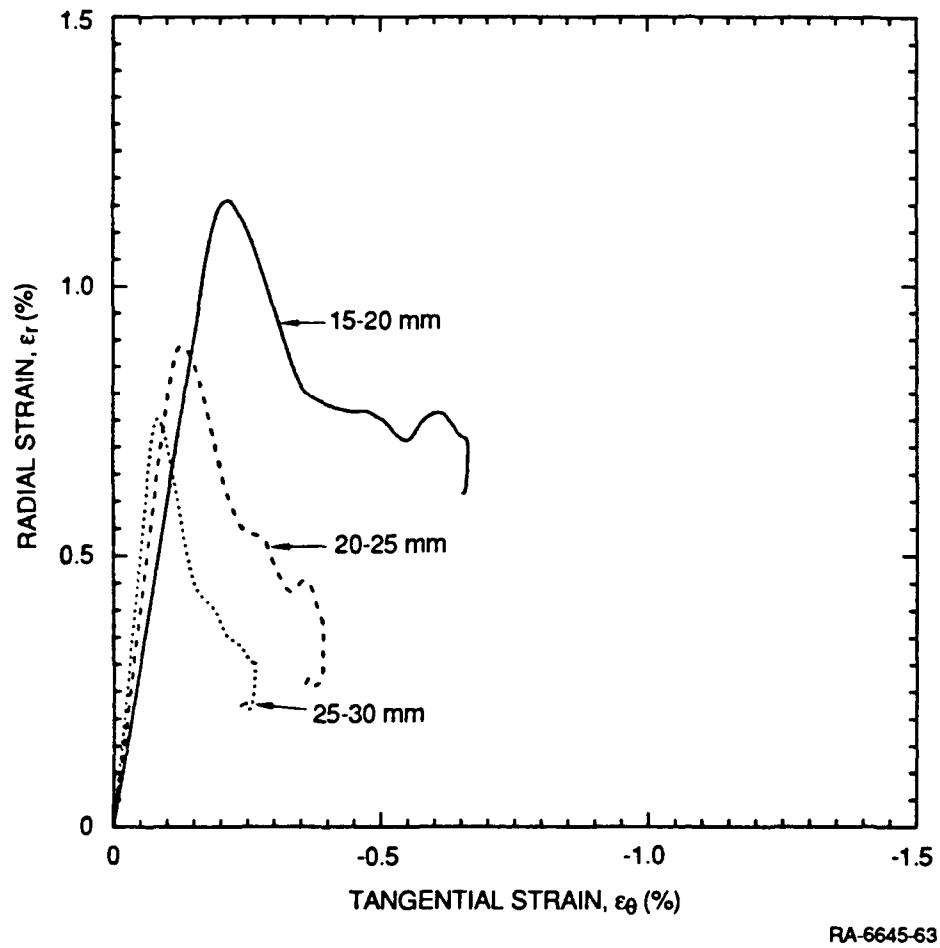
Figure A-8. Strain paths at different ranges in Katahdin fine-grain granite (Test 579).

A-9
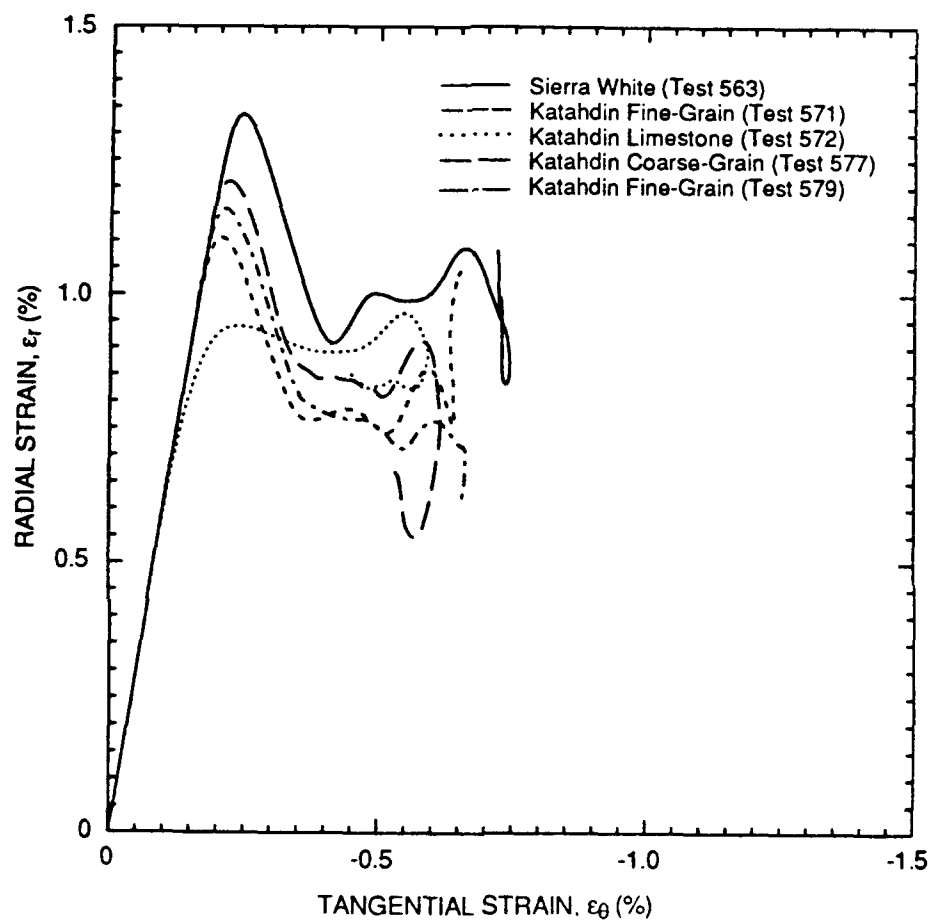
Figure A-9.   Comparison of strain paths for the 15- to 20-mm range in Sierra
White granite and Katahdin granites and limestone.
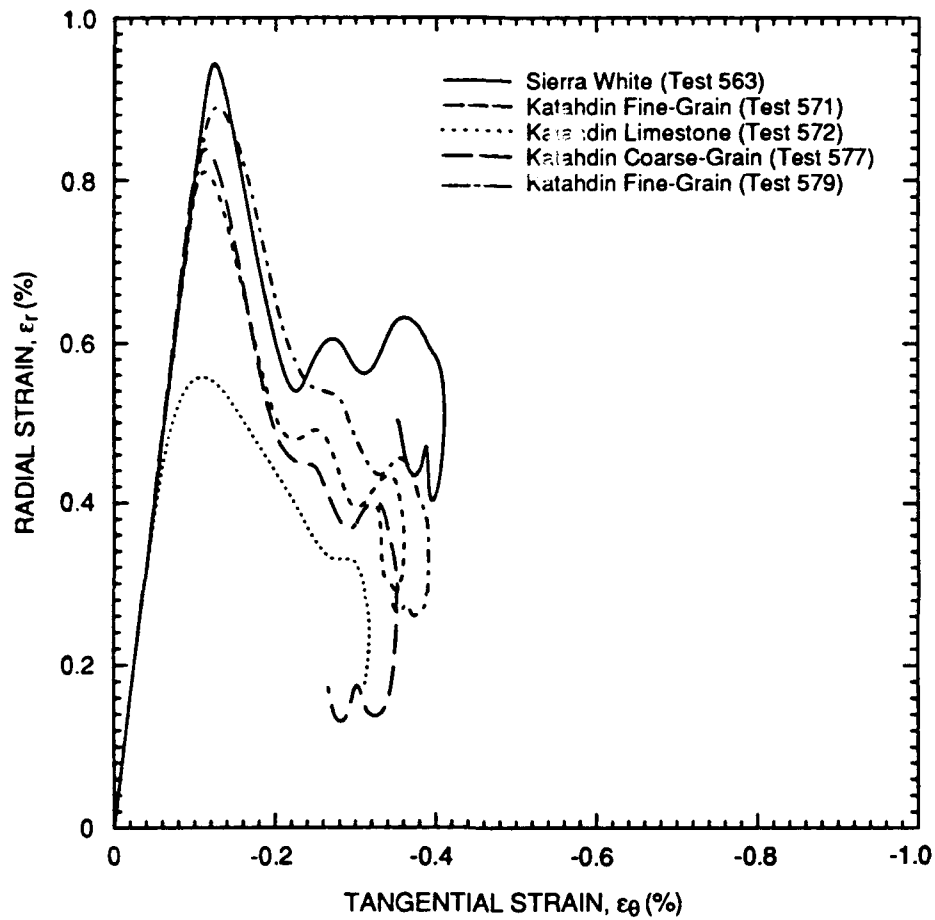
Figure A-10. Comparison of strain paths for the 20 to 25-mm range in Sierra White granite and Katahdin granites and limestone.

RA-6645-65

A-11
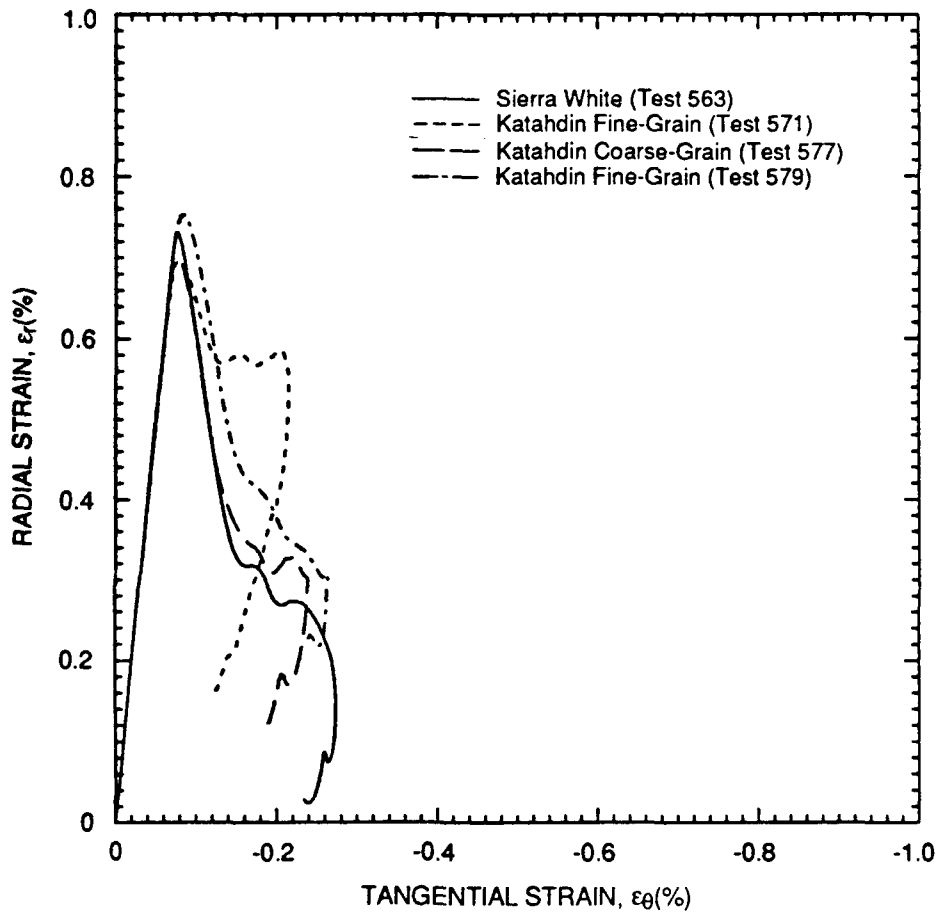
Figure A-11. Comparison of strain paths for the 25 to 30-mm range in Katahdin granites and Sierra White granite.

APPENDIX B

REDUCED DISPLACEMENT POTENTIALS (RDPs) AND REDUCED VELOCITY POTENTIALS (RVPs)

An outline of the treatment of elastic spherical waves is provided here to show how we obtain the reduced velocity and displacement potentials (RVPs and RDPs) from the measured particle velocity histories. The RDPs and RVPs determined from the experimental records are shown in this Appendix.

In spherical coordinates (r,θ,ϕ), a spherically symmetric elastic field has a radial displacement ξ, strains ε_r and $\varepsilon_\phi = \varepsilon_\theta$, and stresses σ_r and $\sigma_\phi = \sigma_\theta$ that depend only on the radial coordinate, r, and the time, t. The kinematic relations are

$$\varepsilon_r = \frac{\partial \xi}{\partial r} \qquad \varepsilon_\theta = \frac{\xi}{r} \tag{B-1}$$

and Hooke's law is

$$\sigma_r = (\lambda + 2\mu)\,\varepsilon_r + 2\lambda\varepsilon_\theta \qquad \sigma_\theta = \lambda\varepsilon_r + 2(\lambda + \mu)\,\varepsilon_\theta \tag{B-2}$$

where λ and μ are the Lamé constants (μ is the shear modulus). In terms of Young's modulus, E, and Poisson's ratio, ϑ,

$$\lambda = \frac{E\vartheta}{(1 + \vartheta)(1 - 2\vartheta)} \qquad \mu = \frac{E}{2(1 + \vartheta)} \qquad \lambda + 2\mu = \frac{(1 - \vartheta)E}{(1 + \vartheta)(1 - 2\vartheta)} \tag{B-3}$$

The equation of motion of an element of material is

$$\frac{\partial \sigma_r}{\partial r} + \frac{2}{r}(\sigma_r - \sigma_\theta) = \rho \frac{\partial^2 \xi}{\partial t^2} \tag{B-4}$$

in which ρ is the material density. Substitution of the stresses, eq. (B-2), and then the strains, eq. (B-1) changes eq. (B-4) to

$$\frac{\partial^2 \xi}{\partial r^2} + \frac{2}{r}\frac{\partial \xi}{\partial r} - \frac{2\xi}{r^2} = \frac{1}{c^2}\frac{\partial^2 \xi}{\partial t^2} \tag{B-5}$$

in which $c^2 = (\lambda + 2\mu)/\rho$, c being the P-wave speed. Differentiation of eq. (B-5) with respect to time t shows that the radial particle velocity $u = \partial\xi/\partial t$ satisfies the same equation.

To find the solution of eq. (B-5), let $\phi(r,t)$ be a displacement potential so that

$$\xi = \frac{\partial\phi}{\partial r} \tag{B-6}$$

Then, eq. (B-5) becomes

$$\frac{\partial^2(r\phi)}{\partial r^2} = \frac{1}{c^2}\frac{\partial^2(r\phi)}{\partial t^2} \tag{B-7}$$

which is the standard form of the wave equation. The solution of eq. (B-7) that describes P waves propagating outwards from a spherical source of radius r = a is

$$\phi = \frac{1}{r}\psi\left(t - \frac{r-a}{c}\right) \tag{B-8}$$

where the function ψ is the reduced displacement potential (RDP). If the wave starts from the source at radius r = a at time t = 0, the wave arrival time at radius r is $t_a = (r - a)/c$, so the RDP applies at this radius only when $t > t_a$. Let $\tau = t - (r - a)/c$ be the the time measured from the time of arrival. Then,

$$\phi = \frac{1}{r}\psi(\tau) \qquad \tau = t - (r-a)/c \tag{B-9}$$

According to eqs. (B-6) and (B-9), the displacement is related to the RDP by

$$\xi = -\frac{\dot{\psi}(\tau)}{rc} - \frac{\psi(\tau)}{r^2} \tag{B-10}$$

where the dot indicates differentiation with respect to the argument, τ. The choice of the displacement potential value at the wave front given by $\phi(0)$ is arbitrary, so we choose $\phi(0) = 0$. Also, the displacement at the wave front is zero, so $\partial\phi/\partial r = 0$ at $\tau = 0$. Hence, by eqs. (B-9) and (B-10), we have

$$\psi(0) = 0 \qquad \dot{\psi}(0) = 0 \tag{B-11}$$

The solution of eq. (B-10) giving the RDP at the radius, r, where the displacement history is measured is simply

$$\psi(\tau) = -cr\, e^{-c\tau/r} \int_0^\tau \xi(r,\tau')\, e^{c\tau'/r}\, d\tau' \qquad \text{(B-12)}$$

Equation (B-12) was used to calculate the RDPs for the spherical wave experiments in the Katahdin granite and limestone experiments, which are shown in Figures B-1 through B-5.

An analogous expression for the reduced velocity potential (RVP) is derived in the same way. The particle velocity, u, satisfies eq. (B-5) and when a velocity potential, χ, is introduced through the definition

$$u = \frac{\partial \chi}{\partial r} \qquad \text{(B-13)}$$

we find that $r\chi$ replaces $r\phi$ in the standard wave equation, eq. (B-7). For outgoing waves,

$$\chi = \frac{1}{r}\gamma(t - \frac{r-a}{c}) \qquad \text{(B-14)}$$

or

$$\chi = \frac{1}{r}\gamma(\tau) \qquad \tau = t - (r-a)/c \qquad \text{(B-15)}$$

and $\gamma(\tau)$ is the RVP. Consequently, the particle velocity is related to the RVP by the equation

$$u = -\frac{\dot{\gamma}(\tau)}{rc} - \frac{\gamma(\tau)}{r^2} \qquad \text{(B-16)}$$

The value of the velocity potential is arbitrary at the wave front, so we choose $\chi(0) = 0$. However, the value of the particle velocity at the wave front need not be zero, and we have

$$\gamma(0) = 0 \qquad \dot{\gamma}(0) = rcu(r,0) \qquad \text{(B-17)}$$

where u(r,0) is the jump in velocity at the wave front. The solution of eq. (B-16) with $\gamma(0) = 0$ gives the RVP in the form

$$\gamma(\tau) = cr\, e^{-c\tau/r} \int_0^\tau u(r,\tau')\, e^{c\tau'/r}\, d\tau' \qquad \text{(B-18)}$$

RVP histories determined from the experimental records by using eq. (B-18) are shown in Figures B-6 through B-10.

If a pulse in a cavity causes permanent deformation around the spherical cavity, we let the radius $r = a$ be the radius beyond which the material remains elastic. In these cases, the final displacement in the elastic region will not be zero; the final particle velocity will still be zero. Let the final displacement, $\xi_{\infty}(r)$, be established at radius $r > a$ at time τ_d. Formula (B-12) then gives

$$\psi(\tau) = - cr\, e^{-c\tau/r} \int_0^{\tau_d} \xi(r,\tau')\, e^{c\tau'/r}\, d\tau' - r^2 \xi_{\infty}(r) \left\{ 1 - e^{-c(\tau-\tau_d)/r} \right\}$$

for $\tau > \tau_d$, so $\psi(\infty) = \psi_{\infty}$ is

$$\psi_{\infty} = - r^2\, \xi_{\infty}(r) \tag{B-19}$$

A similar treatment of formula (18) gives $\gamma_{\infty} = 0$ because $u_{\infty}(r) = 0$.

B-4
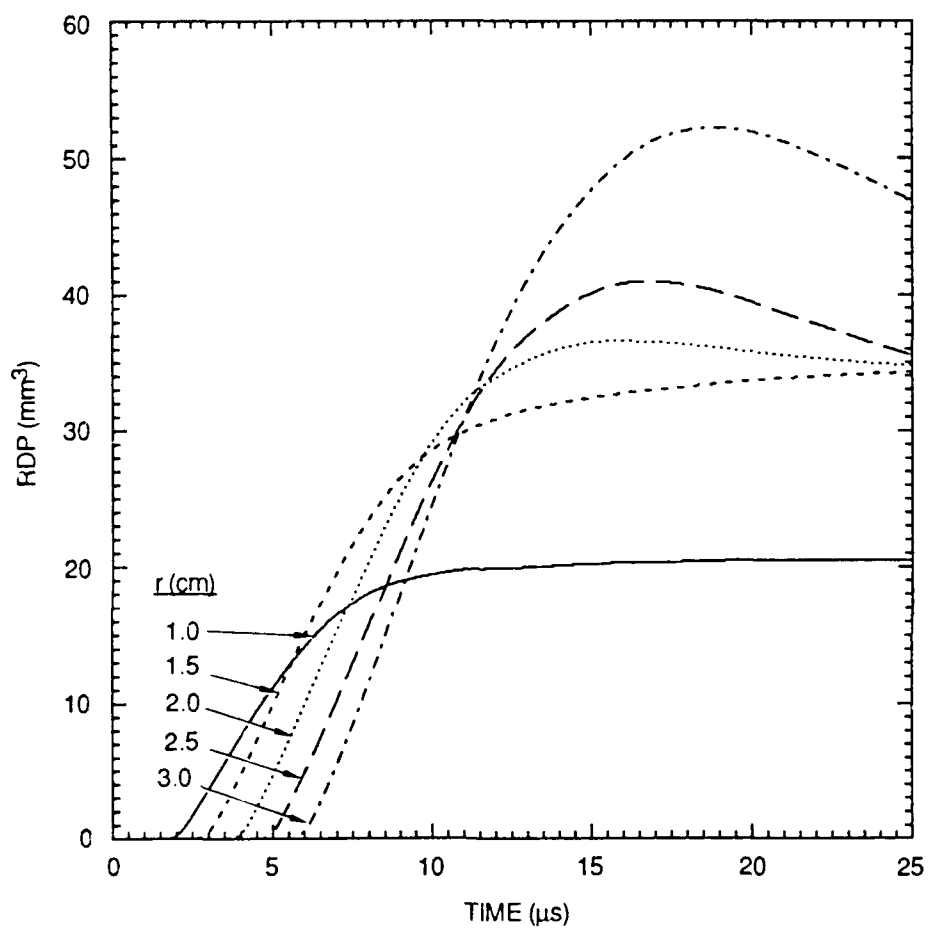
RA-6645-78

Figure B-1.   Reduced displacement potentials (RDPs) in Sierra White granite
(Test 563).
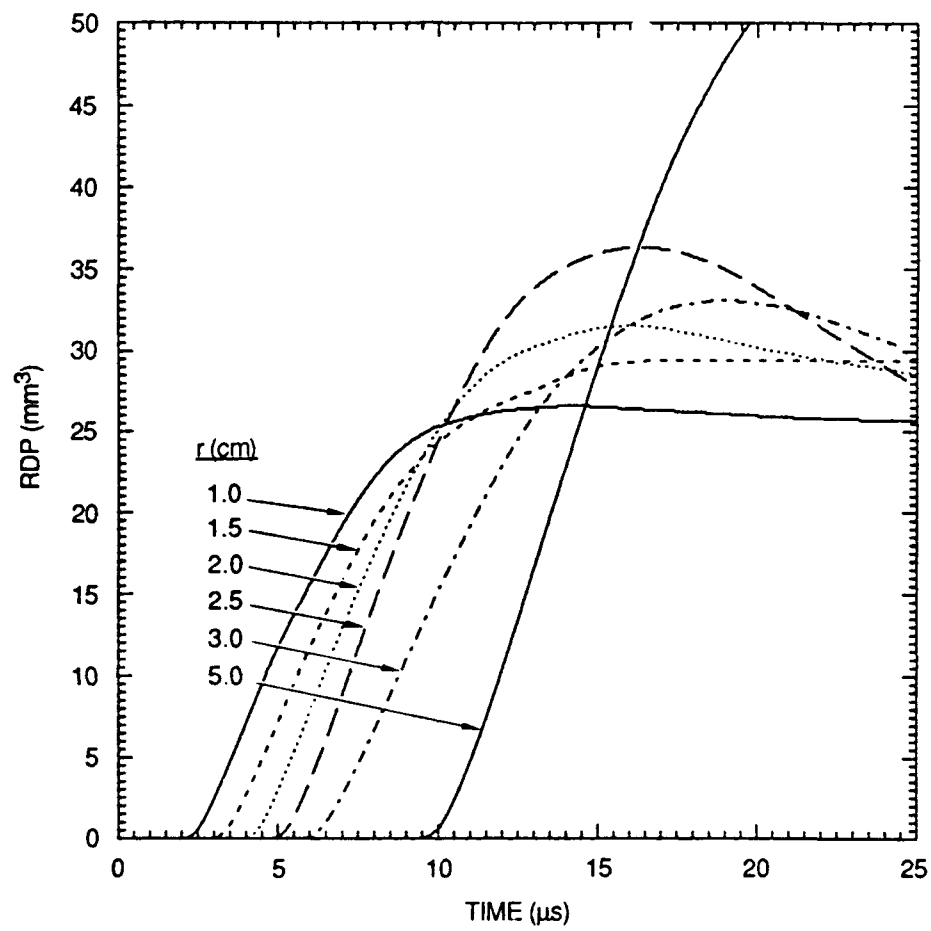
Figure B-2. Reduced displacement potentials (RDPs) in fine-grain Katahdin granite (Test 571).
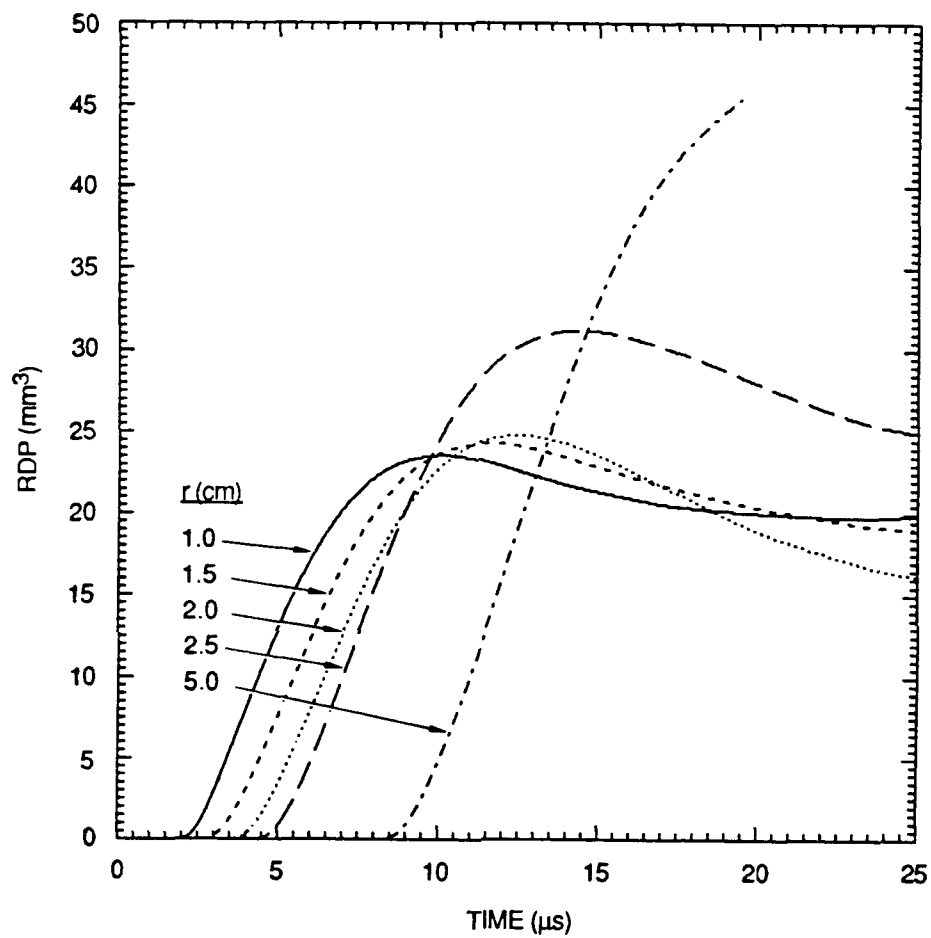
RA-6645-79

RA-6645-80

Figure B-3. Reduced displacement potentials (RDPs) in Katahdin limestone
(Test 572).
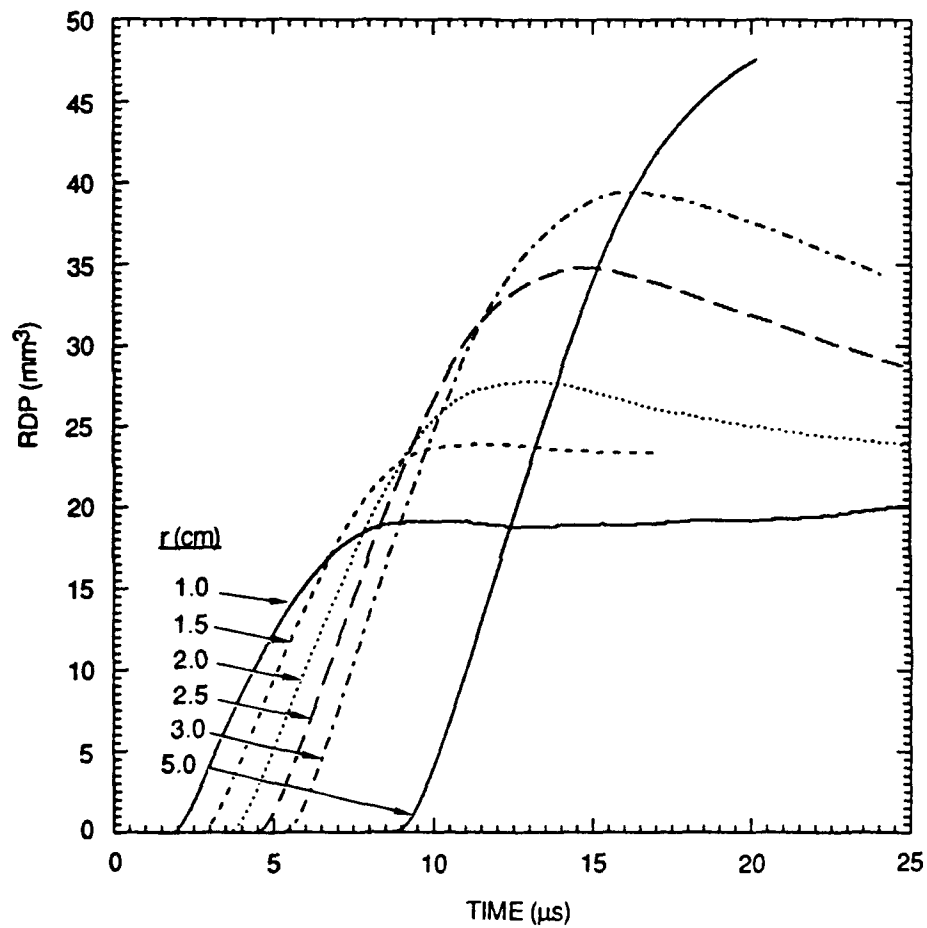
RA-6645-81

Figure B-4.   Reduced displacement potentials (RDPs) in coarse-grain
              Katahdin granite (Test 577).
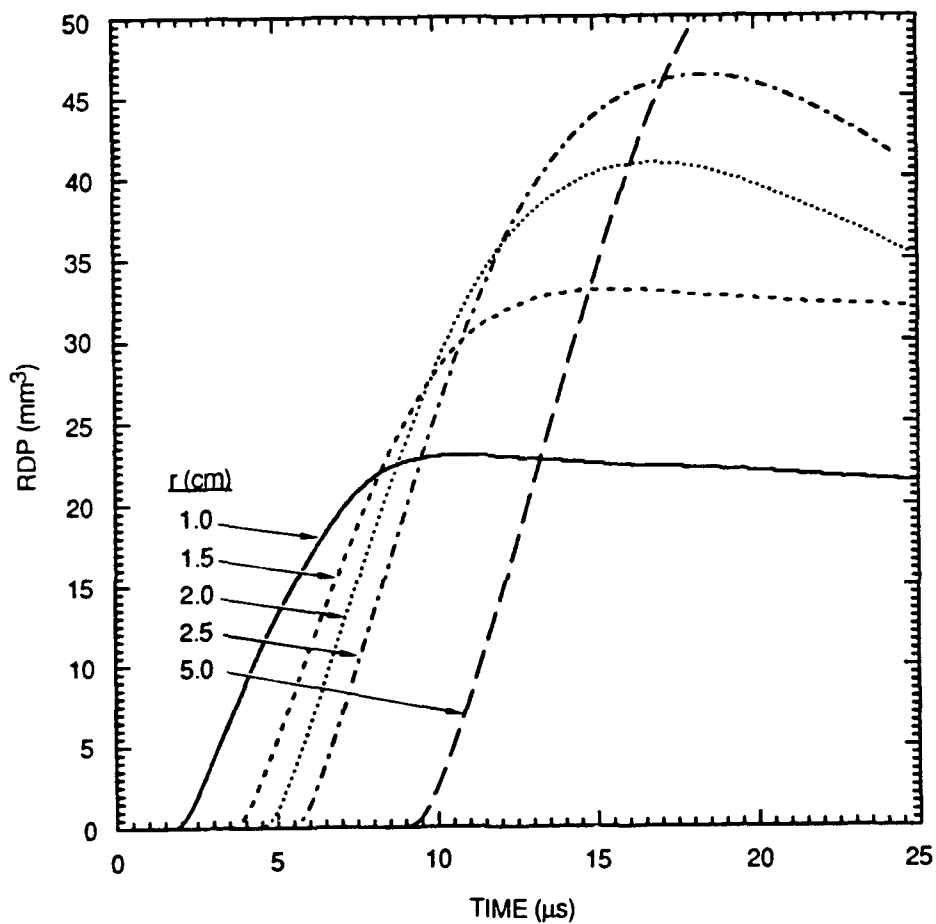
RA-6645-82

Figure B-5. Reduced displacement potentials (RDPs) in fine-grain Katahdin granite (Test 579).
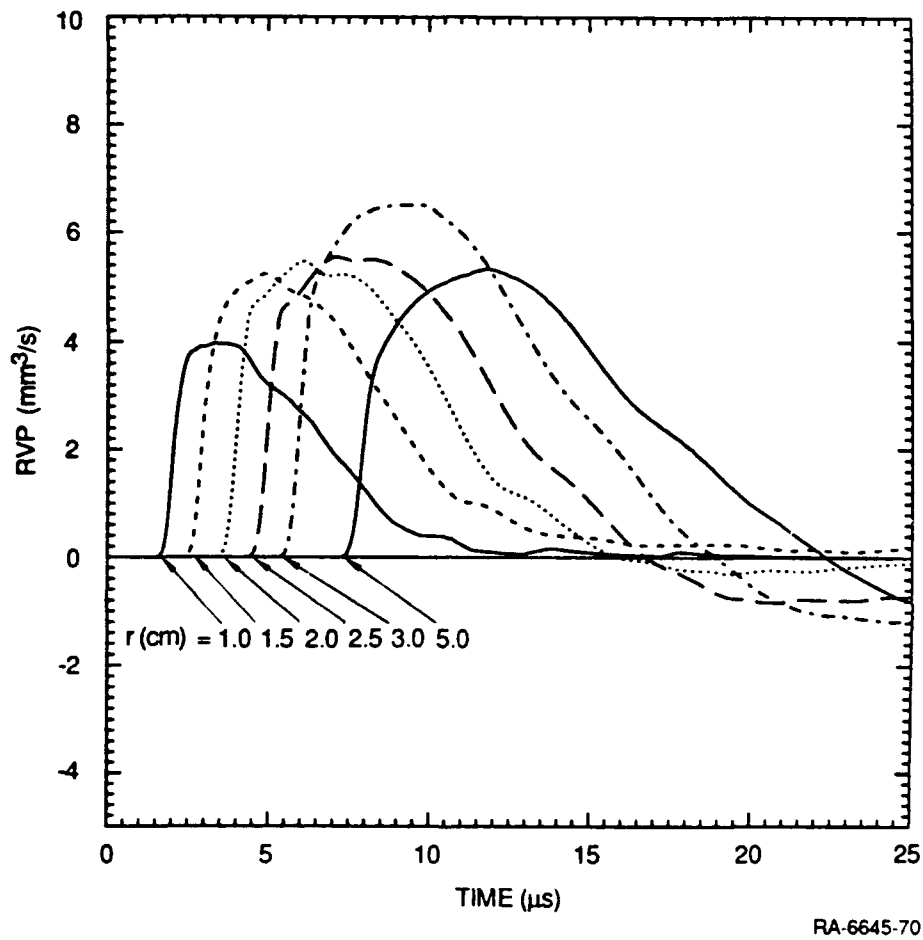
RA-6645-70

Figure B-6. Time histories of reduced velocity potentials (RVPs) in Sierra
White granite (Test 563).
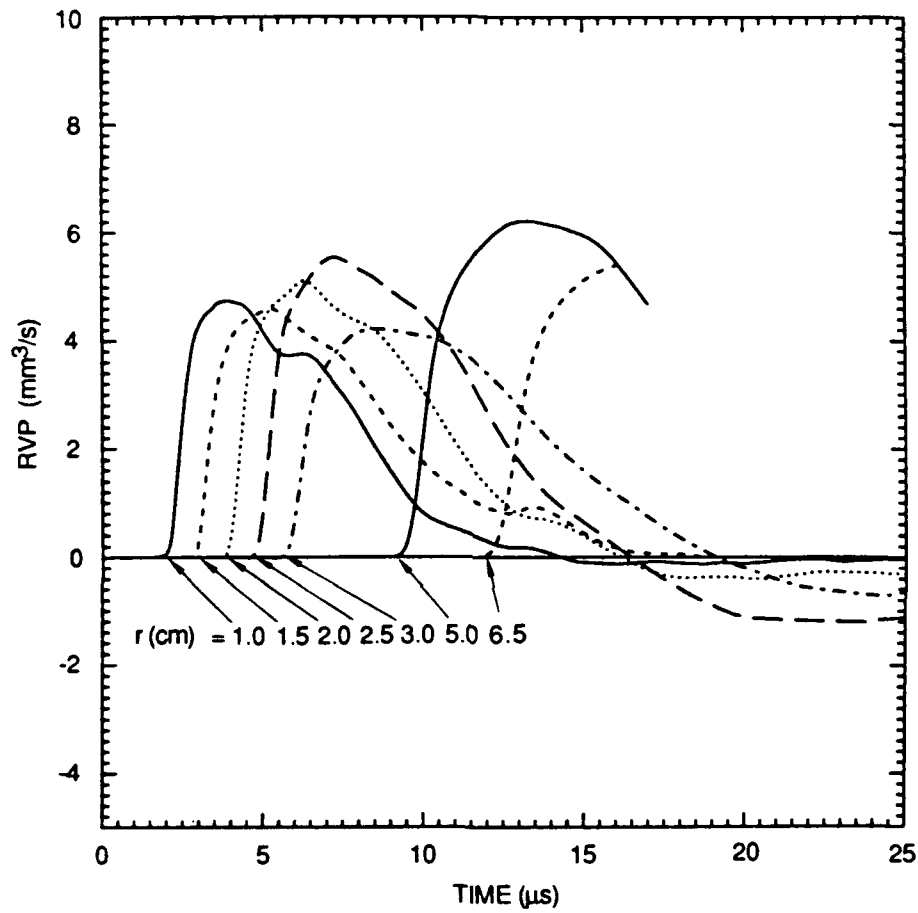
Figure B-7. Time histories of reduced velocity potentials (RVPs) in fine-grain Katahdin granite (Test 571).

RA-6645-71

B-11
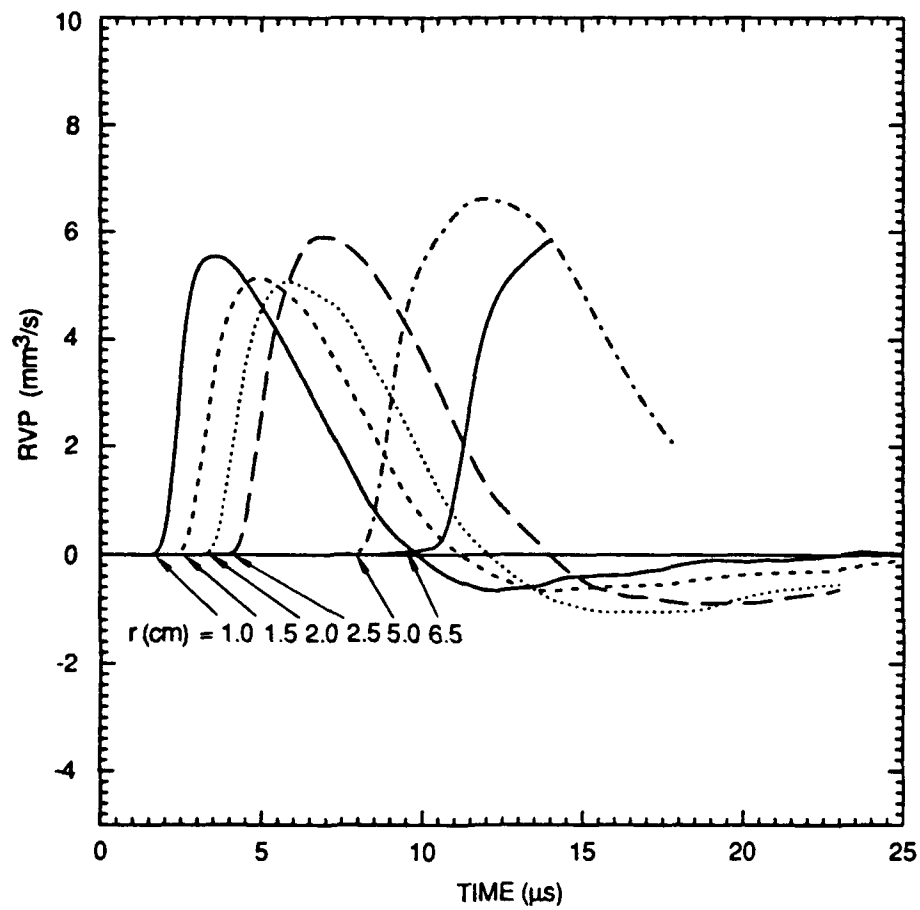
Figure B-8. Time history of reduced velocity potentials (RVPs) in Katahdin limestone (Test 572).
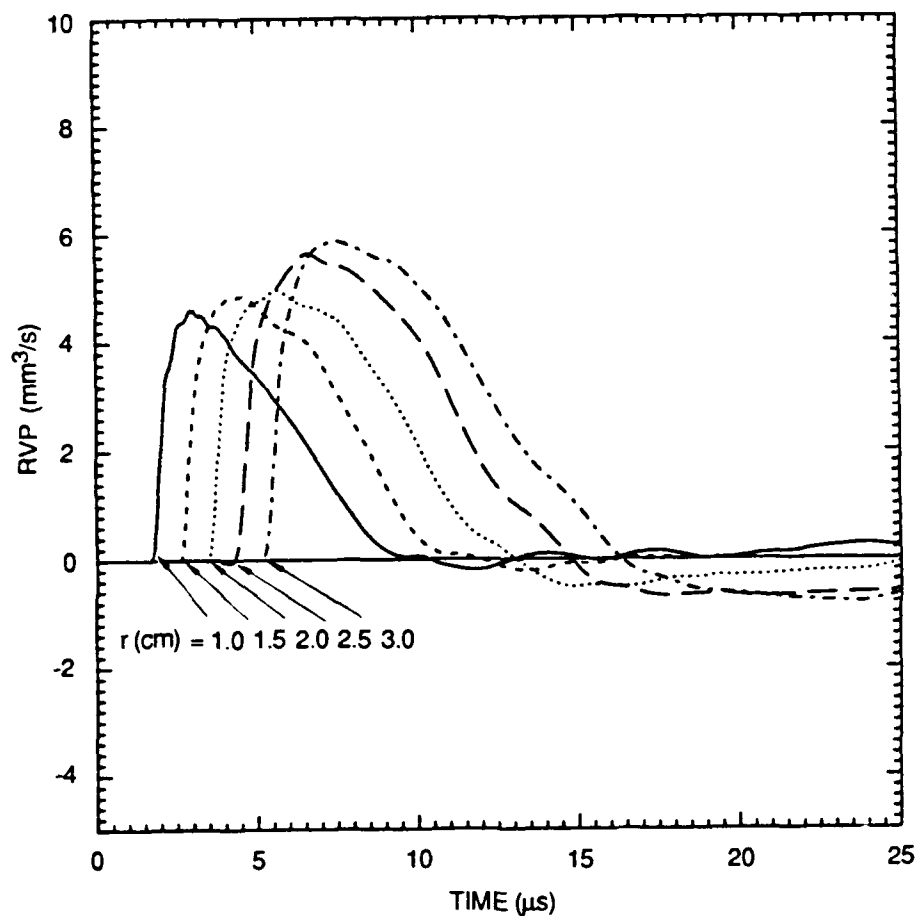
RA-6645-72

RA-6645-73

Figure B-9. Time history of reduced velocity potentials (RVPs) in coarse-grain Katahdin granite (Test 577).
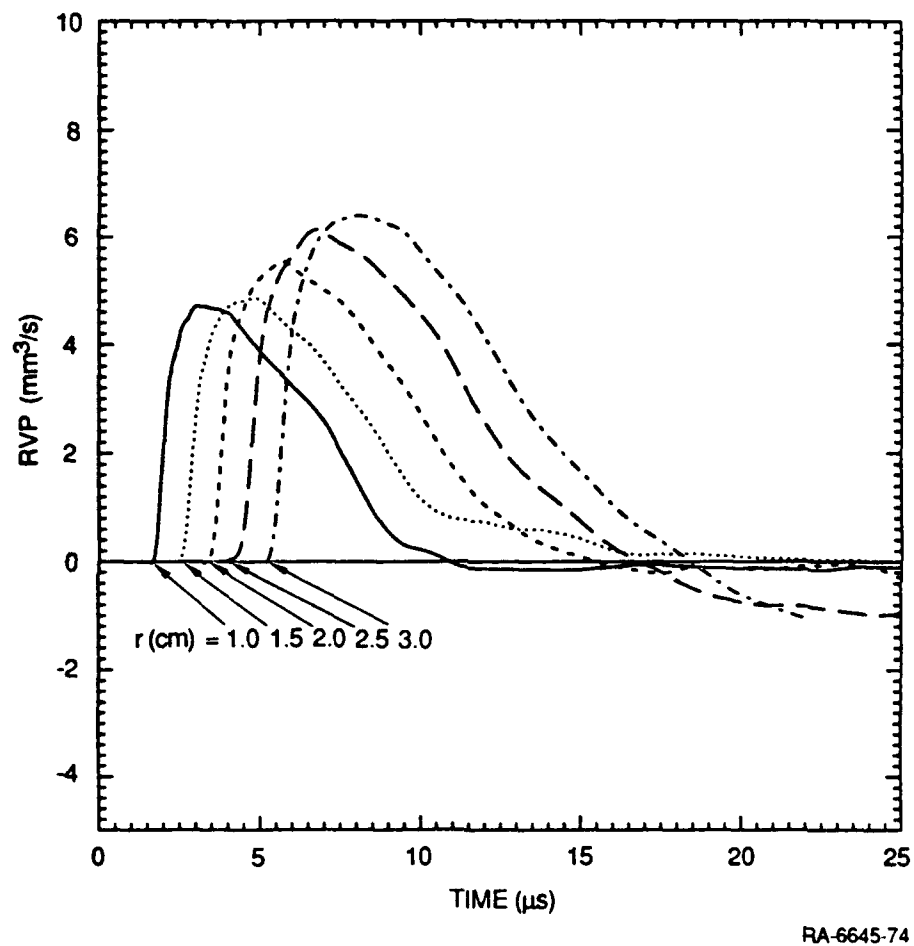
Figure B-10. Time history of reduced velocity potentials (RVPs) in fine-grain
Katahdin granite (Test 579).

RA-6645-74

B-14

Prof. Thomas Ahrens
Seismological Lab, 252-21
Division of Geological & Planetary Sciences
California Institute of Technology
Pasadena, CA 91125

Prof. Charles B. Archambeau
CIRES
University of Colorado
Boulder, CO 80309

Dr. Thomas C. Bache, Jr.
Science Applications Int'l Corp.
10260 Campus Point Drive
San Diego, CA 92121   (2 copies)

Prof. Muawia Barazangi
Institute for the Study of the Continent
Cornell University
Ithaca, NY 14853

Dr. Douglas R. Baumgardt
ENSCO, Inc
5400 Port Royal Road
Springfield, VA 22151-2388

Prof. Jonathan Berger
IGPP, A-025
Scripps Institution of Oceanography
University of California, San Diego
La Jolla, CA 92093

Dr. Lawrence J. Burdick
Woodward-Clyde Consultants
566 El Dorado Street
Pasadena, CA 91109-3245

Dr. Jerry Carter
Center for Seismic Studies
1300 North 17th St., Suite 1450
Arlington, VA 22209-2308

Dr. Karl Coyner
New England Research, Inc.
76 Olcott Drive
White River Junction, VT 05001

Prof. Vernon F. Cormier
Department of Geology & Geophysics
U-45, Room 207
The University of Connecticut
Storrs, CT 06268

Professor Anton W. Dainty
Earth Resources Laboratory
Massachusetts Institute of Technology
42 Carleton Street
Cambridge, MA 02142

Prof. Steven Day
Department of Geological Sciences
San Diego State University
San Diego, CA 92182

Dr. Zoltan A. Der
ENSCO, Inc.
5400 Port Royal Road
Springfield, VA 22151-2388

Prof. John Ferguson
Center for Lithospheric Studies
The University of Texas at Dallas
P.O. Box 830688
Richardson, TX 75083-0688

Dr. Mark D. Fisk
Mission Research Corporation
735 State Street
P. O. Drawer 719
Santa Barbara, CA 93102

Prof. Stanley Flatte
Applied Sciences Building
University of California
Santa Cruz, CA 95064

Dr. Alexander Florence
SRI International
333 Ravenswood Avenue
Menlo Park, CA 94025-3493

Prof. Henry L. Gray
Vice Provost and Dean
Department of Statistical Sciences
Southern Methodist University
Dallas, TX 75275

Dr. Indra Gupta
Teledyne Geotech
314 Montgomery Street
Alexandria, VA 22314

Prof. David G. Harkrider
Seismological Laboratory
Division of Geological & Planetary Sciences
California Institute of Technology
Pasadena, CA 91125

1

Prof. Donald V. Helmberger
Seismological Laboratory
Division of Geological & Planetary Sciences
California Institute of Technology
Pasadena, CA 91125

Prof. Eugene Herrin
Institute for the Study of Earth and Man
Geophysical Laboratory
Southern Methodist University
Dallas, TX 75275

Prof. Bryan Isacks
Cornell University
Department of Geological Sciences
SNEE Hall
Ithaca, NY 14850

Dr. Rong-Song Jih
Teledyne Geotech
314 Montgomery Street
Alexandria, VA 22314

Prof. Lane R. Johnson
Seismographic Station
University of California
Berkeley, CA 94720

Dr. Richard LaCoss
MIT-Lincoln Laboratory
M-200B
P. O. Box 73
Lexington, MA 02173-0073   (3 copies)

Prof Fred K. Lamb
University of Illinois at Urbana-Champaign
Department of Physics
1110 West Green Street
Urbana, IL 61801

Prof. Charles A. Langston
Geosciences Department
403 Deike Building
The Pennsylvania State University
University Park, PA 16802

Prof. Thorne Lay
Institute of Tectonics
Earth Science Board
University of California, Santa Cruz
Santa Cruz, CA 95064

Prof. Arthur Lerner-Lam
Lamont-Doherty Geological Observatory
of Columbia University
Palisades, NY 10964

Dr. Christopher Lynnes
Teledyne Geotech
314 Montgomery Street
Alexandria, VA 22314

Prof. Peter Malin
University of California at Santa Barbara
Institute for Crustal Studies
Santa Barbara, CA 93106

Dr. Randolph Martin, III
New England Research, Inc.
76 Olcott Drive
White River Junction, VT 05001

Prof. Thomas V. McEvilly
Seismographic Station
University of California
Berkeley, CA 94720

Dr. Keith L. McLaughlin
S-CUBED
A Division of Maxwell Laboratory
P.O. Box 1620
La Jolla, CA 92038-1620

Prof. William Menke
Lamont-Doherty Geological Observatory
of Columbia University
Palisades, NY 10964

Stephen Miller
SRI International
333 Ravenswood Avenue
Box AF 116
Menlo Park, CA 94025-3493

Prof. Bernard Minster
IGPP, A-025
Scripps Institute of Oceanography
University of California, San Diego
La Jolla, CA 92093

Prof. Brian J. Mitchell
Department of Earth & Atmospheric Sciences
St. Louis University
St. Louis, MO 63156

Mr. Jack Murphy
S-CUBED, A Division of Maxwell Laboratory
11800 Sunrise Valley Drive
Suite 1212
Reston, VA 22091 (2 copies)

Prof. John A. Orcutt
IGPP, A-025
Scripps Institute of Oceanography
University of California, San Diego
La Jolla, CA 92093

Prof. Keith Priestley
University of Cambridge
Bullard Labs, Dept. of Earth Sciences
Madingley Rise, Madingley Rd.
Cambridge CB3 0EZ, ENGLAND

Dr. Jay J. Pulli
Radix Systems, Inc.
2 Taft Court, Suite 203
Rockville, MD 20850

Prof. Paul G. Richards
Lamont Doherty Geological Observatory
 of Columbia University
Palisades, NY 10964

Dr. Wilmer Rivers
Teledyne Geotech
314 Montgomery Street
Alexandria, VA 22314

Prof. Charles G. Sammis
Center for Earth Sciences
University of Southern California
University Park
Los Angeles, CA 90089-0741

Prof. Christopher H. Scholz
Lamont-Doherty Geological Observatory
of Columbia University
Palisades, NY 10964

Thomas J. Sereno, Jr.
Science Application Int'l Corp.
10260 Campus Point Drive
San Diego, CA 92121

Prof. David G. Simpson
Lamont-Doherty Geological Observatory
of Columbia University
Palisades, NY 10964

Dr. Jeffrey Stevens
S-CUBED
A Division of Maxwell Laboratory
P.O. Box 1620
La Jolla, CA 92038-1620

Prof. Brian Stump
Institute for the Study of Earth & Man
Geophysical Laboratory
Southern Methodist University
Dallas, TX 75275

Prof. Jeremiah Sullivan
University of Illinois at Urbana-Champaign
Department of Physics
1110 West Green Street
Urbana, IL 61801

Prof. Clifford Thurber
University of Wisconsin-Madison
Department of Geology & Geophysics
1215 West Dayton Street
Madison, WS 53706

Prof. M. Nafi Toksoz
Earth Resources Lab
Massachusetts Institute of Technology
42 Carleton Street
Cambridge, MA 02142

Prof. John E. Vidale
University of California at Santa Cruz
Seismological Laboratory
Santa Cruz, CA 95064

Prof. Terry C. Wallace
Department of Geosciences
Building #77
University of Arizona
Tucson, AZ 85721

Dr. William Wortman
Mission Research Corporation
8560 Cinderbed Rd.
Suite # 700
Newington, VA 22122

3

Dr. Monem Abdel-Gawad
Rockwell International Science Center
1049 Camino Dos Rios
Thousand Oaks, CA 91360

Dr. G.A. Bollinger
Department of Geological Sciences
Virginia Polytechnical Institute
21044 Derring Hall
Blacksburg, VA 24061

Prof. Keiiti Aki
Center for Earth Sciences
University of Southern California
University Park
Los Angeles, CA 90089-0741

Dr. Stephen Bratt
Center for Seismic Studies
1300 North 17th Street
Suite 1450
Arlington, VA 22209

Prof. Shelton S. Alexander
Geosciences Department
403 Deike Building
The Pennsylvania State University
University Park, PA 16802

Michael Browne
Teledyne Geotech
3401 Shiloh Road
Garland, TX 75041

Dr. Kenneth Anderson
BBNSTC
Mail Stop 14/1B
Cambridge, MA 02238

Mr. Roy Burger
1221 Serry Road
Schenectady, NY 12309

Dr. Ralph Archuleta
Department of Geological Sciences
University of California at Santa Barbara
Santa Barbara, CA 93102

Dr. Robert Burridge
Schlumberger-Doll Research Center
Old Quarry Road
Ridgefield, CT 06877

Dr. Jeff Barker
Department of Geological Sciences
State University of New York
at Binghamton
Vestal, NY 13901

Dr. W. Winston Chan
Teledyne Geotech
314 Montgomery Street
Alexandria, VA 22314-1581

Dr. Susan Beck
Department of Geosciences, Bldg # 77
University of Arizona
Tucson, AZ 85721

Dr. Theodore Cherry
Science Horizons, Inc.
710 Encinitas Blvd., Suite 200
Encinitas, CA 92024 (2 copies)

Dr. T.J. Bennett
S-CUBED
A Division of Maxwell Laboratory
11800 Sunrise Valley Drive, Suite 1212
Reston, VA 22091

Prof. Jon F. Claerbout
Department of Geophysics
Stanford University
Stanford, CA 94305

Mr. William J. Best
907 Westwood Drive
Vienna, VA 22180

Prof. Robert W. Clayton
Seismological Laboratory
Division of Geological & Planetary Sciences
California Institute of Technology
Pasadena, CA 91125

Dr. N. Biswas
Geophysical Institute
University of Alaska
Fairbanks, AK 99701

Prof. F. A. Dahlen
Geological and Geophysical Sciences
Princeton University
Princeton, NJ 08544-0636

4

Prof. Adam Dziewonski
Hoffman Laboratory
Harvard University
20 Oxford St
Cambridge, MA 02138

Prof. John Ebel
Department of Geology & Geophysics
Boston College
Chestnut Hill, MA 02167

Eric Fielding
SNEE Hall
INSTOC
Cornell University
Ithaca, NY 14853

Prof. Donald Forsyth
Department of Geological Sciences
Brown University
Providence, RI 02912

Dr. Cliff Frolich
Institute of Geophysics
8701 North Mopac
Austin, TX 78759

Dr. Anthony Gangi
Texas A&M University
Department of Geophysics
College Station, TX 77843

Dr. Freeman Gilbert
IGPP, A-025
Scripps Institute of Oceanography
University of California
La Jolla, CA 92093

Mr. Edward Giller
Pacific Sierra Research Corp.
1401 Wilson Boulevard
Arlington, VA 22209

Dr. Jeffrey W. Given
SAIC
10260 Campus Point Drive
San Diego, CA 92121

Prof. Stephen Grand
University of Texas at Austin
Department of Geological Sciences
Austin, TX 78713-7909

Prof. Roy Greenfield
Geosciences Department
403 Deike Building
The Pennsylvania State University
University Park, PA 16802

Dan N. Hagedorn
Battelle
Pacific Northwest Laboratories
Battelle Boulevard
Richland, WA 99352

Dr. James Hannon
Lawrence Livermore National Laboratory
P. O. Box 808
Livermore, CA 94550

Prof. Robert B. Herrmann
Dept. of Earth & Atmospheric Sciences
St. Louis University
St. Louis, MO 63156

Ms. Heidi Houston
Seismological Laboratory
University of California
Santa Cruz, CA 95064

Kevin Hutchenson
Department of Earth Sciences
St. Louis University
3507 Laclede
St. Louis, MO 63103

Dr. Hans Israelsson
Center for Seismic Studies
1300 N. 17th Street, Suite 1450
Arlington, VA 22209-2308

Prof. Thomas H. Jordan
Department of Earth, Atmospheric
   and Planetary Sciences
Massachusetts Institute of Technology
Cambridge, MA 02139

Prof. Alan Kafka
Department of Geology & Geophysics
Boston College
Chestnut Hill, MA 02167

Robert C. Kemerait
ENSCO, Inc.
445 Pineda Court
Melbourne, FL 32940

William Kikendall
Teledyne Geotech
3401 Shiloh Road
Garland, TX 75041

Prof. Amos Nur
Department of Geophysics
Stanford University
Stanford, CA 94305

Prof. Leon Knopoff
University of California
Institute of Geophysics & Planetary Physics
Los Angeles, CA 90024

Prof. Jack Oliver
Department of Geology
Cornell University
Ithaca, NY 14850

Prof. L. Timothy Long
School of Geophysical Sciences
Georgia Institute of Technology
Atlanta, GA 30332

Dr. Kenneth Olsen
P. O. Box 1273
Linwood, WA 98046-1273

Dr. Gary McCartor
Department of Physics
Southern Methodist University
Dallas, TX 75275

Howard J. Patton
Lawrence Livermore National Laboratory
L-205
P. O. Box 808
Livermore, CA 94550

Prof. Art McGarr
Mail Stop 977
Geological Survey
345 Middlefield Rd.
Menlo Park, CA 94025

Prof. Robert Phinney
Geological & Geophysical Sciences
Princeton University
Princeton, NJ 08544-0636

Dr. George Mellman
Sierra Geophysics
11255 Kirkland Way
Kirkland, WA 98033

Dr. Paul Pomeroy
Rondout Associates
P.O. Box 224
Stone Ridge, NY 12484

Prof. John Nabelek
College of Oceanography
Oregon State University
Corvallis, OR 97331

Dr. Jay Pulli
RADIX System, Inc.
2 Taft Court, Suite 203
Rockville, MD 20850

Prof. Geza Nagy
University of California, San Diego
Department of Ames, M.S. B-010
La Jolla, CA 92093

Dr. Norton Rimer
S-CUBED
A Division of Maxwell Laboratory
P.O. Box 1620
La Jolla, CA 92038-1620

Dr. Keith K. Nakanishi
Lawrence Livermore National Laboratory
L-205
P. O. Box 808
Livermore, CA 94550

Prof. Larry J. Ruff
Department of Geological Sciences
1006 C.C. Little Building
University of Michigan
Ann Arbor, MI 48109-1063

Dr. Bao Nguyen
GL/LWH
Hanscom AFB, MA 01731-5000

Dr. Richard Sailor
TASC Inc.
55 Walkers Brook Drive
Reading, MA 01867

Dr. Susan Schwartz
Institute of Tectonics
1156 High St.
Santa Cruz, CA 95064

John Sherwin
Teledyne Geotech
3401 Shiloh Road
Garland, TX 75041

Dr. Matthew Sibol
Virginia Tech
Seismological Observatory
4044 Derring Hall
Blacksburg, VA 24061-0420

Dr. Albert Smith
Lawrence Livermore National Laboratory
L-205
P. O. Box 808
Livermore, CA 94550

Prof. Robert Smith
Department of Geophysics
University of Utah
1400 East 2nd South
Salt Lake City, UT 84112

Dr. Stewart W. Smith
Geophysics AK-50
University of Washington
Seattle, WA 98195

Donald L. Springer
Lawrence Livermore National Laboratory
L-205
P. O. Box 808
Livermore, CA 94550

Dr. George Sutton
Rondout Associates
P.O. Box 224
Stone Ridge, NY 12484

Prof. L. Sykes
Lamont-Doherty Geological Observatory
of Columbia University
Palisades, NY 10964

Prof. Pradeep Talwani
Department of Geological Sciences
University of South Carolina
Columbia, SC 29208

Dr. David Taylor
ENSCO, Inc.
445 Pineda Court
Melbourne, FL 32940

Dr. Steven R. Taylor
Lawrence Livermore National Laboratory
L-205
P. O. Box 808
Livermore, CA 94550

Professor Ta-Liang Teng
Center for Earth Sciences
University of Southern California
University Park
Los Angeles, CA 90089-0741

Dr. R.B. Tittmann
Rockwell International Science Center
1049 Camino Dos Rios
P.O. Box 1085
Thousand Oaks, CA 91360

Dr. Gregory van der Vink
IRIS, Inc.
1616 North Fort Myer Drive
Suite 1440
Arlington, VA 22209

Professor Daniel Walker
University of Hawaii
Institute of Geophysics
Honolulu, HI 96822

William R. Walter
Seismological Laboratory
University of Nevada
Reno, NV 89557

Dr. Raymond Willeman
GL/LWH
Hanscom AFB, MA 01731-5000

Dr. Gregory Wojcik
Weidlinger Associates
4410 El Camino Real
Suite 110
Los Altos, CA 94022

Dr. Lorraine Wolf
GL/LWH
Hanscom AFB, MA 01731-5000

7

Prof. Francis T. Wu
Department of Geological Sciences
State University of New York
at Binghamton
Vestal, NY 13901

Dr. Gregory B. Young
ENSCO, Inc.
5400 Port Royal Road
Springfield, VA 22151-2388

Dr. Eileen Vergino
Lawrence Livermore National Laboratory
L-205
P. O. Box 808
Livermore, CA 94550

J. J. Zucca
Lawrence Livermore National Laboratory
P. O. Box 808
Livermore, CA 94550

Dr. Ralph Alewine III
DARPA/NMRO
1400 Wilson Boulevard
Arlington, VA 22209-2308

Mr. James C. Battis
GL/LWH
Hanscom AFB, MA 01731-5000

Dr. Robert Blandford
AFTAC/TT
Center for Seismic Studies
1300 North 17th St., Suite 1450
Arlington, VA 22209-2308

Eric Chael
Division 9241
Sandia Laboratory
Albuquerque, NM 87185

Dr. John J. Cipar
GL/LWH
Hanscom AFB, MA 01731-5000

Cecil Davis
Group P-15, Mail Stop D406
P.O. Box 1663
Los Alamos National Laboratory
Los Alamos, NM 87544

Mr. Jeff Duncan
Office of Congressman Markey
2133 Rayburn House Bldg.
Washington, DC 20515

Dr. Jack Evernden
USGS - Earthquake Studies
345 Middlefield Road
Menlo Park, CA 94025

Art Frankel
USGS
922 National Center
Reston, VA 22092

Dr. Dale Glover
DIA/DT-1B
Washington, DC 20301

Dr. T. Hanks
USGS
Nat'l Earthquake Research Center
345 Middlefield Road
Menlo Park, CA 94025

Paul Johnson
ESS-4, Mail Stop J979
Los Alamos National Laboratory
Los Alamos, NM 87545

Janet Johnston
GL/LWH
Hanscom AFB, MA 01731-5000

Dr. Katharine Kadinsky-Cade
GL/LWH
Hanscom AFB, MA 01731-5000

Ms. Ann Kerr
IGPP, A-025
Scripps Institute of Oceanography
University of California, San Diego
La Jolla, CA 92093

Dr. Max Koontz
US Dept of Energy/DP 5
Forrestal Building
1000 Independence Avenue
Washington, DC 20585

Dr. W.H.K. Lee
Office of Earthquakes, Volcanoes,
& Engineering
345 Middlefield Road
Menlo Park, CA 94025

Dr. William Leith
U.S. Geological Survey
Mail Stop 928
Reston, VA 22092

Dr. Richard Lewis
Director, Earthquake Engineering & Geophysics
U.S. Army Corps of Engineers
Box 631
Vicksburg, MS 39180

James F. Lewkowicz
GL/LWH
Hanscom AFB, MA 01731-5000

Mr. Alfred Lieberman
ACDA/VI-OA'State Department Bldg
Room 5726
320 - 21st Street, NW
Washington, DC 20451

Stephen Mangino
GL/LWH
Hanscom AFB, MA 01731-5000

Dr. Robert Masse
Box 25046, Mail Stop 967
Denver Federal Center
Denver, CO 80225

Art McGarr
U.S. Geological Survey, MS-977
345 Middlefield Road
Menlo Park, CA 94025

Richard Morrow
ACDA/VI, Room 5741
320 21st Street N.W
Washington, DC 20451

Dr. Carl Newton
Los Alamos National Laboratory
P.O. Box 1663
Mail Stop C335, Group ESS-3
Los Alamos, NM 87545

Dr. Kenneth H. Olsen
Los Alamos Scientific Laboratory
P. O. Box 1663
Mail Stop D-406
Los Alamos, NM 87545

Mr. Chris Paine
Office of Senator Kennedy
SR 315
United States Senate
Washington, DC 20510

Colonel Jerry J. Perrizo
AFOSR/NP, Building 410
Bolling AFB
Washington, DC 20332-6448

Dr. Frank F. Pilotte
HQ AFTAC/TT
Patrick AFB, FL 32925-6001

Katie Poley
CIA-ACIS/TMC
Room 4X16NHB
Washington, DC 20505

Mr. Jack Rachlin
U.S. Geological Survey
Geology, Rm 3 C136
Mail Stop 928 National Center
Reston, VA 22092

Dr. Robert Reinke
WL/NTESG
Kirtland AFB, NM 87117-6008

Dr. Byron Ristvet
HQ DNA, Nevada Operations Office
Attn: NVCG
P.O. Box 98539
Las Vegas, NV 89193

Dr. George Rothe
HQ AFTAC/TTR
Patrick AFB, FL 32925-6001

Dr. Alan S. Ryall, Jr.
DARPA/NMRO
1400 Wilson Boulevard
Arlington, VA 22209-2308

Dr. Michael Shore
Defense Nuclear Agency/SPSS
6801 Telegraph Road
Alexandria, VA 22310

Mr. Charles L. Taylor
GL/LWG
Hanscom AFB, MA 01731-5000

Dr. Larry Turnbull
CIA-OSWR/NED
Washington, DC 20505

Dr. Thomas Weaver
Los Alamos National Laboratory
P.O. Box 1663, Mail Stop C335
Los Alamos, NM 87545

GL/SULL
Research Library
Hanscom AFB , MA 01731-5000 (2 copies)

Defense Intelligence Agency
Directorate for Scientific & Technical Intelligence
Attn: DT1B
Washington, DC 20340-6158

Secretary of the Air Force
(SAFRD)
Washington, DC 20330

AFTAC/CA
(STINFO)
Patrick AFB, FL 32925-6001

Office of the Secretary Defense
DDR & E
Washington, DC 20330

TACTEC
Battelle Memorial Institute
505 King Avenue
Columbus, OH 43201 (Final Report Only)

HQ DNA
Attn: Technical Library
Washington, DC 20305

DARPA/RMO/RETRIEVAL
1400 Wilson Boulevard
Arlington, VA 22209

DARPA/RMO/Security Office
1400 Wilson Boulevard
Arlington, VA 22209

Geophysics Laboratory
Attn: XO
Hanscom AFB, MA 01731-5000

Geophysics Laboratory
Attn: LW
Hanscom AFB, MA 01731-5000

DARPA/PM
1400 Wilson Boulevard
Arlington, VA 22209

Defense Technical Information Center
Cameron Station
Alexandria, VA 22314 (5 copies)

Dr. Ramon Cabre, S.J.
Observatorio San Calixto
Casilla 5939
La Paz, Bolivia

Prof. Hans-Peter Harjes
Institute for Geophysik
Ruhr University/Bochum
P.O. Box 102148
4630 Bochum 1, FRG

Prof. Eystein Husebye
NTNF/NORSAR
P.O. Box 51
N-2007 Kjeller, NORWAY

Prof. Brian L.N. Kennett
Research School of Earth Sciences
Institute of Advanced Studies
G.P.O. Box 4
Canberra 2601, AUSTRALIA

Dr. Bernard Massinon
Societe Radiomana
27 rue Claude Bernard
75005 Paris, FRANCE   (2 Copies)

Dr. Pierre Mecheler
Societe Radiomana
27 rue Claude Bernard
75005 Paris, FRANCE

Dr. Svein Mykkeltveit
NTNF/NORSAR
P.O. Box 51
N-2007 Kjeller, NORWAY   (3 copies)

FOREIGN (OTHER)

Dr. Peter Basham
Earth Physics Branch
Geological Survey of Canada
1 Observatory Crescent
Ottawa, Ontario, CANADA K1A 0Y3

Dr. Eduard Berg
Institute of Geophysics
University of Hawaii
Honolulu, HI 96822

Dr. Michel Bouchon
I.R.I.G.M.-B.P. 68
38402 St. Martin D'Heres
Cedex, FRANCE

Dr. Hilmar Bungum
NTNF/NORSAR
P.O. Box 51
N-2007 Kjeller, NORWAY

Dr. Michel Campillo
Observatoire de Grenoble
I.R.I.G.M.-B.P. 53
38041 Grenoble, FRANCE

Dr. Kin Yip Chun
Geophysics Division
Physics Department
University of Toronto
Ontario, CANADA M5S 1A7

Dr. Alan Douglas
Ministry of Defense
Blacknest, Brimpton
Reading RG7-4RS, UNITED KINGDOM

Dr. Roger Hansen
NTNF/NORSAR
P.O. Box 51
N-2007 Kjeller, NORWAY

Dr. Manfred Henger
Federal Institute for Geosciences & Nat'l Res.
Postfach 510153
D-3000 Hanover 51, FRG

Ms. Eva Johannisson
Senior Research Officer
National Defense Research Inst.
P.O. Box 27322
S-102 54 Stockholm, SWEDEN

Dr. Fekadu Kebede
Seismological Section
Box 12019
S-750 Uppsala, SWEDEN

Dr. Tormod Kvaerna
NTNF/NORSAR
P.O. Box 51
N-2007 Kjeller, NORWAY

Dr. Peter Marshall
Procurement Executive
Ministry of Defense
Blacknest, Brimpton
Reading FG7-4RS, UNITED KINGDOM

Prof. Ari Ben-Menahem
Department of Applied Mathematics
Weizman Institute of Science
Rehovot, ISRAEL 951729

Dr. Robert North
Geophysics Division
Geological Survey of Canada
1 Observatory Crescent
Ottawa, Ontario, CANADA K1A 0Y3

Dr. Frode Ringdal
NTNF/NORSAR
P.O. Box 51
N-2007 Kjeller, NORWAY

Dr. Jorg Schlittenhardt
Federal Institute for Geosciences & Nat'l Res.
Postfach 510153
D-3000 Hannover 51, FEDERAL REPUBLIC OF
GERMANY

13